Examining the selectivity in the impact of pulmonary P-gp upon the absorption of its substrates using an IPML model with knockout mice.

A thesis submitted in accordance with the conditions governing candidates for the degree of Philosophiae Doctor in Cardiff University

June 2015

Daniel Price

B.Sc.(Hons)

School of Pharmacy

Cardiff University

DECLARATION

This work has not been submitted in substance for any other degree or award at this or any other university or place of learning, nor is being submitted concurrently in candidature for any degree or other award.

Signed …… (candidate) Date ……16/12/2015……

STATEMENT 1

This thesis is being submitted in partial fulfillment of the requirements for the degree of ……PhD……(insert MCh, MD, MPhil, PhD etc, as appropriate)

Signed …… (candidate) Date ……16/12/2015……

STATEMENT 2

This thesis is the result of my own independent work/investigation, except where otherwise stated.

Other sources are acknowledged by explicit references. The views expressed are my own.

Signed …… (candidate) Date ……16/12/2015……

STATEMENT 3

I hereby give consent for my thesis, if accepted, to be available online in the University's Open Access repository and for inter-library loan, and for the title and summary to be made available to outside organisations.

Signed …… (candidate) Date ……16/12/2015……

Student ID Number: C1144707

Summary of Thesis:

P-glycoprotein is an ATPase binding cassette (ABC) drug-transporter protein represented by MDR1 in humans and mdr1a and mdr1b in mice. The substrate specificity of this protein is unusually large due to the polyspecific nature of its binding pocket and as a result a wide range of endogenous and exogenous compounds are effluxed by this transporter. There is a large body of literature about the role of P-glycoprotein in limiting the absorption of drug substrates at a number of barriers but currently data in the lung is limited. P-gp expression and localisation studies have confirmed its presence in lung tissue but there is conflicting data with regards to the functional relevance on lung absorption.

The aims of this project were to establish a knockout, mdr1a/b (-/-), isolated perfused mouse lung model (IPML) to investigate the role of pulmonary P-gp upon lung delivery. Utilising the lungs of knockout mice in the IPML allowed the investigation of P-gp function with the effects of chemical inhibition which may have resulted in the discordance observed in its functional significance in the literature.

IPML experiments were conducted with a panel of 18 P-gp substrates which were chosen for diversity in their physicochemical characteristics. The discordance in P-gp functionality in the lung observed in the literature was replicated in the IPML model. Ten of the substrates showed significant efflux from the lung by pulmonary P-gp whereas the absorption of the remaining eight was unaffected.

Further studies into the mechanism behind the differential effects of pulmonary P-gp showed that it was a barrier specific effect as it was not observed in the intestine. The effect was also not explained by differences in the P-gp binding kinetics off the substrates.

Investigations in to the membrane affinity of the panel revealed a potential mechanism for the selectivity of P-gp in the lung with regards to the passive permeability of the molecules and specifically the paracellular pathway.

Table of contents

Abbreviation list

ABC –	ATP binding cassette
ATP –	Adenosine triphosphate
BBB –	Blood-brain barrier
BCRP –	Breast cancer resistance protein
DMSO –	Dimethyl sulfoxide
GSK –	GlaxoSmithKline plc.
HPLC –	High-performance liquid chromatography
IAM –	Immobilised artificial membrane
IPML –	Isolated perfused mouse lung
IPRL –	Isolated perfused rat lung
KH –	Krebs-Henseleit buffer
LCMS –	Liquid chromatography mass spectrometry
LC-MS/MS –	Liquid chromatography tandem mass spectrometry
MLV –	Multilamellar vesicles
mRNA –	Messenger RNA
MRP –	Multidrug resistance-associated protein
NHBE –	Lonza's normal human bronchial epithelial cells
OAT –	Organic anion transporter
OATP –	Organic anion-transporting polypeptide
OCT –	Organic cation transporter
OCTN –	Sodium dependent organic cation transporter
PBS –	Phosphate buffered saline
PC –	Phosphatidylcholine
PG –	Phosphatidylglycerol
PD -	Pharmacodynamics
P-gp –	P-glycoprotein

PK - Pharmacokinetics

pMDI – Pressurised metered dose inhaler

SAR - Structure-activity relationship

SLC – Solute carrier

Chapter 1

General Introduction

1. GENERAL INTRODUCTION

1.1 Lung Transporters and recognised impact on pulmonary transport

The role of drug-transporters in the absorption and distribution and elimination of low-molecular weight drugs is increasingly well studied at a range of barriers including the lung. The current knowledge of the pulmonary expression and function of drug-transporters places emphasis on three families of transporter proteins, the ABC binding cassette proteins (including P-gp, MRP and BCRP), the solute carrier proteins (including the OCT and OCTN proteins) and the organic anion transporters (OATs and OATPs).

Despite the recent increase in the interest of pulmonary transporters the determination of their effects upon pulmonary pharmacokinetics suffers from a shortage of information. It is the case that for many of the pulmonary transporters data on their localisation within the lung is scarce or contradictory and experiments of transporter functionality in whole lung assays is limited.

ABC binding cassette proteins

P-glycoprotein (P-gp)

P-gp belongs to the ABC subfamily B (ABCB1) and is perhaps the most extensively studied transporter across all barriers. The importance of P-gp to drug disposition is due in part to its large substrate specificity. The crystal structure of P-gp has been elucidated and has led to a greater understanding of the reason for this broad range of substrates (1). The crystal structure of P-gp shows a large binding pocket wherein drug binding is mediated by mainly hydrophobic and aromatic residues located on β-sheets. Aromatic and hydrophobic residues are especially prevalent towards the upper half of the binding pocket, the lower half possessing more polar and charged residues. These charged residues may accommodate the binding of positively charged hydrophobic substrates and subsequently neutralise the charge. Crystal structures generated with P-gp bound to substrate highlight the numerous distinct binding sites within the binding pocket that are thought to be the cause of the broad substrate specificity.

Even though the substrates of P-gp cover a broad range of physicochemical parameters they do share similarities. P-gp substrates tend to be large lipophilic or amphiphilic planar molecules which are able to form weak hydrogen bond associations and often express a weak or delocalised positive charge (2–4).

P-gp expression in the lung has now been demonstrated by multiple groups at both the genetic and protein level. The expression has been localised to a range of pulmonary tissues known to be important for drug absorption. These studies as well as the functional evidence generated from *in vitro*, *ex vivo* and *in vivo* absorption studies is discussed in detail in chapter 4.

Breast cancer resistance protein – BCRP

BCRP (ABCG2) is a member of the ATP binding cassette (ABC) transporters expressed on the apical membranes of epithelial cells where it acts as an efflux transporter for a range of exogenous chemicals from anti-cancer drugs to ion channel blockers.

Data for BCRP activity within the lung is sparse with much fewer studies performed than for the well characterised ABC transporter P-gp. In 2007, Bleasby (5) studied the relative levels of transporter protein mRNA in many organs across a range of species. In the case of BCRP in the lung the expression levels were found to be in the moderate to higher quartile (50-75%) in human lungs. Further investigations were reported across a range of species including dog and rodent, although expression levels were lower in rodent lungs. This relatively high expression of pulmonary BCRP has also been observed by two recent studies in both human lung tissue (6) and immortalised human lung cell lines (7). In these studies it was observed that BCRP protein levels were the third highest of all transporters analysed, with only the expression of MRP1 and OCTN1 higher.

This relatively high level of mRNA presence in the lung is represented by the expression of the protein in *in vitro* cell culture models. In both Calu-3 and 16HBE14o- cells BCRP expression is observed (8) although the protein is much more highly expressed in the 16HBE14o- cell line in which it appears overexpressed.

There are few studies in the literature which have investigated the expression at a protein level and those present appear contradictory. Work by Fetsch et al (9) using immunostaining techniques showed expression of BCRP within unspecified alveolar pneumocytes (it was not mentioned whether these were type I or II or both) and little or no staining of the bronchial epithelia. Discordantly to this observation, earlier work by Scheffer (10) had seen staining of the bronchial epithelial cells and endothelial capillaries but not in alveolar pneumocytes. It appears that staining for the presence of BCRP protein produces varying apparent expression patterns dependent on the stains and techniques used. It is however likely that given the staining seen and the high levels of mRNA present in lung homogenate and in vitro cell lines that BCRP is present in the lung and if assumptions are drawn from other barriers this is likely to be expressed on the apical membranes of epithelia cells.

Multidrug Resistance Proteins

The MRPs are members of the ABC subfamily of ATPase binding cassette (ABC) transporters which consists of at least 13 separate transporters. Of these MRP1 is amongst the most well studied and functions primarily as a co-transporter of glutathione, glucuronic acid or sulphate conjugated drugs; usually at the basolateral membrane of cells. It was primarily identified due to a role in chemotherapy resistance of cancer but plays a role in the pharmacokinetics of many non-cancer drugs as well with relatively large substrate specificity. In the lung the protein is of interest as it has been reported that MRP1 reduces the oxidative stress generated by smoking and therefore may play a therapeutic role in COPD.

The microarray work of Bleasby (5) identifies MRP1 expression as moderate to high (50-75%) in the human and rodent lung, a finding corroborated by other mRNA based studies (11).

The work with mRNA is backed up by evidence of protein staining from intact lungs. Initial work by Flens *et al* in 1996 (12) used immunostaining of wax embedded lung sections to show expression of MRP1 in a normal lung, this was seen as localised around the apical region of the cytoplasm of bronchial epithelia cells. The same study also shows strong expression of the protein using Western blot analyses. Two later studies confirmed the presence of MRP1 using immunohistochemical techniques but instead of localisation below the cilia these studies witnessed localisation of MRP1 on the basolateral membrane (10,13); a finding common with the proteins expression at other barriers. This evidences of the presence of MRP1 is corroborated by a recent study utilising LC-MS/MS techniques to analyse the levels of a variety of transporters from human lung tissue (6). The study found the expression of MRP1 in the human lung was high, second only to OCTN1.

In 2009 a study by Endter *et al* investigated the expression of a wide range of transporters within *in vitro* cell models of respiratory cell lines (8). This study found evidence of a high level of MRP1 expression in all cell lines studied. This *in vitro* activity has been confirmed using functional studies by measuring the reduction in efflux of the substrate carboxydichlorofluorescein in the presence of an MRP inhibitor MK-571 (14).

Despite a large number of studies using *in vitro* cell lines to study the possible roles of MRPs in lung tissue, functional data from an intact lung system is not available. Given the proteins potential role in the protection against oxidative stress in smokers it is of great interest as a lung transporter. The data currently available provides very strong evidence for the presence of MRP1 within the lung, particularly at the basolateral membrane of bronchial epithelia, however this does need to be corroborated with whole lung functional transporter assays.

Organic cation transporters – OCT/N

The OCT proteins are members of the solute carrier (SLC22A) superfamily of proteins. They function as facilitative transporters able to carry a range of endogenous and exogenous molecules across the plasma membrane in either direction.

Localisation

By utilising rtPCR a number of groups have observed the expression of OCT/N in both human and rodent species. Lips *et al*. have shown the expression of OCT1-3 in human (15)and mouse (16) epithelia from the trachea and bronchi. The same study reported the protein expression of OCT1, OCT2 and OCT3 on the apical membrane of ciliated epithelial cells of the trachea and bronchi, it is noted that the level of OCT3 was lower than that of OCT1 and OCT2. The group also showed strong staining of OCT3 on the membranes of basal cells. As well as the presence of the OCTs the expression of OCTN1 and OCTN2 has also been observed in the mouse lung (17). A recent study by Sakamoto *et al.* investigating the expression of a wide range of transporters in human lung tissue by LC-MS/MS has also shown the presence of OCT1, OCT2 and OCTN1. Indeed, the levels of OCTN1 were the highest observed for any transporter in the study.

A microarray analysis performed by Bleasby *et al.* has also shown transcripts of OCT1-3 and OCTN1-2 to be present in the lung (5). The study showed expression of OCT2 to be in the lower quartile in the lung, OCT1 and OCT3 were in the moderate quartile and the expression levels of OCTN1 and 2 were considerably higher in the 50-75 % quartile. It is worth noting that the sampling in the microarray analysis was performed on whole lung homogenates. This means it is possible high levels of localised transporter expression in the lung could be diluted by non-expressing tissues in the sample.

The high levels of OCTN1-2 expression seen in the microarray analysis have also been corroborated in later studies. Horvath *et al.* observed relatively high expression of OCTN1 and OCTN2 transcripts in the epithelial cells of the human airway (18). This mRNA expression was corroborated by localisation of OCTN1 and OCTN2 protein in the airways and strong expression of OCTN2 in the alveolar epithelium. Further, the levels of OCTNs in a range of respiratory epithelial cell models has been shown to be higher than that of the OCTs (8).

Function

A number of the drugs routinely delivered to the lung have been identified as substrates for the OCT/N transporter proteins. For example, salbutamol and formoterol have both been shown to modulate the uptake of model cation substrate in *in vitro* human bronchial cell lines (18,19).

However, despite identifying inhaled drugs which interact with OCTs there is no direct evidence available for a role for the transporters in the pulmonary pharmacokinetics of these drugs.

Organic anion transporters (OATs) and organic anion transporting peptides (OATPs)

The OATs and OATPs belong to the solute carrier family of proteins (SLC22 and SLC21, respectively). Despite implications of a possible role for these transporters at a number of barriers there is a distinct lack of data with regards to their lung distribution.

A review of the relevant data on OAT mRNA expression within the lung (20) concluded that this family of transporters are absent from the lung. It is the case that the microarray study by Bleasby *et al.* recorded no expression for 5 of the 6 isoforms, although the study did suggest relatively high expression of OAT2 in pulmonary tissue (5).

Conversely, the expression of a range of the OATP isoforms has been detected in the lung tissue. At the mRNA level the expression of OATP4A1 was shown to be very strong in lung tissue, OATP3A1 and OATP2A1 also showed strong expression with lower levels of expression seen for OATP2B1 (21). The microarray analysis of Bleasby *et al.* is in agreement with these findings with similar high expression of these OATPs observed whilst the expression of the other OATPs were in the lowest quartile, essentially absent from the lung (5).

1.2 P-gp efflux – the effect of passive membrane permeability

It is now generally accepted that P-glycoprotein is present within the lung tissue, a finding corroborated by studies across multiple groups, however, functional studies in intact lungs have so far provided conflicting data. The effect of P-gp upon the absorption of rhodamine 123 and digoxin from an intact lung has been investigated in multiple studies and in both mice and rat lungs (22–25). Despite both molecules being well established substrates in both *in vitro* assays and as seen by efflux in the intestine the effect of P-gp upon their pulmonary absorption has proved discordant.

The absorption of rhodamine 123 has been assessed from an IPRL model. The study shows the absorption of rhodamine 123 from the rat lungs is a saturable process, suggesting an active component in the pulmonary absorption of rhodamine 123. The active component was identified as P-gp by studies with a chemical inhibitor (GF120918). The absorption of rhodamine 123 was significantly increased in the presence of the chemical inhibitor providing strong evidence for an effect of P-gp to attenuate the pulmonary absorption of this substrate (22).

Subsequent studies utilising digoxin as the model substrate did not show the same effect of P-gp. In a study comparable to that of rhodamine 123 the addition of a P-gp inhibitor did not enhance pulmonary absorption of digoxin. Likewise, absorption from the lungs of spontaneous mdr1a (-/-) CF-1 mice was no different to that from the wild type counterparts. This data would suggest that pulmonary P-gp does not play a role in the absorption of digoxin.

This discordance in the efflux of recognised substrates has been observed at other barriers and attributed to the contribution of passive transport overcoming P-gp efflux. A more complete discussion of the mechanism behind this is presented in chapter 5. Briefly, as explained earlier P-gp substrates tend to be lipophilic molecules which partition readily to the membrane. Absorption of these drugs across a membrane is not that of a continuous diffusion gradient, rather they are absorbed by distinct flip-flop events whose rate is compound specific. The flip-flop event is a mechanism of transport across a lipid bilayer (26) and explained in detail in chapter 6. The flip-flop event is the rate limiting step in passive absorption for these molecules and therefore determines the transmembrane movement rate. Work by Eytan *et al.* (26) has shown that the rate of these flip-flop events contributes to the overall net effect of efflux. In some cases, as for verapamil, the rate of transmembrane movement is significantly higher than the possible extrusion rate of P-gp. Therefore, despite being a P-gp substrate with good affinity to the protein verapamil absorption across a P-gp expressing membrane is unaffected by efflux.

In this thesis this contribution of passive permeability to the overall effect of efflux will be repeatedly discussed as to its role in pulmonary efflux. The evidence provided by studies in the intestine will be used to develop a hypothesis for the discordance in pulmonary efflux and ultimately used to predict pulmonary drugs likely to exhibit efflux from the lung.

1.3 Lung perfusion models in physiology and pharmaceutical sciences

History of the technique

Isolated organ perfusions have been utilised for the study of physiology since the mid 1800's. Isolated organs proved vital tools for many early scientific discoveries such as the work of Claude Bernard on the role of the pancreas in digestion and the glycogenic function of the liver.

The original uses of the lungs in isolated organ models was a respirator for heart-lung preparation (27,28) in which it functioned purely to maintain the viability of the heart tissue. The use of the isolated perfused lung (IPL) itself as a model for studying lung physiology began in the 1950's. The initial lungs utilised were those of the larger species such as rabbits, dogs and guinea pigs (29) presumably due to the relative ease of their setup and maintenance.

The first documented use of the isolated perfused rat lung (IPRL) came shortly after in 1970 by Leary and Smith. The model used in these primary experiments was developed and represented the first standardised IPL model from which current IPL setups are established. Following the development of these early IPL protocols the usage of the technique has increased and as a consequence there now exists a variation of preparations regularly utilised for studies of lung pharmacology. This range of IPL preparations are routinely utilised for a wide array of investigations including drug delivery applications, drug discovery, physiology and histology.

Adaptation for drug absorption and deposition studies

The use of the IPL model for drug absorption studies was pioneered by the studies of Ryrfeldt *et al.* in the lungs of rats and guinea pigs. The group utilised the model to investigate the absorption of a range of molecules including but not limited to ibuterol, terbutaline (30) and budesonide (31). The group not only utilised the IPL models for the study of drug absorption but also applied it to studies of pharmacodynamics of drugs delivered both in the perfusate and as aerosol doses.

One particular IPRL setup, that of Byron and Niven (32), stands out as a model that has been used repeatedly to investigate drug deposition and absorption from the lung (32–34).The Byron and Niven model allows the delivery of an aerosolised dose to the rat lungs in a manner more consistent with human dosing than the tracheal instillation commonly used *in vivo.* This model allowed the development of the IPL preparations for the purpose of drug delivery and absorption investigations, a field in which they are now routinely used. There now exists a body of data on the absorption of a range of solutes from the Byron and Niven model (34–37) and it has been established as the standard model in this field. Another example of the use of IPL experiments in drug absorption studies is the work of Tronde. A large study by Tronde generated absorption profiles of a range of inhaled drugs from the IPRL and determined the physicochemical properties which resulted in enhanced absorption from the lungs (38).

Compared to *in vivo* models the IPL experiments allow increased control over the ventilation and perfusion of the lung as well as facilitating dosing strategies unavailable in *in vivo* experiments. The

ease of sampling and ability to sample multiple times from the same animal an absorption profile can be determined from a single lung and therefore without the inter-animal variability necessary with *in vivo* investigations. This also has the benefit of markedly reducing the animal usage of the IPL models. The absorption profile is also generated without the confounding effects of systemic ADME present in whole body studies.

Isolated perfused mouse lung studies of absorption

As discussed more fully in chapter 2, there is currently little data on the use of an isolated perfused mouse lung (IPML) for studies of drug absorption. However the model is particularly well used for studies of pharmacodynamic effects such as vasoconstriction and mediator release (39–43). These studies of pharmacodynamics provide sufficient data on the methodology of the IPML to adapt the model of Byron and Niven for use with the mouse lungs.

The prevalence of data for the IPML is pharmacodynamic studies is in party due to the availability of a number of knockout mice strains. The adaption of the IPML for the absorption studies will enable a similar use of a range of genetic knockouts to elucidate the role of transporters upon pulmonary pharmacokinetics, of particular interest here are mdr1a/b (-/-) mice.

1.4 Thesis aims and objectives

- The adaptation of a current IPRL setup for use with mouse lungs.
    - Validate the setup and maintenance of the IPML by determining tissue viability over the time course of the experiments.
    - Develop a means of reproducible aerosol dose to the mouse lungs with deposition at the absorptive airways.
    - Validate the barrier properties of the IPML by the absorption of paracellular probes
    - Investigate the applicability of the IPML to drug transporter studies by investigating the absorption of digoxin and rhodamine 123 with chemical inhibition and comparing the effect of P-gp to that seen previously in the literature.
- Establish a stable breeding colony of both mdr1a (-/-) and (+/+) mice in order to investigate the effect of P-gp knockout in the IPML.
    - Validate the ability of the knockout model to identify P-gp mediated effects by comparing the absorption of rhodamine 123 and digoxin to that obtained in CD1 mice with chemical inhibition.

- Investigate the absorption of a panel of P-gp substrates in the IPML with both knockout and wild type mice. The panel will then form the dataset used to investigate the discordance seen in digoxin and rhodamine 123 absorption.
- Investigate the effect of P-gp upon the intestinal absorption of the panel as a means of identifying if the discordance seen in the lung is present at other barriers.
- Establish the P-gp binding kinetics of the panel in order to investigate whether the discordance in efflux is attributable to variations in the affinity of the substrates to P-gp.
- Investigate the membrane partitioning in both an IAM and liposome experiment. This will be used to advance the hypothesis for the role of passive permeability in the discordance seen in the lung by highlighting the possible importance of the paracellular pathway in this organ.
- The physicochemical properties of the panel will then be established and used as a predictive tool to highlight other substrates which may show P-gp attenuated absorption in the lung.

Chapter 2

Development and Validation of the IPML

2.1 INTRODUCTION

2.1.1 General Lung Physiology

The airways

The primary function of the lung is to facilitate the gaseous exchange between inspired air and the circulatory system, i.e. the oxygenation of the blood and removal of carbon dioxide from the body. For optimum efficiency this process requires a large surface area for gaseous exchange coupled with ample blood perfusion to the gas exchange tissues. As a consequence of the large surface area and thin barrier properties of the lung it is a promising route for drug delivery for both local and systemic actions (44,45).

As a result of its function the mammalian lung is a particularly heterogeneous organ consisting of over 60 cell types in two main regions (46). The upper region of the lung, roughly 10 % of the volume of the lung, forms the conducting region of the airways. As shown in figure 2.1.1 this region consists of the sinuses, nasal cavity, pharynx, larynx (all not shown), trachea, bronchi and bronchioles. At the bifurcation, at the terminus of the trachea, the airways split in to two branches forming the bronchi; each subsequent airway bifurcation results in an exponential increase in airway surface area and a decrease in epithelial cell size. In humans the conducting region of the airways is generally formed from generation 0-16 (trachea to terminal bronchioles) whilst generations 17-23 form the respiratory region. However, the number of airway branchings before the respiratory region is reached can vary greatly from as few as 6 to as many as 30 (47).

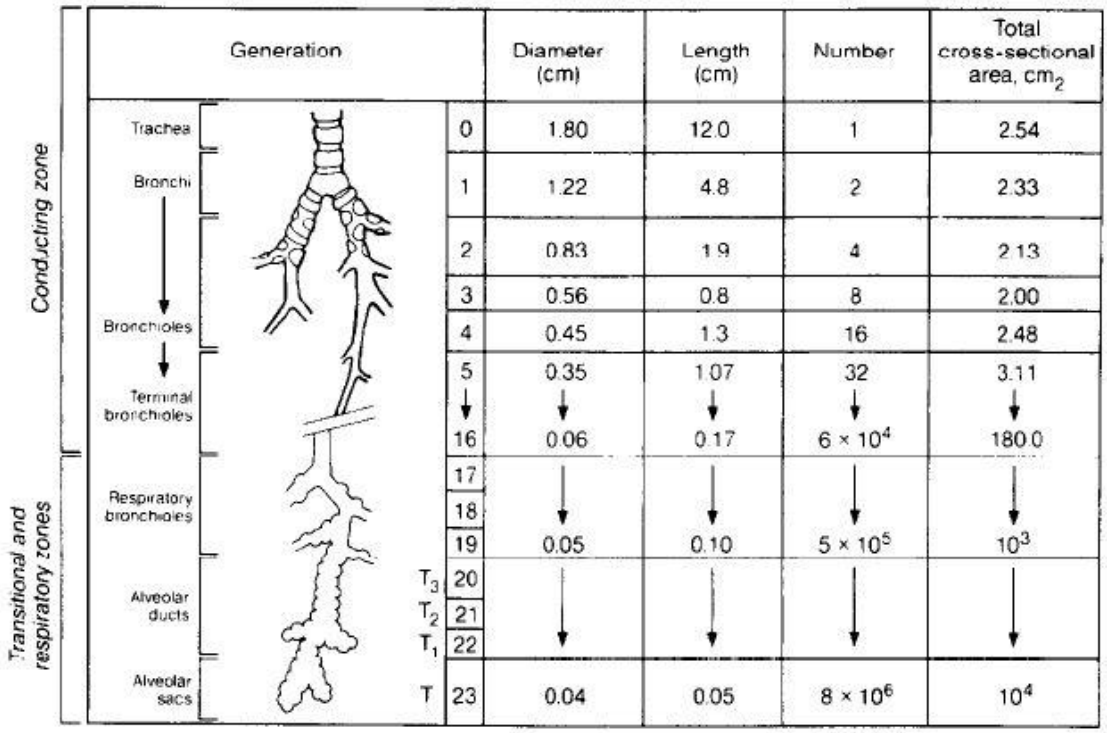

Generation		Diameter (cm)	Length (cm)	Number	Total cross-sectional area, cm_2
0		1.80	12.0	1	2.54
1		1.22	4.8	2	2.33
2		0.83	1.9	4	2.13
3		0.56	0.8	8	2.00
4		0.45	1.3	16	2.48
5 ↓ 16		0.35 ↓ 0.06	1.07 ↓ 0.17	32 ↓ 6×10^4	3.11 ↓ 180.0
17 18 19		↓ 0.05	↓ 0.10	↓ 5×10^5	↓ 10^3
T_3 20 T_2 21 T_1 22		↓	↓	↓	↓
T	23	0.04	0.05	8×10^6	10^4

Figure 2.1.1 A schematic of the airway branching of the lung highlighting the two main regions, the conducting and respiratory zones. Taken from Patton, 1996 (48).

The respiratory region accounts for the majority of lung tissue, roughly 85 % of the total lung volume, and is composed of alveolar epithelial cells and the capillary bed on either side of a thin basement membrane (46). The alveolar region is the most important for both gaseous exchange and drug absorption. The region consists of epithelial type I and II cells, brush cells and alveolar macrophages. From a drug delivery perspective absorption across the alveolar type I cells is the most prevalent route of transcellular absorption with regards to absorption from the lung; they have a smaller cell thickness, fewer organelles, higher cytoplasmic volume and cover the majority of the alveolar surface (roughly 96%) in comparison to the type II cuboidal cells (49). The effect of lung physiology on drug absorption is discussed in more detail in chapter 5, where it is compared with the intestine with regards to their drug permeability.

Respiratory rates and volume

The tidal volume of the lungs is a measure of the total volume of air inspired and expired with a normal breath and is well below the maximum volume (vital capacity) of the lung. For the mouse lung the tidal volume differs across strains and ages and averages approximately 0.2 mL for mice of 9-12 weeks of age (50). Similarly, the respiratory rate of the mouse has also shown variability between strains and animal sizes with documented rates of between 60 and 230 breaths/min

(51,52). The lung must be inflated with an adequate volume and rate to prevent the collapse of the respiratory surfaces, atelectasis.

Blood circulation to the lungs

The circulatory system of the mouse lungs is distinct from that of other common laboratory lung models, e.g. rat lungs, due to the lack of a bronchial circulation in the upper airways of the mouse (53). In the majority of model mammalian species the blood is perfused through the lungs as part of two separate circulations (54). The conducting region of the airways is perfused by the bronchial circulation, connected to the systemic circulation of the body. As such the bronchial circulation receives approximately 1% of the cardiac output and provides oxygenated blood and nutrients to the trachea and bronchioles. It has been suggested that the bronchial circulation may play an important role in the uptake of systemic drugs to the lung (55).

The respiratory regions of the airways are perfused by the pulmonary circulation. Here the blood supply originates from the pulmonary artery and consequently provides the complete cardiac output to the alveolar capillaries. This ensures efficient gas exchange due to the low oxygen concentration of the blood as well as providing nutrients to the alveolar cells. The two circulations are not completely distinct and are linked by anastomoses in the bronchioles of the lung (56).

The lack of the bronchial circulation in the mouse lung sets it apart from the lungs of the rat and larger mammalian models in that no systemic (bronchial) circulation is present (53). The entirety of the lung's blood supply is delivered by the pulmonary circulation, i.e. both the conducting and respiratory regions are perfused by the pulmonary circulation. As the entirety of the lungs blood supply therefore originates from the pulmonary artery it is possible to determine the rate of perfusion of the lung vasculature by measurements in the pulmonary artery. Previous literature suggests the heart rate of a mouse is approximately 450 beats per minute and produces a mean blood velocity of 90 cm/s. As the aortic diameter of a mouse is approximately 1.2 mm the resulting perfusion rate to the lungs is 14.8 mL/min (57).

With regards to the isolated perfused lung (IPL) studies the presence of a singular pulmonary circulation may prove advantageous for the mouse lung model. In the IPL models perfusion is achieved by cannulation of the pulmonary artery and therefore, perfusion occurs through the pulmonary circulation. In the rat and other models this results in limited perfusion of the conducting region due to the restricted supply of blood/perfusate via the anastomoses of the two circulations. For studies which are influenced by events in the upper airways it may be the case that a mouse lung

model may prove advantageous as the conducting regions would be perfused to a normal physiological level.

2.1.2 IPL models for drug absorption

The IPL model is now well established for studies of lung physiology and drug absorption, as discussed in chapter 1. In comparison to *in vivo* studies the IPL provides a model with precise control over perfusion and ventilation, simple administration to the airways or blood and easy sampling of the perfusate or lavage fluid with ready determination of mass balance. Also, as the organ is isolated from the systemic circulation it is possible to study lung specific events in an intact lung without the confounding effects of systemic actions (58). The IPL model may also prove more ethically sound as multiple samples can be taken from the perfusate following drug administration whereas in an *in vivo* model an animal would be sacrificed at each time point. This has the additional benefit of reducing inter-animal variability in drug absorption. The major limitation of the IPL is the period of viability, for the rat lungs this is approximately 3-5 hours and is considerably lower in mice with viability of 1-2 hours common. However, for the study of the absorption of low molecular weight drugs this may prove adequate as the absorption of these molecules from the lung tends to be relatively rapid. Currently, most reports utilising the IPL for drug delivery applications have been in the form of the isolated perfused rat lung (IPRL) and these have been summarised previously by Tronde (59).

Despite the lack of literature reporting drug absorption from an IPML the model is well established for investigations of lung physiology. The model is particularly well used for studies of pulmonary vasoconstriction and mediator release (39–43) where knockout mice strains for relevant proteins provide a useful insight in to the physiological mechanisms in an intact organ. The IPL lends itself well to these studies as the physical effects of vasoconstriction are easily measured by increases in pressure at the perfusate pump and regular samples can be taken from the perfusate to measure the release of mediators such as cytokines. The use of the isolated perfused mouse lung in published literature is discussed in more detail in chapter 1.

These physiological studies provide useful information on the mechanics of performing an IPML, such as ventilation rates, tidal volumes and perfusion flow rates. Past research using IPML models has used perfusate flow rates of 1 mL/min (60–64), approximately 7% of the total cardiac output received by the lungs in an *in vivo* situation (15 mL/min). Efforts have been made to adjust perfusate flow rate to mouse size (65), however, the adjustments necessary are small and the majority of studies instead use mice of a similar size to minimise the variation in the flow rate to lung

size ratio. Ventilation volumes utilised in the IPML generally mimic the tidal volumes observed *in vivo* in order to prevent atelectasis, on average the tidal volume of a mouse is approximately 0.2 mL/min.

The respiratory rate of the mouse is also significantly different from that of the rat, with rat rates documented as 70-115 breaths/min (66) and mice significantly faster at 80-230 breaths/min (51,52) with variations dependent upon the size and strain of mouse used. The in house IPRL model has previously been used to study drug absorption (22) and utilises a respiratory rate of 20 breaths/min, roughly a fifth of the normal respiratory rate of the rat. This proved adequate to prevent atelectasis whilst improving lung viability. Similarly IPML models from the literature use respiratory rates below that of the normal *in vivo* situation, with rates of 50-100 breaths/min utilised (60,62,65,67).

The current in house IPRL model utilises a dosing method proposed by Byron (32) involving horizontal dosing of the lungs using a metered dose inhaler (MDI). This dosing strategy has been shown to be reproducible and able to deliver more than 90 % of the dose to the lobar regions of the lung (68). As discussed previously, it is the lobar regions which are most important for drug absorption and therefore delivery to the lung periphery is key to the success of the model. Ideally, this MDI method of lung dosing would be applicable to the mouse lung although there is no evidence in the literature of its use with this species. Other dosing methods will also be investigated for their applicability to the mouse lung model and delivery to the lung periphery. Delivery of the dose in the form of small droplets can increase the deposition in to the deep lung. To this end a Penn Century Microsprayer™ is available and can be utilised to generate a liquid aerosol for delivery to the lung. However, particle size and therefore lung deposition have been shown to be effected by a drug's physicochemical properties (69) which could be seen to result in drug specific differences in absorption following delivery by this method.

The simplest methods reported in the literature utilise intratracheal instillation of the dose via a syringe and a bolus of air (23,65,70). This method provides a convenient way of ensuring identical volumes are delivered to the lung in a reproducible manner with easy determination of mass balance possible. This method has been shown to produce an even distribution of drug to the lungs and avoids the complications of particle size apparent with the previously discussed aerosolisation methods.

Here we aim to use the mechanics of the IPML and *in vivo* mouse studies reported in the literature in order to adapt an in house IPRL methodology for use with a mouse lung. The use of a mouse model will enable us to develop transgenic animals for the purpose of the study of the role of P-gp upon

the absorption of drugs from the lung without the requirements of a chemical inhibitor. There is already evidence in the literature for the use of IPML techniques with transgenic animals for physiological studies but data regarding the models use for a drug absorption purpose is scarce.

2.1.3 Experimental Objectives

The objective of this chapter is based around the development of an IPML model by using the in house expertise to adapt an existing IPRL system. In order to establish the new model this chapter aims to:

- Show tissue viability for greater than the time periods of the experiments.
- Develop a reproducible drug dosing technique with even deposition of dose in the deep airways.
- Investigate the absorption of model probes and a small number of substrates to compare the IPML to previous studies using rat lungs.

2.2 Materials and Methods

2.2.1 IPML Setup

Materials

Mechanical ventilator – 50 1718 (Harvard Apparatus, Cambs, UK)

Peristaltic pump - MINIPULS 3 (Gilson Inc., WI, USA)

Circulating water bath

Glassware

Water jacketed artificial glass thorax, custom made (Radleys, Essex, UK)

Water jacketed perfusate reservoir, custom made (School of Chemistry, Cardiff University, UK)

Artificial thorax lid and perfusate reservoir lid, custom made (School of Chemistry, Cardiff University, UK)

Perfusate line warmer, B14 socket and cone, SQ13 side arms, custom made (Radleys, Essex, UK)

SQ13 Plastic hose connector (Radleys, Essex, UK, product: 451002)

Plastic tubing and connectors

Perfusate tubing: PE50, 0.965 mm OD and 0.58 mm ID (VWR, PA, USA)

Pump tubing: Accu-rated PVC pump tubing, 2.972 mm OD, flow 1 mL/min (Fisher Scientific, Loughborough, UK)

Water lines: Tygon R-1000, 11.1 mm OD and 6.3 mm ID (VWR, PA, USA)

T-shape waterline connector: ADF-715-070W (Fisher Scientific, Loughborough, UK)

Perfusate

D-glucose anhydrous; C6H12O6, (Fisher Scientific, Loughborough, UK, G/0450/60)

Potassium chloride; KCl, (Fisher Scientific, Loughborough, UK, Cat: P/4280/53)

Magnesium sulphate heptahydrate; $MgSO_4.7H_2O$, (Fisher Scientific, Loughborough, UK, Cat: M/0600/53)

Sodium bicarbonate; $NaHCO_3$, (Fisher Scientific, Loughborough, UK, Cat: S/4200/60)

Calcium chloride dihydrate; $CaCl_2.2H_2O$, (Fisher Scientific, Loughborough, UK, Cat: C/1500/50)

Sodium chloride; NaCl, (Fisher Scientific, Loughborough, UK, Cat: S/3105/63)

Potassium dihydrogen phosphate; KH_2PO_4, (Fisher Scientific, Loughborough, UK, Cat: P/4800/53)

Bovine serum albumin; BSA, (Sigma-Aldrich, Dorset, UK, Cat: A7906-1kg)

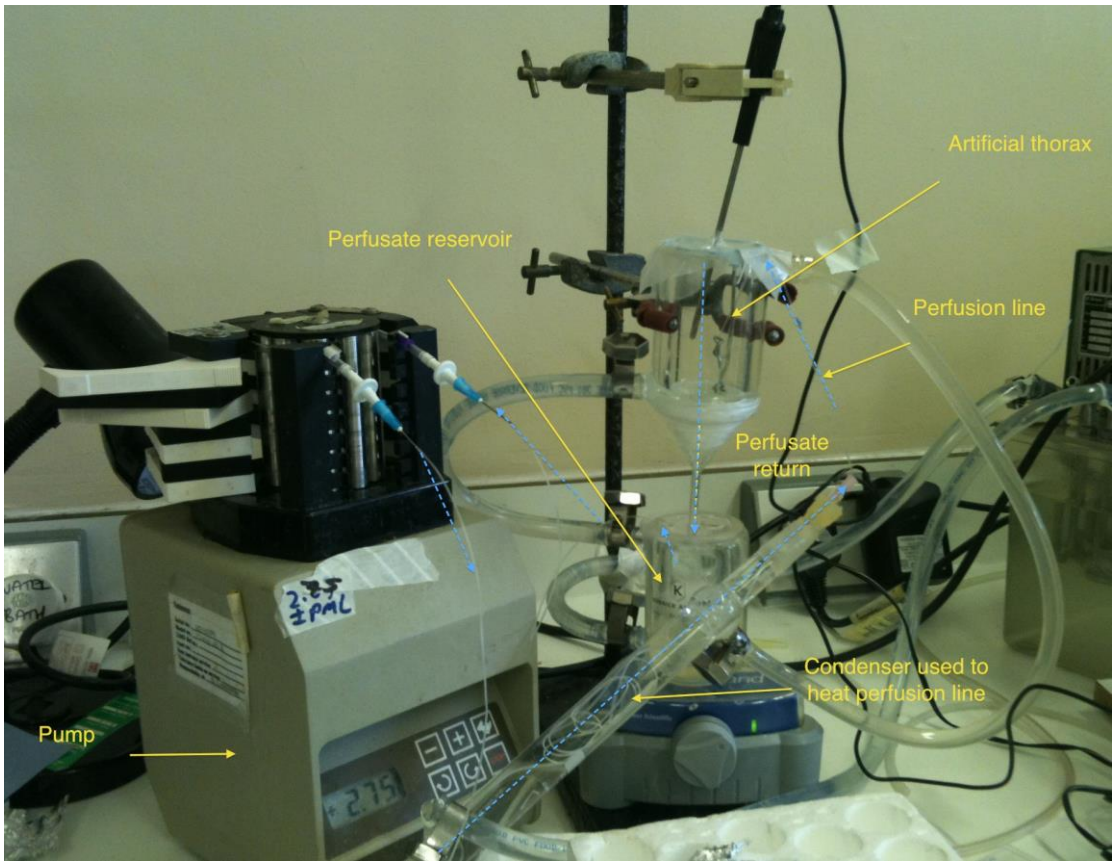

Figure 2.2.1 A photograph showing the equipment setup used for all IPML experiments, note: the artificial thorax lid is replaced with parafilm in the photograph for the purpose of temperature measurement inside the thorax. Blue arrows indicate the perfusate flow during normal experimental conditions.

The IPML equipment is setup as shown in figure 2.2.1 with recirculation of perfusate from the reservoir via the lungs. The recirculation from the reservoir makes it easy to sample from the reservoir and simple to maintain a constant perfusate volume throughout all experiments. The water jacketed glassware is supplied by water from the water bath at a constant 37 ^{o}C. Within the perfusate line warmer a metre of perfusate tubing is coiled to ensure the perfusate is warmed to 37

^{O}C before being passed through the lung vasculature. The setup is adapted from that of the Byron and Niven IPRL experiments (as seen in figure 2.2.2).

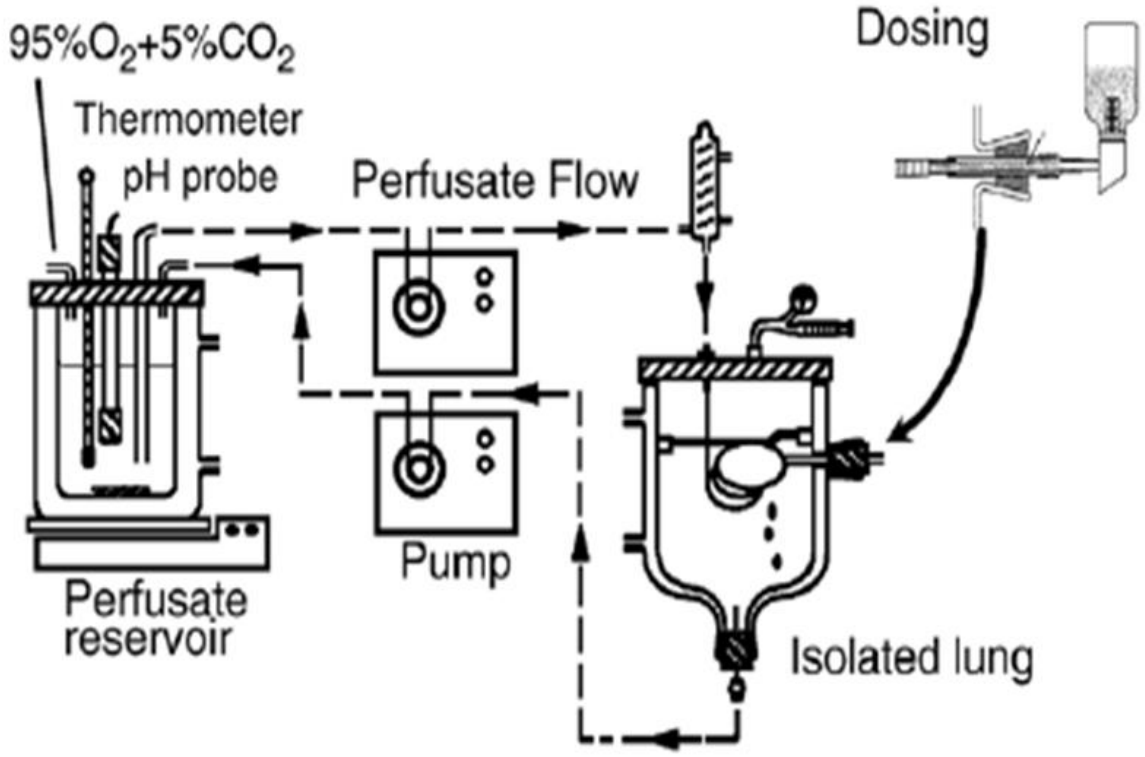

Figure 2.2.2 A schematic of the Byron and Nivel based IPRL setup from which the IPML was adapted.

Ventilation

The volume and rate of ventilation for inflation of the lungs is determined by the mechanical ventilator. Literature discussed in the introduction suggests an average tidal volume of 0.2 mL for a mouse lung but it was found that increasing this to 0.3 mL decreased the rate of oedema formation within the experiments and therefore 0.3 mL was chosen as the ventilation volume throughout the experiments. Restrictions, due to the model of ventilator available, mean it is not possible to make small adjustments to the volume to compensate for changes in mouse size, instead the size of mice used in the experiments is kept constant at 30 g ± 3 g. In all experiments performed in the IPML a ventilation rate of 70 breaths/min was used, this in within the range of ventilation rates used with similar models in the literature (see Introduction).

Perfusion Rate

The perfusion rate of the lungs in the IPML is determined by the peristaltic pump. A perfusion rate of 1 mL/min was chosen (setting 7.15 on the pump) similar to values used in previous literature studies

(see Introduction). This flow rate was decreased during cannulation of the pulmonary artery to 0.5 mL/min (setting 3.6 on the pump) to ease this process of the surgery.

2.2.2 IPML Surgery

Materials

Mouse tracheal cannula, 1.3 mm OD and 1.0 mm ID (Harvard Apparatus, Cambs, UK, Cat: 730028)

Euthatal (200 mg/ml) (Merial Animal Health Ltd., Harlow, UK)

1 ml syringe (Fisher Scientific, Loughborough, UK, Cat: SZR-150-011Q).

25G x 5/8IN needles orange (Fisher Scientific, Loughborough, UK, Cat: SZR-175-510A).

Cotton thread

Isolation and perfusion of the lungs

Animals

Male pathogen-free CD1 mice (Harlan, UK) were used throughout the preliminary method development experiments. The mice were housed in temperature and humidity controlled rooms (19-21 ^{o}C and 40-60 % humidity) with a 12 hour dark-light cycle. All mice had access to food and water *ad libitum* and were acclimatised for at least 24 hours following transport to the experimental laboratories. All animal experiments were performed in adherence to the Animal (Scientific Procedures) Act 1986 and were approved by Cardiff University and GSK, Stevenage.

Perfusate

Perfusate solution was prepared as a Krebs-Henseleit (pH 7.4) buffer containing 10 % w/v BSA and filtered using Whatman grade No.91 filter paper under vacuum. All perfusate batches were made between 16 and 24 h before an experiment and were stirred continuously at 4 ^{o}C for 16 hours before use. Batches not used within 48 h were discarded.

Preparation

All glassware and 15 mL of perfusate in the reservoir were brought to the experimental temperature (37 ^{o}C) for at least 30 min prior to surgery. The perfusate reservoir was constantly oxygenated by a

gas line pumping 95% O_2, 5% CO_2 in to the reservoir throughout the experiment. Once at temperature the perfusate was pumped through the system and the first 5 mL of circulated perfusate was discarded. Surgical implements were thoroughly cleaned in 50 % ethanol and a Euthatal dose was prepared (60 mg/kg dose or approximately 0.1mL of the 200 mg/mL stock) in a 1 mL sterile syringe with a 25G needle attached.

Animals were then retrieved from housing and euthanised with the dose of Euthatal via an IP injection as per Schedule 1. After animals stopped responding to applied stimuli (blink test and foot pinch test) death was guaranteed by separation of the spinal cord in the neck. From this point surgery took an average of 6 min to result in suspension of perfused lungs in the artificial thorax.

Surgery

Following euthanasia, an incision was made in the throat and expanded to expose the trachea, taking care not to sever any of the major blood vessels of the neck. Once the trachea was exposed a small incision of about half of the tracheas circumference was made below the 4^{th} cartilage ring. This allowed the tracheal cannula to be inserted until 2-3mm short of the first bifurcation. The cannula was then secured in the trachea by tying with cotton thread.

The abdominal cavity was then opened across its entire width to expose the diaphragm. The diaphragm could then be removed, great care must be taken to avoid touching any lung tissue, this is made simpler by first making a small incision in the diaphragm causing the pressure to be released in the cavity and the lungs to fall away from it. The ribcage was then dissected on both sides in a single large cut from the base of the ribs to the neck in order to expose the lungs and heart. The sternum was then clamped and secured above the head of the animal.

The base of the heart was then clamped with plastic forceps and held firmly. Both atria were then cut to allow free flow of perfusate. A small incision was then made roughly 3-5 mm below the entry of the pulmonary artery. The cut was made perpendicular to the path of the artery and roughly 5mm long. Through this incision it was possible to insert perfusate tubing from the reservoir (perfusion rate of 0.5 mL/min), 5 mm in to the pulmonary artery from the ventricle of the heart. The perfusate tubing acts as the pulmonary artery catheter in these experiments. Once inserted an artery clamp was utilised to hold the tubing in place whilst the catheter was secured by tying with cotton thread between the clamp and the incision in the ventricle. Two cotton loops were used to tie off the catheter to ensure redundancy if one was loose. Both ventricles of the lung were then cut to allow perfusate from the lungs to drain freely from the heart.

Removal of the lungs from the thoracic cavity was initiated at the trachea. The cannula was held with forceps and lifted as the trachea was cut above the cannula. Thoracic connections were then severed as the lungs were lifted gently by the trachea until the lungs were removed completely. Care was taken to ensure the lungs did not contact the severed rib cage at this point. Once removed, the lungs were suspended vertically in the artificial glass thorax by suspending them from the tracheal cannula. The cannula was then attached to the mechanical ventilator and ventilation initiated.

The first 2 mL of perfusate pumped through the lungs was discarded to waste (as it was high in blood) and the perfusate flow rate was increased to the experimental rate of 1 mL/min. The perfusate reservoir was topped up with warmed perfusate to a predetermined mark indicating 10 mL of perfusate was present in the system.

Lung perfusion and viability

Complete and effective perfusion of the lungs is easily confirmed in the IPML model; the lungs change from a reddish-pink colour to a brilliant white (figure 2.2.3) when properly perfused. Loss of lung viability is also easy to distinguish as area of the lung turn transparent due to pulmonary oedema. Visual observations in early experiments suggest that pulmonary oedema begins to form in the mouse lungs between 45 and 75 min after experimental setup.

This viability throughout the duration of the experiment (approximately 40 min after isolation) was confirmed by measuring the wet/dry weight ratio of the lungs. Lung tissue was removed from the IPML setup upon termination of the experiment and blotted dry and weighed in a 50 mL centrifuge tube (the centrifuge tube was previously weighed and its mass subtracted). The tissue was then frozen in liquid nitrogen and lyophilised (Thermo Systems, UK) for 48 hours under vacuum. The lung tissue was them reweighed to determine the dry weight of the lungs.

Viability of an hour is considerably shorter than that observed in the rat lung, a model which has shown to be viable for more than two hours (38). Due to the shorter viability of the mouse lungs the absorption experiments were run for 30 min instead of the 60 min our group has used previously for the IPRL.

Figure 2.2.3 Isolated perfused mouse lungs suspended in an artificial thorax by the tracheal cannula. Note the brilliant white colouration of the lungs indicating effective perfusion.

2.2.3 Dosing strategies

Following the isolation and perfusion of the lungs they were maintained in the artificial thorax for 5 min to ensure the perfusion and ventilation of the lungs was performed effectively. An initial perfusate sample (0.5 mL) was taken before dosing by extraction from the perfusate reservoir using a Gilson pipette. The perfusate volume was then restored by the addition of 0.5 mL fresh perfusate at 37 ^{o}C in to the reservoir. The lungs were then dosed via the tracheal cannula using the methods described in detail below.

pMDI and PE50 loop

Two MDI actuators (one HFA227 and the other HFA134A) with 25 µl valves were acquired. A short length of PE50 (length can be varied to exactly account for dose volume to be administered) was connected to the MDI actuators using a 25G needle. The tubing was used to hold the dose and replicate the dosing port used previously by our group for the IPRL model (71,72). With a 12 mm length of PE10 inserted into the end of the PE50, the dose does not drip out when held vertically.

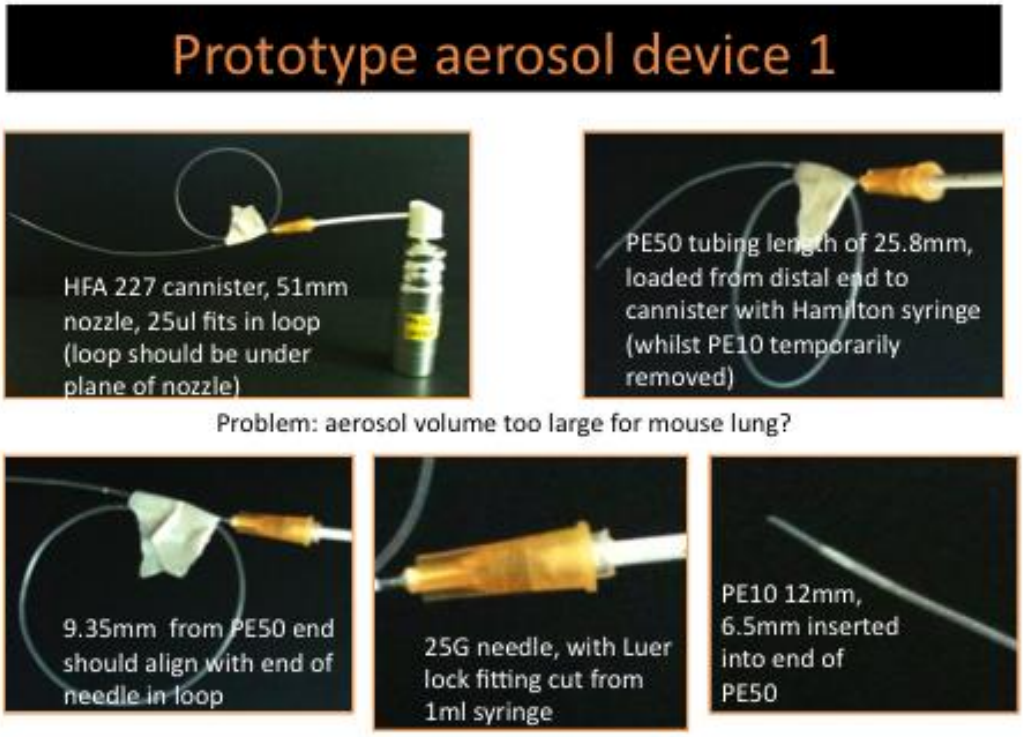

Figure 2.2.4 The setup of the prototype pMDI delivery device for the aerosol delivery of small volumes of dose (15-25 µL) to the IPML. The setup proved unsuitable for the model providing either too large an aerosol volume or too little force to expel the dose as an aerosol.

The volume of gas expelled by the device was measured by connecting to a gas tight syringe to the dose delivery end of the PE50 tubing and measuring the displacement. The aerosol generated with this device is excellent; however the volume of the aerosol is too large for delivery to mouse lungs. The total lung capacity for a mouse varies with the size of the animal but is in general 0.9-1.5 mL (51).

Attempts were made to reduce the aerosol volume of the device. For instance, a spacer was included in the system between the PE50 tube holding the dose and the MDI in order to increase the dead volume. However, this either created too little pressure to expel the dose as an aerosol or still gave too large a volume of expelled gas (although over a longer timescale).

Boring holes in the spacer tubing was attempted to divert fractions of the generated aerosol out of the system, to achieve a relevant volume of air passing through the dose tubing. This proved difficult to engineer, and the hole could easily be stretched by escaping gas and change size, making the system inherently inconsistent. Also, with small tubing such as the PE50, it is difficult to ensure an airtight connection. No IPML or deposition experiments were attempted using this device due engineering difficulties in producing an aerosol of adequate volume for dosing the IPML.

Hamilton syringe- pre-inflated lungs

There is a precedent in the literature for dosing the lungs via tracheal instillation of a liquid dose. To increase the penetration of the dose to the lower airways attempts were made to dose the lung whilst it was pre-inflated. Pre-inflation was achieved by utilising a 1 mL air filled syringe and a 3-way valve. This setup allowed the lungs to be inflated by the injection of air from the syringe, the valve was then closed and the upper valve opened. The upper valve was made air-tight by the inclusion of a suba-seal through which dose could be injected using a Hamilton syringe. Mechanical problems with the setup lead to the method being discarded before deposition experiments were possible.

Penn-Century Microsprayer

The Microsprayer (Model 1A-1C-M, Penn-Century, Philadelphia, USA) is a delivery device designed to create an air-free aerosol specifically for intratracheal delivery to mouse lungs. The atomiser generates an aerosol using the manual pressure from the syringe alone, i.e. it does not rely on compressed air or gas, indeed if any air is present in the system the dose is expelled as a liquid stream rather than an aerosol. Similarly, if the plunger is not depressed with sufficient force an aerosol is not produced.

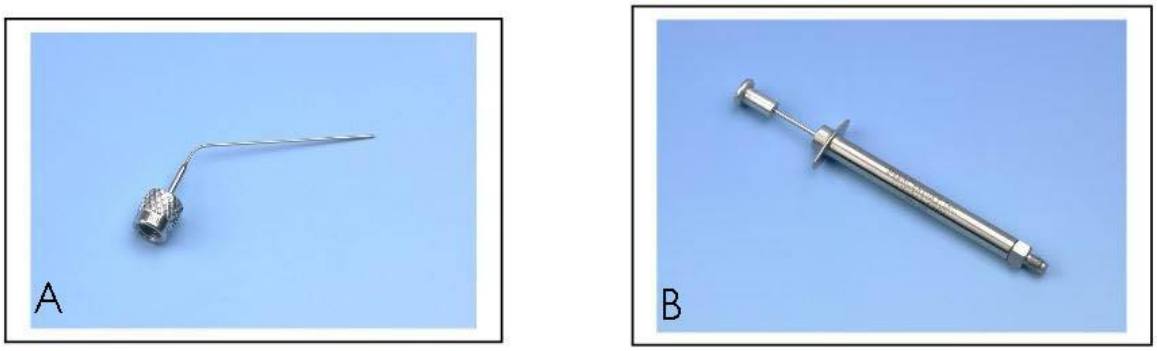

Figure 2.2.5 The two components of the Penn-Century Microsprayer, the Aerosolizer (A) and the high pressure syringe (B). Images from the online manual for the device.

Whilst the isolated lungs were equilibrated following surgery the dosing system was setup. The high pressure syringe was first purged of all air by the injection of water in to the base of the syringe using the provided Air Purge syringe and needle. The high pressure syringe was held vertically and the dose injected in to the base of the syringe as the needle was withdrawn. This was repeated until no more air bubbles were seen to escape the syringe and a meniscus of liquid was seen at the top of the syringe. The Aerosolizer was then attached and dose forced through by the syringe until all air had been removed. The 25 µL spacer was then attached to the plunger and the plunger depressed

until the spacer was tight to both the handle of the plunger and the syringe, the spacer was then removed. The dose remaining in the syringe and Aerosolizer at this point is the 25 µL dose for delivery.

The Aerosolizer is then inserted in to the trachea to a depth just short of the first bifurcation and the plunger rapidly depressed to deliver the aerosolised dose.

Hamilton syringe with an air bolus

Two variants of a simple dosing solution were also investigated utilising a Hamilton syringe. The first simply drew 25 µL of the dose solution in to a 50 µL Hamilton syringe, this was then instilled in to the trachea by rapid depression of the plunger. Care was needed to ensure the plunger did not depress under gravity prior to dosing. The second method was similar but differed in that prior to drawing the dose solution in to a 250 µL Hamilton, 250 µL of air were drawn in to the syringe. This was achieved by drawing the plunger back to the 250 µL marker and then inserting the tip of the needle into the dosing solution and drawing the plunger further until the dose reached the 15 µL marker. Dose was not drawn to the 25 µL marker to the expulsion of the dead volume of the syringe (10 µL) when the instillation was forced with the bolus of air. Again this was dosed by simply depressing the plunger rapidly whilst the needle was maintained just above the first bifurcation of the lungs.

Stoplock Hamilton syringe

The dosing methods above were improved by the inclusion of the gas-tight Stoplock Hamilton syringe (250 µL, 1700 series). The method utilised was similar to the air bolus method above except after the syringe was loaded the valve could be closed. The Hamilton could then be positioned without fear of the plunger depressing due to gravity. Dosing was achieved by depressing the plunger to the 25 µL marker and then opening the valve, this pressurised the air in a reproducible manner to ensure more consistent dosing.

Dosing volume studies

In order to ensure the same volume of the dose was being delivered to the lungs in a reproducible manner by each dosing device, the variability in dosing volume was investigated. The dosing systems were prepared as described above with solutions of ^{14}[C]-mannitol (5 nCi per 25 µL dose) in PBS. The dose was then injected in to a micro-centrifuge tube in the same manner as it would be delivered to the lungs. Following this, 1 mL of water was added to the tube and the concentration of the resulting solution was determined as per the methods described below. By calculating the amount of mannitol present following dosing it was possible to determine the percentage of the dose delivered

by each device, this was repeated ten times in order to gauge the variability inherent with each dosing system.

Deposition studies

In order to ensure the delivery systems were able to deliver the dose to the lungs in a reproducible manner studies were undertaken to investigate the lobar distribution of the dose following a particular dosing strategy. The IPML surgery was carried out and the lungs were dosed as described above with a dose of ^{14}[C]-mannitol (5 nCi per 25 µL dose) in PBS. Immediately following dosing, the lungs were removed from the artificial thorax and the lobes separated into micro-centrifuge tubes. To calculate the amount of dose present in each lobe 1 mL of PBS was added and the lobe homogenised using an Ultra-turrax t25 homogeniser for 2 minutes per sample. Concentrations of the radiolabelled dose were then determined by scintillation as described below.

In order to account for the differences in lobar mass, the percentage of dose present in each lobe was corrected according to the ratio of lobar mass to total lung mass. The mass of each lobe in relation to the mass of the complete animal and the lung mass was determined by sacrificing 5 animals and weighing each lobe, the lobar mass to animal and lung mass ratios are shown in table 2.2.1 below.

Lobe	Lobar mass to body mass ratio (%)	Lobar mass to lung mass ratio (%)
Left	0.175	34
Superior	0.101	19.61
Middle	0.064	12.43
Inferior	0.13	25.06
Postcaval	0.046	8.94

Table 2.2.1 The ratios of the masses of the lobes of the lung in comparison to the total body mass of the mice (average = 38.51 g) and the total mass of the lung (average = 0.516 g). Data is presented as an average from 5 animals and expressed as percentages.

2.2.4 Absorption studies

Absorption studies- paracellular probes

The variability in IPML experiments utilising different delivery systems was investigated. The surgery and dosing was performed as described above for the deposition studies. Following dosing the delivery device was left in the tracheal cannula for the first 5 minutes of the experiment. At set time points (0, 1, 2, 3, 4, 5, 10, 15, 20 and 30 minutes) 500 µL samples were removed from the perfusate reservoir and transferred to micro-centrifuge tubes. After the 5 minute time point was removed from the reservoir the tubing from the ventilator was reattached to the tracheal cannula and lung ventilation reinitiated.

At 30 minutes the experiment was terminated and the samples were centrifuged at 16,000 rcf to pellet any blood cells and other contaminants. The supernatant was then transferred to a clean micro-centrifuge tube and analysed as described below.

The concentration of the dose present in each sample was compared to the amount of drug initially deposited in the lung in order to ascertain the percentage of deposited dose absorbed during the time course of the experiment.

Chemical inhibition studies- P-gp substrates

In order for comparisons of the P-gp functionality present in the lungs of the IPML model developed here and the rat lung model used in the literature previously, investigations were conducted in to the effect of a chemical P-gp inhibitor upon the absorption of two P-gp substrates (rhodamine 123 and digoxin) from the mouse lungs. The chemical inhibitor used in these studies was GF120918 (GSK, Stevenage, UK), an inhibitor which has been widely used in the literature for the purpose of inhibiting P-gp functionality. A summary of previous uses of GF120918 in the literature is available in table 2.2.2 as well as the concentrations at which it was utilised in these studies. To investigate the effect of P-gp inhibition on lung absorption characteristics, the pulmonary absorption of both substrates was compared in the presence and absence of the inhbitor.

In the inhibitor experiments presented here, GF120918 was utilised at a concentration of 500 nM, a level at which previous work from our laboratory has shown efficient inhibition of pulmonary P-gp (71,72) and one which is consistent with the level used in previous literature, table 2.2.1. A 25 µL pre-dose of GF120918 (0.5 % DMSO) was delivered to the lungs via the delivery device 5 minutes prior to the experimental dose, the inhibitor was also present in the perfusate at 500 nM, this ensured even inhibition of P-gp functionality throughout the lung. The same concentration (i.e. 500

nM) was also present in the 25 µL substrate dose delivered to the lungs. In the non-inhibitor experiments the GF120918 was replaced by a 0.5 % DMSO solution and the dosing schedule was identical; a pre-dose was delivered 5 minutes prior to the substrate dose.

Other than the pre-dose the experiments were carried out in the same manner as those above for the absorption studies. Substrate doses were prepared as described in detail in chapter 4.2 with a 25 µL dose of 50 µM rhodamine 123 and 0.25 Ci (16 pM) of ^{3}[H]-digoxin. A marker of the paracellular barrier integrity was present in all doses in the form of 0.25 µCi of ^{14}[C]-mannitol (17 pM).

Mass Balance

Following experimentation both the dosing system and tracheal cannula were washed with 1 mL of water. The concentration of the dose present in the wash fluid of the syringe enabled calculations of the actual dose instilled in to the lungs during dosing by allowing the subtraction of dose remaining in the dosing device. Likewise, the concentration of the dose present in the wash fluid of the cannula allowed the portion of drug refluxed during dosing to be subtracted from the overall dose. Together this allowed an accurate estimation of the actual deposited dose in the lungs from which percentage dose absorbed was calculated.

Analytical Methods

Radiolabelled doses were analysed by liquid scintillation as described in detail in chapter 4.2. Briefly perfusate samples (200 µL) were added to translucent scintillation tubes. Scintillation cocktail was added (3 mL) and the samples were measured in a Tri-Carb scintillation counter on dual-counting mode. By comparing the DPM of the sample to that of the standard curve it is possible to calculate the concentration present in each sample.

In order to analyse the doses of the non-radiolabelled rhodamine 123 HPLC-MS/MS was utilised. This technique provided sufficient lower limits of quantification (LLQ) for the analysis of rhodamine 123 in the sample and is described fully in chapter 4.2.

Data Analysis

The absorption profiles of the two experimental groups were compared in a non-compartmental manner using area under the curve analysis (AUC). AUC analysis was performed on the % deposited dose absorbed at all time points using Graphpad Prism 5 software.

To determine the significance of the differences in absorption between the wild type mdr1a/b (+/+) and the knockout mdr1a/b (-/-) mice an independent T-test was performed upon the percentage of deposited dose absorbed at 30 min and the AUC analyses. In all cases significance was accepted as $p< 0.05$.

Correlations between datasets were performed using Microsoft Excel 2010 by calculating the Pearson's moment of correlation. Graphs representing these correlations were generated using Graphpad Prism 5 software.

GF120918 Concentration	Cell Type	Substrate	Inhibitor Solvent	Reference
2, 10, 20, 70 µM	Whole lung (rabbit)	rhodamine 123	DMSO	(73)
1 µM	HeLa cells	rhodamine 123	N/A	(74)
0.5-2 µM	Primary hepatocytes (rat)	rhodamine 123	N/A	(75)
100 nM	EMT6/P cells	rhodamine 123	N/A	(76)
100 mg/kg (5 mg/mouse)	Whole animal (mouse)	saquinavir	N/A	(77)
500 mg/kg (animal) 0.5 µM (*in vitro*)	Whole animal (rat) BBCEC Cells	rhodamine 123 morphine	HPMC: Tween 80: H_2O	(78)
25 mg/kg	Whole animal (mouse)	paclitaxel	WFI: Tween 80: H_2O	(79)
250 mg/kg (animal) 300-800 nM (*in vitro*)	Whole animal (mouse)	coelenterazine	HPMC: Tween 80: H_2O	(80)
0.001- 10 µM	MDCKII cells	calcein-AM colchicine digoxin prazosin vinblastine	DMSO	(81)
250 mg/kg (animal) 300 nM (*in vitro*)	Whole animal (rat) NIH3T cells	99mTc-sestamibi	HPMC: Tween 80: H_2O	(82)
0.5, 2, 10 µM	Caco-2 cells	fexofenadine	N/A	(83)
1 µM	MDCKII cells	saquinavir	DMSO	(84)
500 nM	Caco-2 cells	amprenavir	HPMC: Tween 80: H_2O	(85)

Table 2.2.1 A compilation of experiments from the literature which utilise GF120918 as a chemical inhibitor of P-gp and the concentrations at which it was used. Adapted from Francombe, 2011 (86). HPMC: Hydroxypropyl methylcellulose, DMSO: dimethyl sulfoxide

2.2 Results

2.2.1 IPML tissue viability

In order to assess the viability of the IPML following forced instillation and a 30 minute experiment the wet:dry weight ratio of the lungs at the end of the experimental timeframe and freshly isolated lungs was investigated (table 2.3.1). It was apparent that lungs with no visible oedema after the completion of a 30 minute absorption experiment showed no difference in wet:dry ratio to lungs freshly removed from the animal ($p = 0.63$). This indicates that the lung tissue is still viable at the end of an absorption experiment if no visible oedema is seen.

In experiments where damage has occurred to the lung tissue, either during surgery or dosing oedema can form rapidly (seen within the first 10 minutes of an experiment). On these occasions the wet:dry ratio of the lung mass is seen to be significantly increased from that of healthy lungs ($p = 0.024$). Taken together this shows that in the absence of damage caused to the lungs during surgery or dosing the IPML remains viable for the time course of the experiment. In examples where damage has occurred this is easily identified by visible oedema which correlates well with increases in lung wet:dry mass ratios providing a useful visual check for lung viability in each experiment.

	Lung wet mass (mg)	Lung dry mass (mg)	Wet:Dry Ratio
Freshly isolated lungs	256 ± 41	78 ± 14	3.32 ± 0.34
No visible oedema	280 ± 50	87 ± 13	3.23 ± 0.27
Visible oedema	522 ± 83	81 ± 18	6.89 ± 2.76

Table 2.3.1 The mass of lungs before and after lyophilisation was established for lungs immediately after removal from the animal, following a 30 minute absorption experiment where no oedema is visible at the end of the experiment and after a 30 minute absorption experiment where oedema is visible. As can be seen the wet:dry ratio of the lung mass is increased when oedema is present. Data are presented as mean ± S.D, n = 5.

2.2.2 Dosing validation

Reproducible dosing volumes

In the isolated perfused rat lung model (IPRL) already established within the group dosing is achieved using a modified pMDI device. The same was attempted with the mouse lungs using both an HFA227 and HFA134a pMDIs. These devices proved unsuitable for use with the mouse lungs due to the large volume of aerosol generated (approximately 5 ml for HFA227 and 7.2 ml for HFA134a). As the tidal volume of the mouse lungs is approximately 1 ml this aerosol volume would have caused unacceptable damage to the lung tissue. Attempts to reduce the volume generated by the addition of spacers or by boring holes in the tubing to release gas resulted in either too small a reduction in volume or insufficient aerosol generation for the experiments. It was therefore decided not to proceed with the pMDIs as a mechanism for dose delivery to the IPML.

Likewise, pre-inflation of the lungs was discarded as a possible dosing technique early on in the method development. In practice this setup proved unsuitable for the IPML experiments. There were problems encountered with the orientation of the valves, syringes and dosing needle during experimentation which resulted in inconsistent dosing. It also proved difficult to maintain the air-tight nature of the system; a prerequisite necessary to ensure the lungs remained inflated throughout dosing. Due to these issues this dosing setup was not used for any deposition experiments with the IPML.

Three remaining possible dosing strategies showed potential for dosing in to the IPML experiments, the Penn-Century Microsprayer, a Hamilton syringe with an air bolus and a Stoplock Hamilton also with a bolus of air. The air bolus in the syringes helped to inflate the lungs upon dosing in order to encourage dosing deeper in to the airways.

In order to evaluate the fraction of dose delivered from the three potential dosing devices a number of test doses of ^{3}[H]-mannitol were expelled from the dosing mechanisms into micro-centrifuge tubes and the volume of dose emitted was determined. It was observed that the Hamilton syringe which relied on operator pressure to expel the dose and air bolus was unacceptably variable with regards to the volume of dose delivered (table 2.3.2). This was greatly improved by the more consistent pressure applied by the Stoplock Hamilton. The valve in the Stoplock syringe allowed the plunger to be depressed to the same point (30 µL) with the valve closed and therefore the air bolus

was pressurised to the same extent with each dose. Sudden release of the valve then generated a more consistent dose. The Microsprayer also showed low variability in the volume of dose expelled from the device although it is of note that the device often blocked due to the presence of air bubbles which were introduced during loading (experiments with a blocked device were not included in the variability analysis). Due to the poor variability in the dosing with the 250 µL Hamilton no further experiments were conducted with this technique.

	Percentage of dose expelled (%)	Standard deviation (%)
Penn-Century Microsprayer	87.28	8.99
250 µL Hamilton with air bolus	91.26	23.15
250 µL Stoplock Hamilton with air bolus	96.09	1.15

Table 2.3.2 The reproducibility of the doses delivered from the three dosing devices selected for delivery to the IPML. Data shows the percentage of mannitol initially loaded in to the device which was measured in the delivered dose. N=10 for each device.

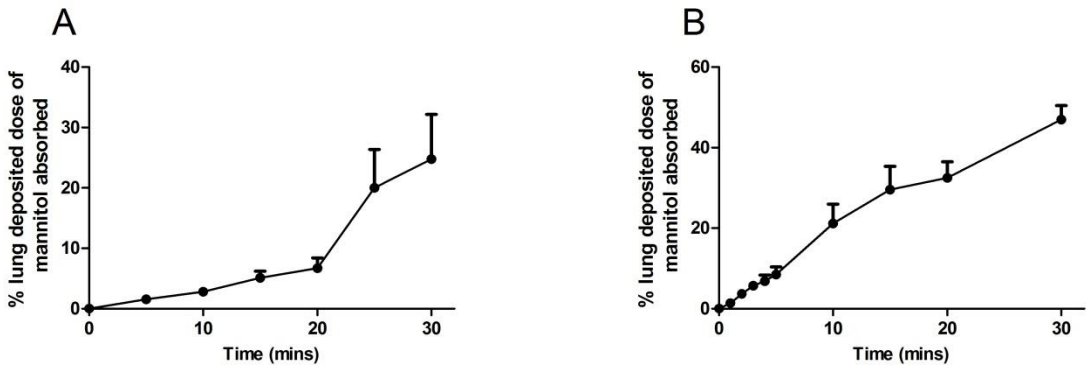

Figure 2.3.1 Absorption profiles of the paracellular probe mannitol from the IPML with the lungs of CD1 mice after deliver by [A] the Penn-Century Microsprayer and [B] the Stoplock Hamilton syringe with a 250 µL bolus of air. Data are presented as the mean ± S.D and n=6 for both experiments.

The increased variability off the Microsprayer in comparison to the Stoplock Hamilton, seen in the simple dose volume reproducibility experiments, was also observed in the absorption profiles of the paracellular probe mannitol from the IPML (figure 2.3.1). During these early absorption experiments with the Microsprayer it became apparent that the device blocking was an issue, in total 10 IPML experiments were performed with the Microsprayer and the results of 4 produced no meaningful

data and recorded no absorption of mannitol observed above background levels. This is due to the device failing to generate an aerosol if air bubbles are introduced during loading. Unfortunately this does not become apparent until after the experiment is analysed and if carried forward would result in unacceptable animal and resource use. Due to the increased reliability and dose volume reproducibility the Stoplock Hamilton was chosen as the preferred dosing device going forward.

Reproducible deposition

The deposition profile following dosing with the Stoplock Hamilton syringe was investigated to ensure the profile was consistent across experiments and dosing to the peripheral airways was achieved. The depth of dose penetration in to the lung was observed visually by dosing with a solution of Evans Blue. As can be seen in figure 2.3.2 the dye can be seen in the parenchyma of the lung lobes immediately after dosing, however, it is of note that concentrations of dye are also observed in the lower trachea and major bronchi of the lungs.

Figure 2.3.2 The distribution of Evan's Blue dye seen following forced instillation with a Stoplock Hamilton in the IPML.

The reproducibility of this dosing pattern was investigated by identifying the proportion of a ^{3}[H]-sucrose associated with each lobe immediately after dosing. Following the dosing of sucrose 80 % of the total deposited dose was recovered from the lung tissue, 2 % is lost in the trachea and tracheal cannula and the remaining 18 % is unaccounted for in the tissue processing and analysis. The largest proportion of the dose (27 %) was recovered from the left lobe of the lung; this lobe is also the largest with an average mass of 85 ± 15 mg. The remaining lobes also show proportions relative to their mass as can be seen in figure 2.3.3

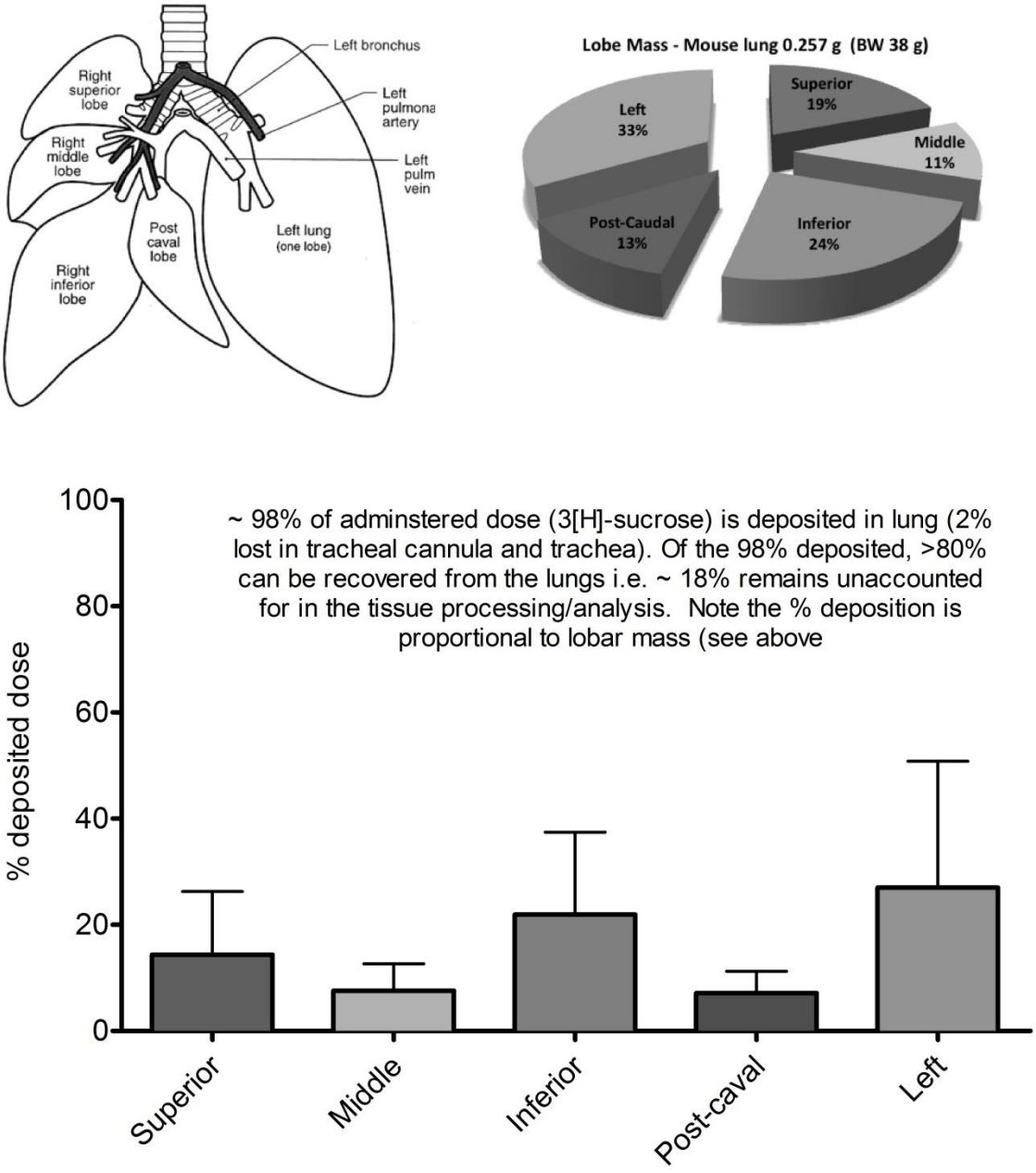

Figure 2.3.3 The deposition of sucrose in each lobe of the mouse lung following forced instillation with a Stoplock Hamilton and a bolus of air is both consistent and relative to lobar mass. Data is presented as a mean ± S.D, n=5. BW= body weight

2.3.2 IPML validation – permeability

Permeability to paracellular markers

The general permeability of the CD1 mouse lungs was assessed by investigating the absorption of two paracellular probes, mannitol and sodium fluorescein (F-Na). The probes were delivered to the

lung using the Stoplock Hamilton and the percentage of the dose present in the perfusate was measured at intervals to produce an absorption profile for each (figure 2.3.4). It was observed that the absorption of F-Na from the lung was extensive with 87% of the deposited dose absorbed within 30 minutes. The lungs of CD1 mice proved less restrictive to mannitol absorption with 40% of the deposited dose absorbed within 30 minutes.

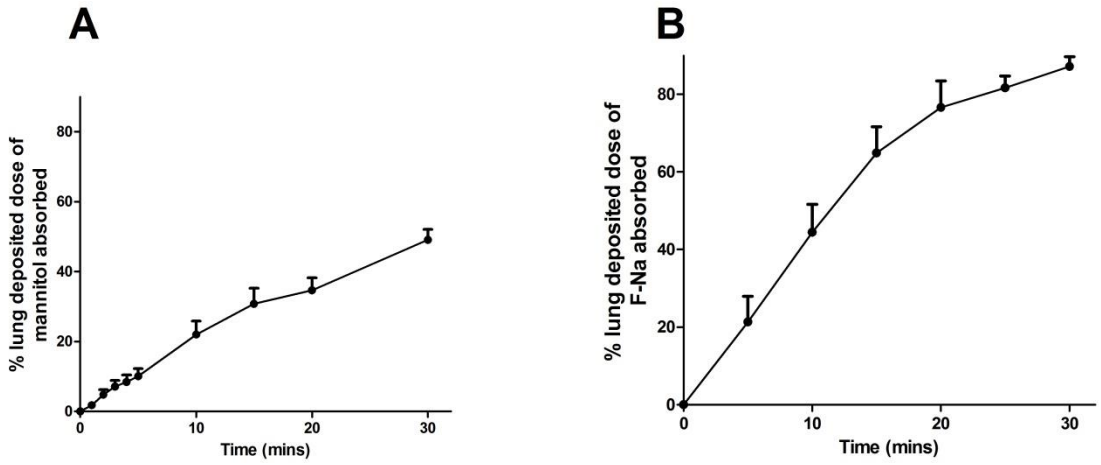

Figure 2.3.4 The permeability of the lungs of CD1 mice in the IPML to the paracellular probes [A] mannitol and [B] F-Na. Data are presented as mean ± S.D, n = 5-6.

Due to the restrictive nature of the pulmonary barrier to the absorption of mannitol a radiolabelled dose (^{3}[H]-mannitol) was included in all experiments of pulmonary absorption going forward. Experiments which showed mannitol absorption outside the range of 49 ± 9 % of deposited dose absorbed at 30 minutes (1 S.D from the mean) from the lungs of CD1 mice were discarded.

Permeability to P-gp substrates – effect of GF120918 on absorption

In order to evaluate the suitability of the IPML model for the investigation of the effect of P-gp upon the pulmonary absorption of its substrates transport studies were carried out with rhodamine 123 and digoxin. These two substrates are well characterised and have been utilised in studies of pulmonary P-gp in the literature previously.

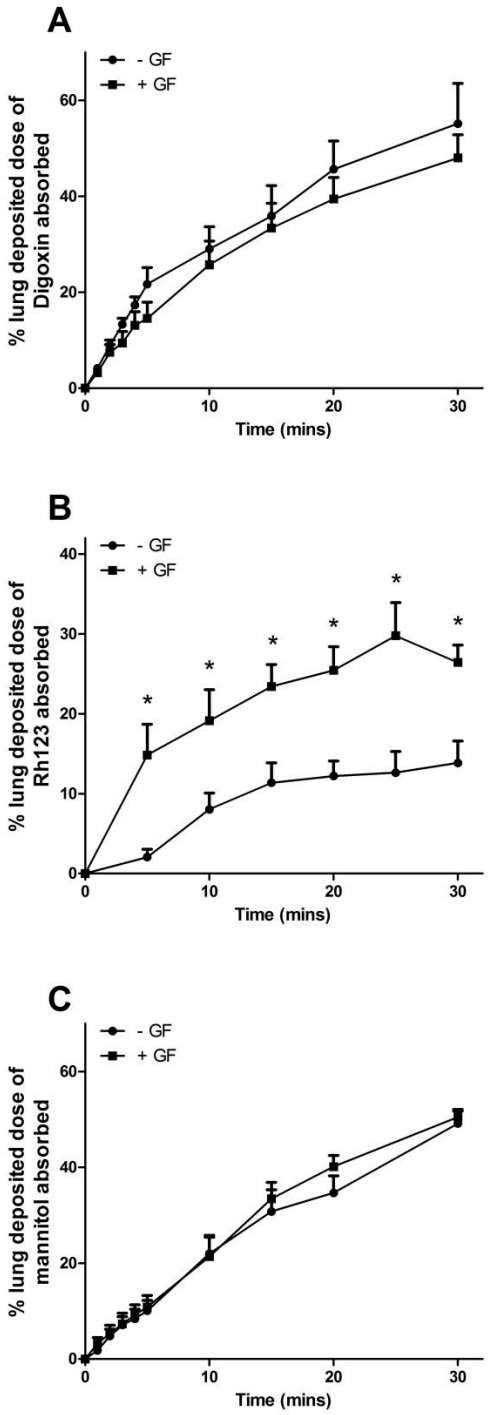

Figure 2.3.5 The absorption of the P-gp substrates [A] digoxin and [B] rhodamine 123 from the lungs of CD1 mice in the presence and absence of the selective P-gp inhibitor GF120918. Data is also shown for the paracellular control, [C] mannitol, included as a co-dose with the rhodamine 123 experiments showing no change in the general permeability of the lung with the addition of GF120918. Data are presented as mean ± S.D, n = 5-6, * indicates a significant difference ($p < 0.05$).

Results for rhodamine 123 show that in the absence of P-gp functionality the percentage of deposited dose absorbed is increased over the no-inhibitor controls (AUC = 250 ± 122 %.min^{-1}. in the

absence of GF120918 and 629 ± 181 %.min^{-1} in experiments where the inhibitor was present, p= 0.007). This suggests that P-gp functions to attenuate the absorption of rhodamine 123 from the mouse lungs in the absence of the inhibitor (figure 2.3.5 A).

The absorption profile of digoxin in the presence and absence of GF120918 does not suggest a role for P-gp in its absorption. There is no difference in the percentage of the dose absorbed or the AUC in the presence and absence of the inhibitor (AUC = 1051 ± 308 and 908 ± 219 %.min^{-1} respectively, p = 0.835) suggesting GF120918 does not enhance digoxin absorption (figure 2.3.5 B)

The difference seen in the absorption of rhodamine 123 in the presence of the inhibitor is not explained by a general increase in the permeability of the lungs for this group of experiments. The paracellular probe mannitol was included in all of the IPML experiments and its absorption shows no significant difference between any of the experimental groups (figure 2.3.5 C)

The difference observed in the absorption of rhodamine 123 in the presence of GF120918 verifies that the IPML model developed here is able to determine the effects of P-gp attenuation upon the absorption of its substrates. The lack of effect seen in the absorption of digoxin highlights the lack of effect seen in the absorption of this substrate previously in the literature.

2.4 DISCUSSION

There is an increased interest in the delivery of drugs to the systemic circulation via the pulmonary route in recent times; it is being investigated as a route of delivery with the potential for rapid and extensive uptake for drug candidates with poor oral bioavailability. It is therefore important to develop suitable models for the assessment of pulmonary pharmacokinetics for the examination of drug transport across the lung. The isolated perfused lung (IPL) models have been well utilised in this regard for a considerable time (87) and have been shown to be well suited for establishing the pharmacokinetics of a range of low molecular weight drugs (38). Previous studies, both in the literature and within our group, utilise an isolated perfused rat lung (IPRL) for drug absorption studies and here the Byron IPRL setup is adapted for use with mouse lungs. These studies in the IPRL are summarised in the introduction to this chapter.

Utilising the lungs of mice rather than rats will allow us to investigate the role of P-gp on lung absorption by the development of P-gp deficient mice. Due to the reduced breeding time and current availability of P-gp deficient mice they are a far more suited species to genetic knockout applications than rats. To this end the chapter presented here focuses on the development and validation of the *ex vivo* isolated perfused mouse lung (IPML) model by the adaptation of an IPRL setup originally proposed by Byron and Niven (32). The aim of this model is to sufficiently represent the effect of the complex structure of the lungs upon the absorption by maintaining *in vivo* structures whilst allowing the control of experimental factors and eliminating the confounding effects of systemic ADME seen in *in vivo* models.

Validation of the dosing technique

It has been reported previously in the literature that tissue viability in IPL experiments is enhanced by the addition of albumin to the perfusate (88), it was demonstrated that when albumin was added to the perfusate an approximately 5-fold increase in the duration of lung viability was observed (before pulmonary oedema was witnessed) (89). In line with previous studies both in the literature and within our group using the IPRL 4 % bovine serum albumin (BSA) was added to the perfusate buffer in order to increase lung viability.

During the development of the IPML model attempts were made to utilise a similar dosing mechanism to that used previously in IPRL experiments within the laboratory, i.e. a pMDI (71,72).

Unfortunately, this forced instillation technique proved unsuitable for the mouse lung as the volume of the aerosol was too large and would result in unacceptable damage to the lungs. Attempts to reduce the volume of the pMDI aerosol were unsuccessful; the reduction in aerosol volume was either too small or resulted in an insufficient force to generate an aerosol.

Investigations were conducted in to the suitability of a Penn-Century Microsprayer for delivery to the IPML. Despite the device generating a good aerosol when loaded correctly, it proved unreliable as a dosing technique. Experiments in which air was introduced in to the Microsprayer resulted in erratic dosing as the device became blocked and failed to deliver the dose as an aerosol. The failure of the dosing device was not evident until the analysis of the experiment and therefore resulted in the loss of animals and resources. The aerosol generated by the device is not delivered "forced" with a bolus of air/expellant as in the pMDI and there was subsequently no inflation of the lungs during delivery. This is expected to result in a less extensive delivery to the lower lungs.

In order to most closely replicate the forced instillation techniques of the pMDI delivery in the IPRL a bolus of air is needed to inflate the lungs during delivery. This was achieved by using a Stoplock Hamilton syringe, the device allowed a 250 µL bolus of air to be pressurised in a reproducible manner and delivered to the lungs rapidly by opening the valves. This delivery mechanism resulted in the most reproducible dosing volumes of all the devices investigated, with a reproducible fraction of the dose delivered by the device and a reproducible deposition within the lung tissue. The lung deposition of the dose delivered via this technique was investigated visually by dosing Evan's Blue dye and the fraction of dose present in each lobe was established by dosing radiolabelled sucrose. These investigations show that the dosing technique allows efficient dosing to the lung parenchyma with blue staining seen in the lung periphery immediately following dosing of Evan's Blue. It is of note that a concentration of dye was evident in the bronchi and trachea indicating that a portion of the dose does not reach the periphery of the lung. The proportion of the dose which was deposited in the trachea was shown to be consistent between experiments at roughly 2 %. The deposition profile in the lung following dosing with the Stoplock Hamilton was shown to be even and reproducible across multiple experiments. The percentage of the deposited dose recovered from each lobe of the lung showed an acceptable variability and was in relation to the lobar mass, i.e. the largest percentage of the dose was consistently present in the largest lobe (left lobe). The reproducibility of the dosing to the lobes of the lungs witnessed with this dosing device is an improvement on similar results observed with a pMDI in a previous IPRL (68) where consistent deposition to the trachea was observed but the delivery to the lobes showed a large variability between experiments. Preliminary investigations in to the absorption of a paracellular probe

(mannitol) confirmed the reproducibility of this dosing strategy with a consistent absorption profile seen across all experiments. It was determined that the Stoplock Hamilton provided efficient reproducible dosing to the lung in a manner which offers concurrent reproducible inflation, the device was therefore chosen as an acceptable method going forward.

Validation of tissue viability

Following the forced instillation of dose by the Stoplock Hamilton it was important to investigate the duration for which the lung preparation remained viable. During experiments the lungs were constantly observed for signs of pulmonary oedema formation, when present oedema causes the chalky white perfused tissue to become transparent and pink. In addition to this the wet:dry mass of the lungs was determined both before and after the experiment, a technique utilised extensively in the literature to determine tissue viability (90–92). The assumption with this technique is that during the formation of oedema the water content of the lungs will be increased and therefore an increase in the wet:dry ratio will be observed. By comparing the post-experiment ratio to that of healthy lungs the viability of the IPML during the time frame of the experiments can be determined.

The wet:dry mass ratios were determined in three groups, lungs freshly removed from CD1 mice, lungs with no visual oedema at the termination of an absorption experiment and lungs from aborted experiments in which pulmonary oedema was visually apparent. In all cases where no pulmonary oedema was observed following an absorption experiment there was no significant difference between the wet:dry mass ratio and that of the freshly removed lungs. Conversely, lungs with visible oedema showed a significant two-fold increase in the ratios when compared to healthy lungs. The wet:dry ratios reported in the viable lungs post-IPML are in agreement with those reported in the literature where a ratio under four is considered to represent viable lungs (91). These viability studies show that experiments which show no visible sign of oedema during the absorption timeframe are viable and visual formation of pulmonary oedema is a good indicator of tissue viability. It is worth noting that when oedema formation was witnessed it tended to occur soon after the lungs were isolated, it is assumed that oedema formation in this IPML setup is therefore due to accidental damage caused during surgery or dosing and when the technique is performed correctly the lungs remain viable for the duration of the experiments.

Permeability to paracellular probes

In order to validate the IPML model the absorption profile of two paracellular probes, mannitol and sodium fluorescein (F-Na), was investigated in the CD1 mice. The absorption of both was shown to be more extensive than that previously seen in the IPRL (71) with the absorption of F-Na being almost complete at 30 minutes (87 % deposited dose absorbed), in the rat lungs a similar extent of absorption was observed at 60 minutes. The pulmonary barrier was shown to be more restrictive to the absorption of mannitol although the absorption was more extensive than that observed in the rat model with an approximately two-fold increase in the percentage of deposited dose absorbed at 30 minutes in the mouse model. The increased absorption of F-Na in comparison to mannitol is consistent with previous literature and provides evidence to support the validity of the IPML. This data suggests that the mouse lungs may prove generally more permeable than those of the rat model, in particular with regards to the paracellular pathway. The absorption profile of mannitol in the lung lends itself well to a use as a control in experiments going forward. In all absorption experiments a radiolabelled mannitol dose was included and if the extent of absorption of this paracellular control was outside of one standard deviation of the mean (49 ± 9% for CD1 mice) the experiment was considered invalid.

Permeability to P-gp substrates – chemical inhibition

Previous studies in the literature have investigated the role of P-gp in the pulmonary absorption of rhodamine 123 and digoxin from an IPRL (22,24). The results of these two studies appear discordant with a role for P-gp identified in the pulmonary absorption of rhodamine 123 and digoxin absorption unaffected by P-gp attenuation. The two studies are discussed in more detail in chapter 4. Both of these studies utilise chemical inhibition of P-gp function to ascertain its role in the absorption of substrates from the lung and therefore similar experiments were conducted with the IPML using GF120918 as a selective and potent inhibitor of P-gp functionality.

Results from the absorption of the two substrates from the IPML are in agreement with the previous literature studies. The absorption of rhodamine 123 was significantly enhanced in the presence of GF120918 suggesting pulmonary P-gp functions to attenuate rhodamine 123 absorption. Conversely the absorption of digoxin showed no significant difference in the presence or absence of the inhibitor suggesting P-gp does not play a role in its absorption.

The difference seen in the absorption of rhodamine 123 in the presence of GF120918 is unlikely to be due to a general increase in permeability in this group of animals. It was shown that the absorption of the paracellular probe mannitol, included as a control in all experiments, showed no difference in absorption between the two groups. Combined with the lack of difference in the absorption of digoxin this provides strong evidence that GF120918 does not increase the general permeability of the lungs. It is possible that the discrepancy seen in the absorption of the two substrates is due to a non-P-gp related compound specific effect of GF120918; for example the displacement of rhodamine 123 from intraluminal binding sites. However, competition for binding sites would seem unlikely as there are significant chemical differences between rhodamine 123 (a lipophilic amine and GF120918 (a highly lipophilic carboxamide). In order to completely address the issue of the chemical inhibitor the IPML model will be further developed by the inclusion of P-gp deficient mice. These genetic knockouts will remove the need for the inclusion of a chemical inhibitor to assess P-gp function.

Overall, the principle aim of this chapter was the development and validation of the IPML model. The results presented in this chapter confirm the viability and dosing strategies utilised in the IPML are sufficient to provide a model which is well suited for the investigation of pulmonary drug absorption. The use of a mouse model instead of the more conventional rat model will allow the inclusion of genetic knockout mice for the investigation of P-gp functionality in the lung without the confounding effects on a chemical inhibitor.

Chapter 3

Generation and validation of mdr1a/b (-/-) mice

3.1 Introduction

In the previous chapter an IPML model was developed and validated for the investigation of the pulmonary absorption of low molecular weight drugs. One aim of this thesis is the application of this technique to determine the role of P-gp in the pulmonary absorption of its substrates. As discussed in the previous chapter, previous literature studies investigating the role of P-gp in the pulmonary absorption of its substrates have utilised chemical inhibition of P-gp functionality in an IPRL model. In order to avoid the confounding effects of possible non-P-gp mediated functionality of the chemical inhibitors a genetic knockout model is required.

3.1.1 Literature pharmacokinetic (PK) studies utilising P-gp deficient mice

The use of genetic knockout mice is well established in the study of the role of P-gp in the pharmacokinetics of a range of molecules. In rodents there are two P-gp genes expressed, *mdr1a* and *mdr1b*. Of these *mdr1a* is more abundant at all the barriers of interest for drug transport including the lung (5) although the lung does possess relatively higher levels of *mdr1b* in comparison to other barriers. Literature studies with P-gp deficient mice have shown altered pharmacokinetics of a range of P-gp substrates at multiple barriers using the single knockout mdr1a (-/-) mice and the double knockout mdr1a/b (-/-) mice.

The lack of mdr1a/b expression in the P-gp deficient mice has been shown by a range of histological, serochemical and immunological parameters to have no significant biological effect (93). Mice deficient in both mdr1a and mdr1b were shown to display completely normal development, viability and fertility up to 1 year of age. As well as witnessing no abnormalities under macro and microscopic analyses of all the major organs a range of serum and haematological techniques were used to assess the biological effect of P-gp knockout. The study performed a range of analyses such as measurements of the serum levels of bilirubin, alkaline phosphatase, aspartate aminotransferase, alanine aminotransferase, lactate dehydrogenase, creatinine, urea, sodium, potassium, chlorine, calcium, phosphate, total protein and albumin in both sexes. Measurements of the haemoglobin level, haematocrit, erythrocyte, leukocyte and thrombocyte counts were also determined in blood. In all cases the results of the analyses concluded that the biological significance of P-gp knockout was negligible and the only differences identified between the knockout and wild type mice was in their pharmacokinetics and dynamics.

Since the initial use of the P-gp knockout mice in the mid 1990's they have been widely utilised to study the pharmacokinetics of a range of drugs at many barriers. One of the most well studied of

these is the blood-brain barrier. An early observation on the effect of P-gp at the blood brain barrier was an observation of a drastically increased (100-fold) sensitivity of a sub-population of CF-1 mice to ivermectin and avermectin given to the mice as anti-parasitic drugs (94,95). The spontaneous mdr1a deficient sub-population of CF-1 mice has since been isolated and used in a range of studies investigating the impact of P-gp upon drug pharmacokinetics. Increased brain penetration of ivermectin in P-gp deficient mice had been observed earlier in mdr1a (-/-) knockouts by the group of Schinkel (96), they had shown that in the absence of mdr1a functionality sensitivity to both vinblastine and ivermectin was increased due to increased brain penetration in mdr1a deficient mice. An early example of the use of the spontaneous mdr1a deletion in the CF-1 mice investigated the systemic effect of P-gp in these mice on the absorption, metabolism and disposition of ivermectin and cyclosporine-A (97). The study showed that in the absence of P-gp the concentration of both substrates was greatly increased in the brain of the mice, explaining the increased sensitivity of these mice to ivermectin toxicity. An effect of P-gp in the intestine was also shown as following oral dosing blood levels of the drug were higher in the P-gp deficient animals. Interestingly, they observed no difference in the concentrations of the substrates in the liver and a survey of drug-metabolising enzymes in the livers of both deficient and wild type mice suggested there was no difference in the hepatic metabolic activity of either group.

Since these early investigations, there are multiple examples of the spontaneous mdr1a (-/-) CF-1 mice and the double knockout mdr1a/b (-/-) generated by Schinkel being utilised for pharmacokinetic analysis. In the late 1990's, the double knockout mice were used to both investigate the role of P-gp in the pharmacokinetics of digoxin and the ability of a novel chemical inhibitor (SDZ PSC833) to inhibit P-gp activity. The brain penetration of digoxin was markedly increased in the knockout mice suggesting in the wild type animals brain penetration was attenuated by P-gp, the addition of the inhibitor to the wild-type mice showed a similar increase in brain penetration although not to the same extent. Interestingly when the inhibitor was dosed to the knockout mice the hepatobiliary excretion of digoxin was markedly decreased (this was also seen in the wild type animals) this suggests that the inhibitor is not selective for P-gp activity and was causing the inhibition of other drug transporters as well. The study illustrates the power of the P-gp knockout mice in pharmacokinetic studies with P-gp substrates.

The use of the knockout mice has helped to confirm the role of P-gp as a major barrier to blood-brain barrier penetration. Multiple studies have confirmed an increase in absorption of a P-gp substrate across the blood-brain barrier in P-gp knockout mice. A comparison of the blood-brain barrier permeation of a group of substrates (loperamide, domperidone and ondansetron) and non-

substrates (haloperidol, clozapine and flunitrazepam) showed increased brain penetration of the substrates in the knockout mice whilst the non-substrates showed no difference in their absorption over wild type animals. The study highlighted the need to assess P-gp functionality as penetration of loperamide in to the brain caused potent opiate-like activity in the knockout mice, this must be a consideration when dosing multiple drugs as drug-drug interactions could lead to increased concentrations of P-gp substrates in the brain. Multiple studies confirm this increase in brain accumulation in the absence of P-gp functionality across a broad range of drugs including but not limited to vinblastine (98), salinomycin (99), saquinavir and ritonavir (100), digoxin (101), rhodamine 123 (102) and asimadoline (103).

The use of the knockout mouse has not been limited to studies of brain penetration; it has highlighted a role for P-glycoprotein in the pharmacokinetics of drugs at multiple barriers as well as enhancing elimination and reducing toxicity in some cases. For example, a recent study of the pharmacokinetics of salinomycin, a coccidiostatic antibiotic commonly fed to livestock, implicated P-gp in both the oral bioavailability and toxicity of the drug (99). Markedly increased plasma levels of salinomycin were recorded in P-gp deficient mice following oral dosing which was coupled with a decrease in plasma clearance. Coupled with an increase in brain penetration it was shown that the animals deficient in P-gp had an increased sensitivity to the drug.

The mdr1a/b (-/-) mice also show an increase in accumulation of P-gp substrates in cardiac tissue (104). Following IV dosing the retention of doxorubicin was shown to be prolonged in the cardiac tissue (as well as the brain and liver) of P-gp deficient mice. This highlights the risk that decreased P-gp functionality may increase the risk of cardiac toxicity (as well as the well characterised CNS toxicity) for drugs which are substrates of the transporter.

The effect of P-gp expression upon oral bioavailability, observed in a number of the studies discussed above, is also well characterised in the knockout mice models. Indeed the plasma concentration profile of paclitaxel following oral dosing has been shown to be six-fold higher in P-gp deficient mice (105).

The spontaneous mdr1a deficient CF-1 mice have also been utilised to investigate the role of pulmonary P-gp upon the pulmonary absorption of digoxin (23). This is currently the only example of the use of P-gp knockout mice for the study of pulmonary pharmacokinetics. The absorption of digoxin from the knockout mice showed no evidence of a role for P-gp in the pulmonary absorption of digoxin. This is despite the P-gp deficient mice showing increased brain penetration and oral bioavailability of digoxin in previous studies (101). It is possible that due to the relatively high levels

of mdr1b present in the lungs in comparison to the intestine that mdr1b efflux masked the effect of mdr1a. However, this would seem unlikely as the lack of effect of pulmonary P-gp upon the lung absorption of digoxin closely mirrors similar experiments utilising chemical inhibition (24,71)

Whilst the pharmacokinetic studies discussed here are by no means an exhaustive list they represent the large body of literature that has been generated using P-gp deficient mice. The studies highlight the importance of the genetic knockouts in establishing a role for P-gp in the oral bioavailability, brain penetration, organ accumulation, clearance and toxicity of a wide range of drugs. As the knockouts show no obvious biological changes other than P-gp expression they represent a powerful model for the investigation of P-gp mediated effects. The inclusion of the lungs of P-gp knockout mice in the IPML will allow the investigation of the role for P-gp in the absorption of substrates from the lung without the confounding effects of chemical inhibition. The lack of an effect of pulmonary P-gp seen in the absorption of digoxin with these mice should not be interpreted to reduce their usefulness for the study of lung absorption, indeed similar effects have been seen previously with digoxin utilising chemical inhibition.

3.1.2 Experimental objectives

The aim of this chapter is to establish a breeding colony of mdr1a/b (-/-) double knockout mice and their relevant wild type counterparts. The application of this genetic knockout to the investigation of the role of pulmonary P-gp will be validated by the assessment of the absorption of both paracellular markers and a small subset of P-gp substrates (digoxin and rhodamine 123). The absorption from both the double knockout mice and the wild type mice will be compared to the previous absorption experiments carried out with chemical inhibition in CD1 mice.

3.2 Materials and Methods

3.2.1 Establishing a mdr1a/b (-/-) and mdr1a/b (+/+) breeding colony

Animals

FVB/B6 hybrid mice were bred in-house (Cardiff University, UK) and male CD1 mice were purchased from Harlan (UK). All animals were kept under a 12 hour light-dark cycle at 21 ^{o}C and 45-60 % humidity in conventional housing. The animals had access to food and water *ad libitum*. At the point of experimentation all mice weighed 30 ± 3 g. All animal studies were ethically reviewed and carried out as Schedule 1 in accordance with the Animals (Scientific Procedures) Act 1986 and the GSK Policy on the Care, Welfare and Treatment of Animals.

Breeding

A pair of male double knockout mdr1a/b (-/-) FVB mice was purchased from Taconic (Hudson, NY, USA). These knockout mice are from the same background as the double knockout mdr1a/b (-/-) used by the group of Schinkel in the 1990's. The disruption of the mdr1b gene had been achieved by the insertion of a neomycin resistance cassette between the adjacent NcoI fragments containing exons 3, 4 and 5. Secondary targeting of the mdr1a gene was achieved using the insertion of a hygromycin resistance cassette into an XbaI site of the mdr1a gene, as shown in figure 3.2.1 (96,106).

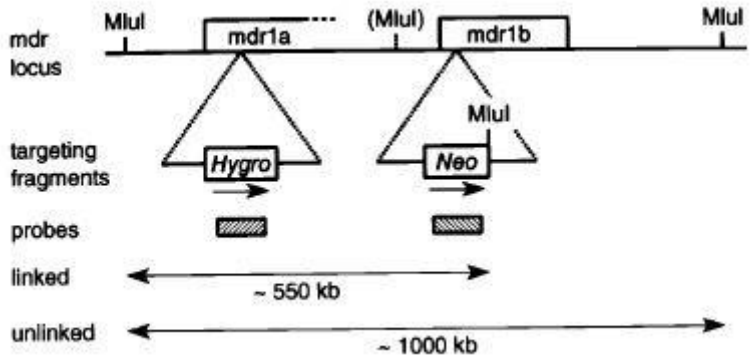

Figure 3.2.1 A diagram showing the disruption of mdr1a and mdr1b in the knockout mice by the interruption of the genome with antibiotic resistance cassettes. Following disruption the genes no longer express functional P-gp. Adapted from Schinkel, 1997 (93).

In accordance with the licencing agreement for their use the male FVB double knockouts were cross-bred in-house (Cardiff University, UK) with wild type B6 females to produce F_1 heterozygous FVB/B6 hybrids. The F_1 hybrids were cross-bred and the F_2 generation were genotyped and bred to form a stable colony of mdr1a/b (-/-) double knockouts and mdr1a/b (+/+) wild types. Mice in generations F_2-F_5 were all genotyped. At F_2 no mice exhibited homozygous double knockout, mdr1a (-/-), mdr1b (+/-) mice were bred with mdr1a (+/-), mdr1b (-/-) mice in generations F_3-F_4 until sufficient numbers of mdr1a/b (-/-) double knockouts were obtained. Concurrently, homozygous wildtype mice were also bred to produce a stable wild type strain as a counterpart to the knockouts. Following the establishment of both breeding colonies one male animal from each litter going forward was genotyped to ensure the genotype was stable and non-breeding females were culled. All females chosen for breeding purposes were genotyped before breeding.

Genotyping

Materials

DNeasyMini Kit (Qiagen, Hilden, Germany)
HotStarTaq DNA Polymerase kit (Qiagen, Hilden, Germany)
Nuclease free water (Ambion, Austin, Texas)
1 kb+ DNA ladder (New England Biolabs, Hitchin, Herts, UK).

DNA Extraction

In order to genotype the animals tail clippings were used as a tissue source and the DNA extracted using the DNeasy Mini Kit. The protocol was performed as per the manufacturer's instructions for tail clipping. In summary, tail clippings were digested overnight in ligase and the resultant supernatant was passed through a filter to which DNA adhered. Several wash steps were performed with solutions containing 40 % ethanol to prevent the solubilisation and subsequent elution of DNA. Elution was then achieved using 100 µL of nuclease free water and the resultant DNA solution was stored at 4 ^{o}C.

Primer Sequences

The primer sequences used for the amplification of mdr1a and mdr1b can be seen in table 3.2.1. The primers for amplification of mdr1a were provided by Taconic. The binding site for MDR1AS2 is downstream of the insertion site of the hygromycin cassette and the primer is therefore common to both knockout and wild type genomes. The MDR1AW2 primer binds to a region of DNA extracted when during the insertion of the hygromycin cassette and therefore amplifies a 269bp segment of DNA only in the wild type genome. The MDR1AKO2 primer binds within the hygromycin cassette and therefore amplifies a segment of 461bp only in the knockout genomes.

Gene	Primer	Sequence	Melting Temperature (^{o}C)	Wild type product size (bp)	Knockout product size (bp)
mdr1a	MDR1AS2	5-CTC CTC CAA GGT GCA TAG ACC-3	55	269	461
	MDR1AW2	5-CCC AGC TCT TCA TCT AAC TAC CCT G-3			
	MDR1AKO2	5-CTT CCC AGC CTC TGA GCC CAG-3			
mdr1b	HSAS6+	5-CAA GCT GTG CAT GAT TCT GGG AAC-3	60	540	453
	HSAS3+	5-GGA GAG AAA CCA TGT CCT TCC AG-3			
	HS5NEO+	5-TGT CAA GAC CGA CCT GTC CGG TG-3			
	HS3NEO2+	5-CAT GAT ATT CGG CAA GCA GGC ATC G-3			

Table 3.2.1 The primers and their respective product sizes used for the genotyping of the mdr1a/b (-/-) mice. All reactions were performed as a multiplex PCR at the stated melting temperature.

Primers for the amplification of mdr1b were designed in house using a murine mdr1b sequence (GenBank ID 18669) and the sequence of the neomycin cassette inserted into the gene during the generation of the knockout mice. Sequences were identified within either the neomycin cassette (for knockout amplification) or the excluded wild type DNA sequence (for wild type amplification) which possessed approximately 50:50 GC:AT ratios. The HSAS6+/3+ primer pair amplified a 540bp segment of the mdr1b gene only present in the wildtype genome. The binding sites for these primers lay within the restriction sites used for the insertion of the neomycin cassette and therefore the binding sites were absent in the knockout genome. The knockout genome was identified by amplifying a 453bp segment from within the neomycin cassette which is present only in the knockout mice. The primers were checked for the possibility of hairpin formation, primer dimerization using the online

tool OligoCalc (107) and designed to include a G/C clamp (for efficient binding primers were designed to begin and terminate with a G or C). Melting temperatures (T_m) were also calculated using the OligoCalc online software with primers designed to possess a T_m of 55-60 ^oC.

PCR amplification

Amplification of the target sequences was achieved by PCR using the HotStarTaq DNA polymerase kit (Qiagen). The reaction was performed by adding:

- 2.5 µL 10x PCR buffer (final concentration of $MgCl_2$ = 1.5 mM)
- 0.5 µL 10 mM dNTPs
- 0.125 µL DNA polymerase
- 0.5 µL primer stock
- Nuclease free water to a final volume of 25 µL

Prior to cycling the reaction was maintained at 95 ^oC for 15 minutes, a necessary step for the activation of HotStarTaq. Following the activation period the amplification was performed with thermal cycling (35 cycles of 94 ^oC for 1 minute, 55 ^oC or 60 ^oC (primer T_m) for 1 minute, 72 ^oC for 1 minute) after cycling the mixture was maintained for a final extension period at 72 ^oC for 10 minutes.

Following PCR the DNA fragments were separated by agarose gel electrophoresis (1.25 % agarose) at 80 V (6.5 V/cm) for 45 minutes. During the formation of the agarose gel 3 drops of ethidium bromide were added to the molten agarose prior to pouring. Ethidium bromide interacts with DNA and emits fluorescence under UV light allowing the visualisation of the DNA bands. A 1kb+ DNA ladder was loaded in to the wells immediately prior and after the PCR products in order to allow the determination of the size of the fragments present in each band.

3.2.2 Validation of the knockouts – absorption experiments

In order to validate the use of the genetic knockout mice lungs for investigating the role of P-gp in pulmonary pharmacokinetics, absorption experiments were conducted with two P-gp substrates (digoxin and rhodamine 123) and the paracellular marker mannitol. The absorption of the molecules was determined from both the wild type mdr1a/b (+/+) and the knockout mdr1a/b (-/-) lungs using the IPML methodology described in detail in chapter 2. Briefly, the 25 µL dose (as described in chapter 4) was administered to the IPML by forced instillation with a bolus of air utilising a Stoplock Hamilton. All of the doses were administered as solutions in PBS (pH 7.4) containing 0.1 % DMSO as

detailed in chapter 4. Following dosing, the concentration of the molecule present in the perfusate at a range of time points (0, 5, 10, 15, 20 and 30 minutes) was determined and the percentage of deposited dose absorbed was calculated. The absorption from the knockout and wild type mice could then be compared in order to draw conclusions about the role of P-gp in the pulmonary absorption of the molecule.

Analysis of rhodamine 123

The perfusate samples from the experiments with rhodamine 123 were analysed by HPLC-MS/MS as described in detail in chapter 4. Briefly, the protein was removed from the samples by precipitation with acetonitrile (60 %) and centrifugation at 16,000 rcf for 10 minutes. Following protein precipitation 10 µL of the sample was injected on to a C18 HPLC column for chromatic separation. The eluted rhodamine 123 and mobile phase were then passed through the mass spectrometer for analysis by MS/MS. Comparison of the peak areas of the samples to those of a standard curve allows the calculation of the concentration present in each sample.

Analysis of mannitol and digoxin

In the absorption experiments detailed in this chapter, mannitol and digoxin were delivered as radiolabelled doses (i.e. ^{14}[C]-mannitol and ^{3}[H]-digoxin). These radiolabelled doses were analysed by liquid scintillation. Perfusate samples (200 µL) were added to translucent scintillation tubes. Scintillation cocktail was added (3 mL) and the samples were measured in a Tri-Carb scintillation counter on dual-counting mode. In the presence of decay the scintillation cocktail emits fluorescence which is detected by the counter, in dual counting mode the fluorescence from both ^{3}[H] and ^{14}[C] decay are measured simultaneously and an output of counts per minute (CPM) is produced. This is converted to decompositions per minute and gives a measure of the total amount of each radiolabel present in the sample. By comparing the DPM of the sample to that of the dose it is possible to calculate the % of dose absorbed to the perfusate at each time point.

Data Analysis

The absorption profiles of the two experimental groups were compared in a non-compartmental manner using area under the curve analysis (AUC). AUC analysis was performed on the % deposited

dose absorbed at all time points using Graphpad Prism 5 software and presented as the mean AUC ± S.D.

To determine the significance of any differences in absorption between the wild type mdr1a/b (+/+) and the knockout mdr1a/b (-/-) mice an independent T-test was performed upon the percentage of deposited dose absorbed at 30 min and the AUC analyses. In all cases significance was accepted as $p< 0.05$.

3.3 Results

3.3.1 Evidence of genetic knockout

In order to establish a breeding colony of mdr1a/b (-/-) and mdr1a/b (+/+) mice, two homozygous, male knockout FVB mice were purchased. As per the licence agreement for their breeding, these were cross bred in-house with a strain of mice which is known to possess no inherent respiratory problems (B6). The resulting F_1 FVB/B6 hybrids were all heterozygous for both mdr1a and mdr1b. By breeding the heterozygotes we were able to produce two homozygous strains, one homozygous wild type, mdr1a/b (+/+), and one homozygous knockout, mdr1a/b (-/-).

In order to select the necessary animals for breeding, it was necessary to establish the genotype of the mice. This was achieved by amplification of the mdr1a/b genes using primers which produced different sized DNA fragments in the knockout and wild type mice; if both fragment sizes were present the genotype was heterozygous for the gene. An example of this is shown in figure 3.3.1 where the results of the amplification on homozygous wild type, heterozygous and homozygous knockout mice are shown for both genes. By selectively breeding the homozygous wild type and homozygous knockout mice stable knockout lines were produced.

After the establishment of the breeding colonies, a single male mouse from each litter was genotyped to ensure the maintenance of the colony. In all cases the genotype proved stable and the homozygotes were maintained throughout the duration of the experiments.

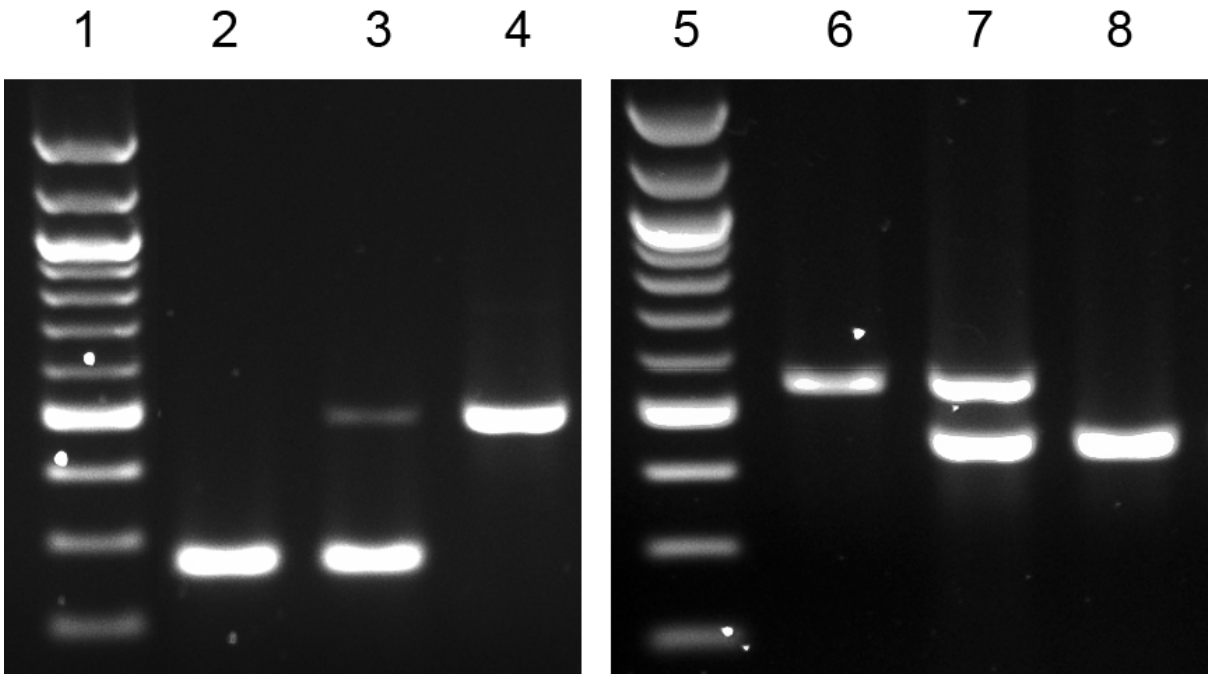

Figure 3.3.1 Images showing examples of the resulting gels from agarose gel electrophoresis of the DNA fragments from all possible genotypes of the FVB/B6 hybrids. Lanes 1 and 5 are loaded with the 1kb+ ladder in order to ascertain the size of the fragments in each band. [2-4] The possible fragment profiles for the genotypes of mdr1a: [2] homozygous wild type, [3] hetorozygote and [4] homozygous knockout. [6-8] The possible fragment profiles for the genotypes of mdr1b: [6] homozygous wild type, [7] heterozygote and [8] homozygous knockout.

3.3.2 Absorption experiments – IPML

Initial absorption experiments in the IPML using the lungs of the knockout mice show similarly discordant results of P-gp functionality as those seen in chapter 2 with chemical inhibition. As seen in figure 3.3.2 the absorption of rhodamine 123 was significantly increased in the knockout mice in comparison to the wild type (AUC = 376 ± 159 and 712 ± 79 %.min, respectively, $p = 0.003$), whereas the absorption of digoxin was unchanged (AUC = 761 ± 128 and 910 ± 242, $p = 0.44$).

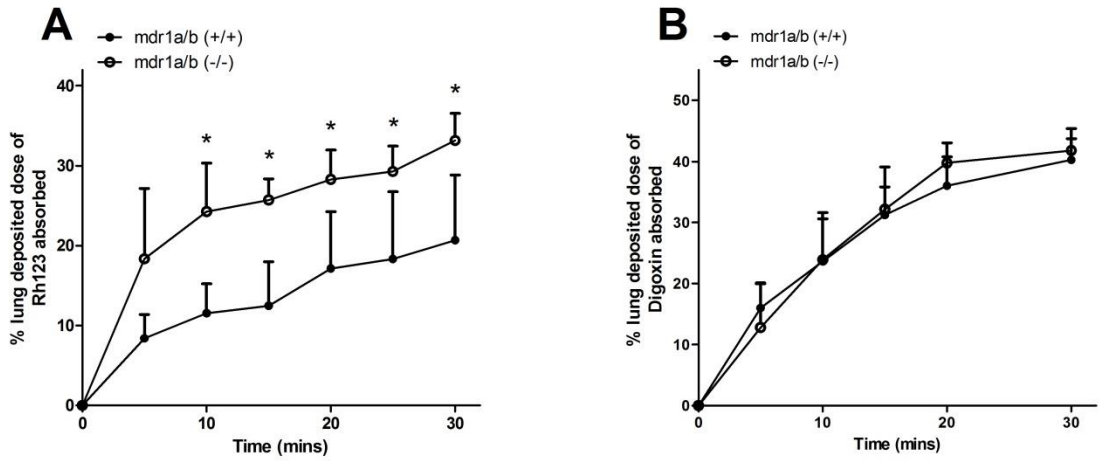

Figure 3.3.2 The absorption profiles of [A] rhodamine 123 and [B] digoxin following dosing to the IPML with the lungs of wild type or mdr1a/b (-/-) mice. Data are presented as mean ± S.D, n = 5-6.

The paracellular permeability of the lungs showed no difference between the wild type and knockout mice (AUC = 717 ± 60 and 734 ± 110, respectively, p = 0.894) with no difference seen in the mannitol absorption in either experiment.

	AUC (%.min) CD1 + 0.1% DMSO	FVB/B6 wild type	T-test (p)	AUC (%.min) CD1 + GF120918	FVB/B6 knockout	T-test (p)
Rhodamine 123	250 ± 122	376 ± 159	0.19	629 ± 181	712 ± 71	0.10
Digoxin	1051 ± 308	761 ± 128	0.58	908 ± 219	910 ± 242	0.15

Table 3.3.1 A comparison of the extent of absorption as determined by AUC between the CD1 and FVB/B6 mice with chemical and genetic knockout of P-gp function. Data are presented as mean ± S.D, n= 5-6.

In order to validate the absorption data from the FVB/B6 breeding colonies comparisons were made to the absorption profiles from CD1 mice with chemical inhibition (table 3.3.1). As measured by AUC the absorption of both rhodamine and digoxin showed no significant difference between both the wild type FVB/B6 mice and the CD1 in the absence of inhibitor, or the knockout FVB/B6 mice and the CD1 mice in the presence of GF120918. The similarity in the absorption profiles of the P-gp substrates in both strains of mice was mirrored by the absorption of the paracellular marker, mannitol. In the CD1 mice the AUC of mannitol absorption was 822 ± 150 %.min, this was not significantly different to the value for the FVB/B6 mice of 717 ± 60 %.min.

The similarity in the extent of absorptions as measured by AUC between the two strains of mice is also witnessed in the percentage of deposited dose absorbed throughout the experiment. Figure 3.3.3 shows the absorption profiles of mannitol, rhodamine 123 and digoxin compared between the FVB/B6 and CD1 mice and the similarities between them are apparent.

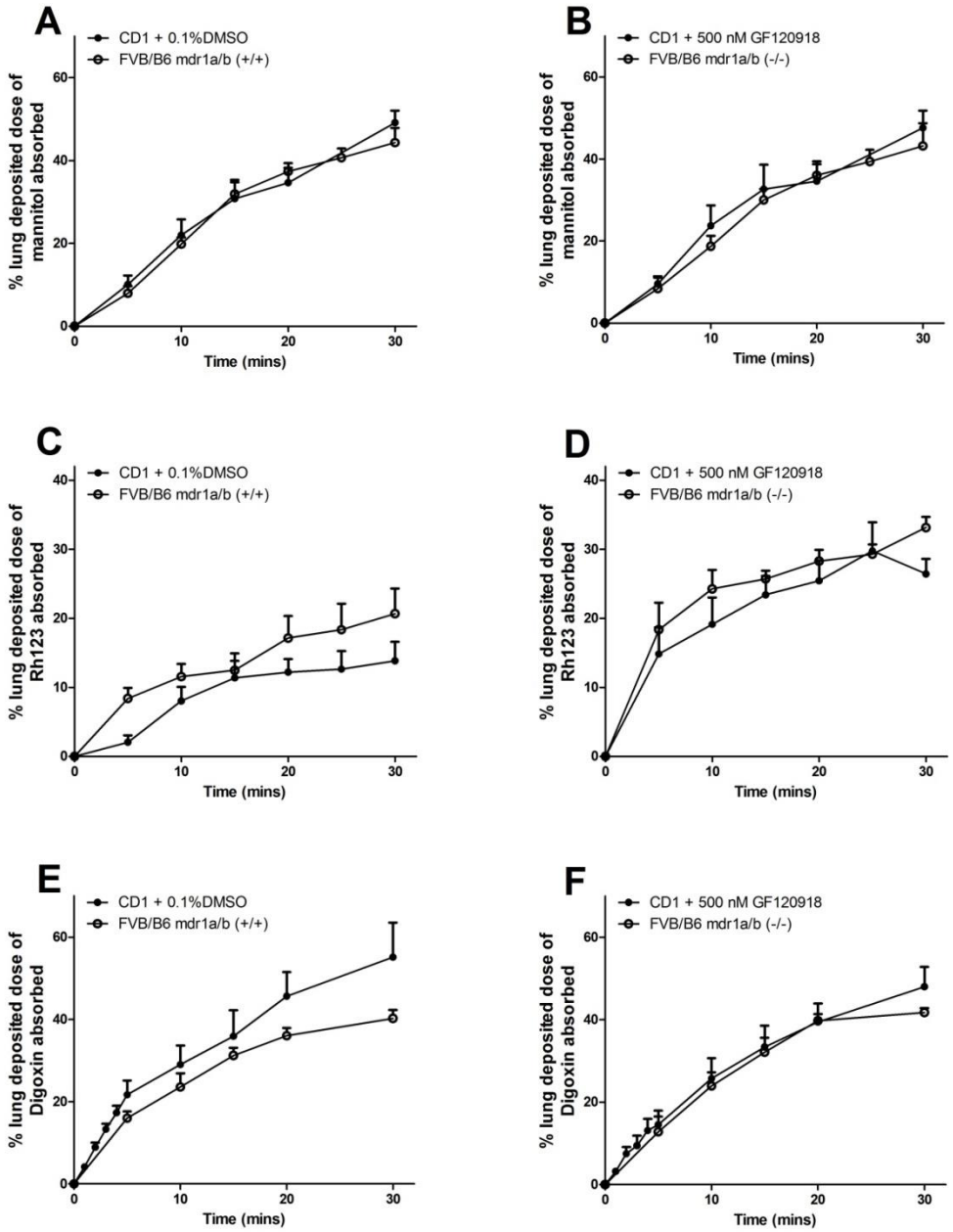

Figure 3.3.3 A comparison of the absorption profiles for [A-B] mannitol, [C-D] rhodamine 123 and [E-F] digoxin in the CD1 mice with chemical inhibition of P-gp and the FVB/B6 mice with genetic knockout. [A, C, E] Show the absorption profile comparison between the wildtype FVB/B6 mice and the CD1 in the absence of inhibitor, [B, D, F] compare the knockout mice to the CD1 experiments with GF120918. All data are presented as mean ± S.D, n = 5-6.

3.4 Discussion

The use of P-gp deficient mice is well established and provides an opportunity to investigate the impact of the drug transporter on pulmonary absorption without the confounding effects of the inhibitor. The aim of this chapter is to generate a breeding colony of knockout mdr1a/b (-/-) FVB/B6 mice and their wild type counterparts and validate their use in studies of lung absorption by comparing the absorption of rhodamine 123 and digoxin to previous studies.

Mice with genetic knockouts of mdr1a/b have been utilised for the investigation of the effects of P-gp upon the pharmacokinetics of its substrates since the mid 1990's (96) when both spontaneous mdr1a deficient CF-1 mice and the mdr1a/b knockouts generated by Schinkel *et al* were first utilised. These knockout mice have been used to demonstrate the role of P-gp in the restriction of transport at many barriers including the brain, liver and intestine as well as the impacts of P-gp upon the toxicity of a range of drugs and possibility of enhanced toxicity with certain dosing combinations.

The CF-1 mice which possess a spontaneous deleterious mutation of the mdr1a gene have previously been utilised to investigate the role of P-gp in the pulmonary absorption of digoxin (23). Manford used an instilled dose of digoxin in an *in vivo* drug absorption model to investigate the effect of pulmonary P-gp upon its absorption from the lung. The study found no difference between the absorption of digoxin from the lung in the spontaneous mdr1a (-/-) mice or the wild type counterparts, suggesting P-gp plays no role in pulmonary absorption of digoxin. However, the same experiments did illustrate a role for P-gp in the systemic pharmacokinetics of digoxin as a 10-fold increase in brain accumulation was seen in the mdr1a (-/-) mice. This lack of effect of pulmonary P-gp upon the absorption of digoxin from the lung seems surprising considering an early observation where digoxin accumulation in the lungs of P-gp deficient mice was increased over that seen in wild type animals (108) suggesting an impact of pulmonary P-gp on digoxin pharmacokinetics. Despite this studies utilising chemical P-gp inhibition to investigate the effect of P-gp upon the pulmonary absorption of digoxin all report the same lack of effect (24,71). Indeed absorption of digoxin from the CD1 mouse lungs in chapter 2 was unaffected by the addition of a chemical inhibitor (GF120918).

There was no difference observed in the absorption of digoxin between the P-gp knockout and wild type mice. This correlates well with the previous studies both in the literature and chapter 2 where no effect of P-gp upon the pulmonary absorption of digoxin has been observed in a variety of models using both chemical and genetic inhibition of P-gp functionality.

Similarly the increase in the absorption of rhodamine 123 seen from the lungs of the knockout mice is in agreement with previous literature. A previous study utilising chemical inhibition of P-gp in an IPRL witnessed a similar effect with an increase in both the rate and extent of rhodamine 123 absorption when co-dosed with an inihibitor (22).

Interestingly the absorption of both substrates (digoxin and rhodamine 123) in the genetic mdr1a/b knockout model showed no significant difference to the comparable chemical inhibition studies in CD1 mice, i.e. the results of chemical and genetic inhibition of P-gp produced similar absorption profiles in the CD1 and FVB/B6 mice. Thus proving that the increase in the pulmonary absorption of rhodamine 123 in the presence of GF120918 is due to the presence of P-gp and not a non-P-gp mediated effect of the inhibitor. This similarity in absorption profiles between the chemical and genetic inhibition models also further validates the use of the knockout mice in the IPML due to the consistency of the results with the published literature.

The lack of difference in the absorption of digoxin and mannitol between the wild type FVB/B6 and the mdr1a/b (-/-) mice illustrates that there is no general increase in the permeability of the knockout lungs. If the genetic knockout of P-gp increased the overall pulmonary permeability we would have expected to see an increase in absorption for all molecules and this is not the case. Conversely the increase witnessed in the absorption of rhodamine 123 from the knockout lungs shows that the model is capable of highlighting an effect of P-gp upon the absorption of a substrate whose pulmonary absorption has previously been shown to be attenuated by P-gp. Therefore showing that the IPML performed with P-gp knockout mice is a suitable model for determining the role of P-gp in the pulmonary absorption of its substrates.

Chapter 4

Pulmonary absorption in the IPML with mdr1a/b (-/-) mice

4.1 Introduction

4.1.1 Pulmonary expression of P-glycoprotein

P-glycoprotein (P-gp) is a broad substrate drug-transporter encoded by the MDR1 gene in humans and the *mdr1a* and *mdr1b* genes in rodents. It is amongst the most highly studied of the ABC transporters with a large volume of published work in a range of barriers including the intestine, kidney, liver and blood-brain barrier (BBB). P-gp substrates cover a broad range of therapeutic classes and physicochemical properties although they tend to be lipophilic or amphipathic (3) enabling entry in to the plasma membrane, a necessity for interaction with the transporter's substrate binding site.

Gene expression in the lung

In 2006 Bleasby *et al.* (5) performed a microarray analysis of transporter expression across a range of species and organs. In all species the expression witnessed in the lung was in the lower quartile, a far lower level than that seen in the intestine or the liver, however, it does need to be considered that the analysis was done on whole organ homogenate and as such the heterogeneous nature of the lung tissue could have served to dilute the mRNA transcript level if only a few cell types show expression. It does seem likely, however, that the expression levels in the lung epithelia are not as high as those seen in the intestine. It is interesting to note that in the rodent species the level of expression of *mdr1b* was higher than *mdr1a* in the lung, whereas in all other studied *mdr1a* is the more abundant (109). This observation has also been made in *in vitro* cell models, specifically those of primary isolated alveolar cells (110).

Protein expression in the lung

A number of groups since the early 1990's have investigated the spatial expression of P-gp within the lung using immunohistochemical (IHC) analyses. All observed P-gp expression within the lung epithelia but there are discrepancies with the localisations dependent on the specific techniques and antibodies used.

Initially Cordon-Cardo *et al.* (111) and van der Valk *et al.* (112)showed positive staining on the luminal surface of bronchial and bronchiolar epithelial cells in frozen tissue samples of human lung. The group of van der Valk also showed variable staining of the alveolar epithelia depending on the antibody used and positive staining of alveolar macrophages. The positive staining of the bronchial epithelia also has been seen by all groups (110,113,114). The alveolar staining witnessed by van der Valk *et al.* has also been more recently confirmed in studies by Campbell *et al.* (110) and Endter *et al.*

(115) with Campbell showing positive staining of the intact alveolar epithelia of rats and Endter with human tissue samples, both groups also showed the presence of the P-gp protein by Western blot analysis in the respective isolated primary alveolar cell lines.

Functional evidence - in vitro studies

Currently there is no standard cell line used in *in vitro* studies of drug permeability instead many cell lines, both immortalised and primary, are used. Work by the group of Endter *et al.* (115) showed polarised transport of the well characterised P-gp substrate rhodamine 123 (rh123) in primary isolated human alveolar epithelial cells, this was both saturable and inhibited by verapamil (a well characterised P-gp inhibitor), together providing good evidence for P-gp mediated efflux. A similar study was performed in rat primary cells by Campbell *et al.* (110) in which the accumulation of rh123 was increased by co-incubation with verapamil. Later work by Madlova *et al.* (24) using the human NHBE and Calu-3 cell lines showed polarised transport of digoxin in both cell types, although transport was less polarised than in the intestinal Caco-2 cells. In all cell lines the polarised transport was abolished by co-dosing with GF120918, a selective P-gp inhibitor. P-gp efflux from Calu-3 cells has also been demonstrated using the fluoroquinolone antibiotic moxifloxacin (116), again using a P-gp inhibitor (PSC-833). Finally Ehrhardt *et al.* (117) showed polarised transport of rh123 in the bronchial epithelia cell line 16HBE14o- which was inhibited by co-dosing with verapamil.

Taken together these studies provide compelling evidence that pulmonary cells grown *in vitro* express functional P-gp at a level high enough to significantly impact the PK/PD of drugs delivered to the lung or indeed drugs with sites of action in the lung delivered systemically. Questions are raised however about the expression of transporter proteins in these *in vitro* cell lines in comparison to intact pulmonary epithelia and whether they are truly models of the pulmonary barrier. To this end studies in intact lungs are necessary to elucidate a role for the transporters if there is one.

Functional evidence – intact lung studies

Although P-gp is the most well studied of the pulmonary drug transporters data in an intact lung system is still scarce. In 2003, the group of Kuhlmann *et al.* (118) looked at the effect of P-gp on the accumulation of idarubicin in lung tissue after dosing via the circulation. They found that in the experiments with the inhibitors the accumulation of the substrate in lung tissue was significantly increased. This would imply that P-gp inhibition is occurring at the endothelial barrier preventing efflux back in to the blood, a finding supported by a similar study by Roerig (73) in a rabbit model with rhodamine 6G performed a year later.

This hypothesis appears to be in agreement with experiments carried out by the group of Tronde *et al.* (38). These experiments investigated the absorption of drugs from the lung in to the blood using both *in vivo* and isolated lung models. In both cases the absorption of losartan was above 95% and it was assumed that there was no attenuating effect of P-gp efflux on absorption from the lung lumen. The experiments were not designed to investigate efflux and therefore the concentrations used were higher than ideal and could cause saturation of the pump and the group did not use P-gp inhibitors to investigate efflux. It therefore could not be determined if P-gp effected the rate of absorption, this could be a distinct possibility due to the observed rate of absorption of losartan being considerably lower than would be predicted from its physicochemical properties.

Manford *et al.* (23) provided further evidence for the lack of effect of P-gp from the lumen to blood using digoxin as a substrate in an isolated rat lung. Then group used spontaneous mdr1a deficient mice and showed that there was no difference in the rate and extent of digoxin absorption between the deficient and control mice. Contrary to this a study in a similar isolated rat lung model using rhodamine 123 as the substrate showed a significant increase in the absorption of rhodamine 123 from the lung to the blood when co-dosed with GF120918 (a selective P-gp inhibitor) (22).

Subsequently a study was published investigating the effects of pulmonary P-gp in an isolated lung on a larger selection of substrates (71). This work corroborates the results of both of the previous two studies using both rat and mouse isolated perfused lung models. In both models a significant increase in the absorption of rhodamine 123 was observed when co-dosed with GF120918, an observation not seen in digoxin where the inhibitor did not alter the absorption profile. This observation was expanded upon in the same publication with two other P-gp substrates, loperamide and saquinavir. A similar pattern was seen with the two new compounds, loperamide appears similar to rhodamine 123 and shows increased absorption in the presence of the inhibitor, and conversely saquinavir absorption was not altered by co-dosing with GF120918.

Summary

The studies discussed above provide persuasive evidence for a role for P-gp in lung tissue, its presence has been observed in a variety of models from *in vitro* cell culture to human sections at both the protein and mRNA levels and functionality has now been observed in isolated perfused lung models in both rat and mouse. P-gp efflux has been shown to reduce the absorption of a set of substrates from the airways to the blood yet the transporter appears to have no effect on other well characterised substrates such as digoxin. Despite this it is apparent that P-gp can affect drug absorption after pulmonary delivery and as such needs to be considered when developing and

delivering drugs which are known substrates as it could well significantly impact their pharmacokinetics/dynamics.

4.1.2 The IPL for studies of pulmonary drug transporters

As described above, the IPL model has been utilised to investigate the role of P-gp upon the pulmonary absorption of a small number of its substrates. In addition to these studies the model has been used to investigate the effects of other pulmonary drug transporters.

Active transport processes have been observed in the IPL model as both active uptake and active efflux. The work of Sakagami (68,119) has shown saturable and inhibitable uptake of both F-PHEA and IgG from the *ex vivo* rat lung. Initial experiments with F-PHEA showed unexpectedly rapid absorption, far more rapid than would be expected from the molecules physicochemical characteristics. The group suggested this was attributable to active uptake within the lung and accounted for high transport rate by adjusting the simple passive model of Byron to include Michaelis-Menton kinetics of active uptake. The evidence for this assumption was provided by IPL experiments performed at lower temperatures and dosed with transcytosis inhibitors, both of which reduced the transport rate back towards the level initially expected.

Despite the scarcity of data on the use of an IPL for the assessment of the role of pulmonary drug transporters on pharmacokinetics in the lung, the experiments discussed here reveal the ability of the isolated perfused lung models to identify the impact of transporter proteins, both for active uptake and for efflux. IPL model shave been used to comprise the first evidence of a role for drug transporters within an intact lung, a role which, though suggested, has yet to be confirmed using the comparable *in vivo* models. This may well be due to the isolated lung models preventing the confounding effects of the transporters at other barriers such as the liver which make whole body experiments more difficult to interpret.

4.1.3 Experimental Objectives

Here we aim to further investigate the apparent discordance in the literature with regards to the effects of pulmonary P-gp upon the absorption of its substrates form the lung. Currently, it appears that not all substrates which are effluxed by P-gp at other barriers are affected by the transporter in the lung. In order to investigate this further, this chapter aims to investigate the absorption of a larger and diverse panel of P-gp substrates in an attempt to ascertain the mechanism behind the discordance.

4.2 Material & Methods

4.2.1 Materials

Chemicals and Equipment

P-glycoprotein (P-gp) substrates dosed to the lungs of the IPML and analysed by tandem mass spectrometry (LC-MS/MS) are shown in table 4.2.1 below.

	Salt	Purity	Purchase Code
Acrivastine		> 98% HPLC	SML0119
Chloroquine	Diphosphate salt	> 98% HPLC	C6628
Colchicine		> 95% HPLC	C9754
Domperidone		> 98% HPLC	D122
Eletriptan	Hydrobromide	>98% HPLC	PZ0011
Erythromycin		> 95%	E5389
GSK1			n/a
GSK2			n/a
GSK3			n/a
Indacaterol			n/a
Mitoxantrone	Dihydrochloride	> 97% HPLC	M6545
Monensin	Sodium salt	90 - 95% TLC	M5273
Puromycin	Dihydrochloride hydrate	99%	10781691
Rhodamine 123		> 98% GC	R8004
Salbutamol		> 96% GC	S8260
Salmeterol	Xinafoate	> 98% HPLC	S5068
Saquinavir	Mesylate	> 98% HPLC	S8451

Table 4.2.1 The non-radiolabelled P-gp substrates delivered to the IPML along with their salts, purities and supplier details.

Digoxin and the mannitol controls were delivered to the lung as radiolabelled doses, allowing the delivery of a much lower amount of drug whilst still retaining the necessary lower limit of quantification (LLQ). The details of these radiolabelled compounds are found in table 4.2.2 below.

Compound	Radiolabel	Radioactivity	Purchase Code	Supplier
Digoxin	[3H(G)]	15-40 Ci/mmol	NET222250UC	PerkinElmer, USA
Mannitol	D-[2-3H]	10-20 Ci/mmol	ART 0263	ARC, St Louis, MO, USA
Mannitol	D-[1-14C]	50-60 mCi/mmol	ARC 0127	ARC, St Louis, MO, USA

Table 4.2.2 Compounds delivered to the IPML as radiolabels either as P-gp substrates or paracellular permeability markers. Compounds are shown along with their relevant radiolabels and supplier details.

The equipment for performing the IPML experiments, as well as the relevant chemicals for the production of the perfusate and phosphate buffered saline (PBS), were the same as those shown in chapter 2.

Chemicals used in the analysis of substrate and control permeability data are shown in table 4.2.3 below. The equipment used for the analysis is summarised in table 4.2.4.

Chemical	Descriptor	Product Code	Supplier
Acetonitrile	HPLC Grade	10407440	Fisher Scientific, Loughborough, UK
Methanol	LCMS Grade	10653963	Fisher Scientific, Loughborough, UK
Formic Acid	98%	10559570	Fisher Scientific, Loughborough, UK
Dimethyl Sulfoxide	n/a	10080110	Fisher Scientific, Loughborough, UK
Scintillation fluid	ScintiSafe 3	SC/9205/21	Fisher Scientific, Loughborough, UK

Table 4.2.3 Chemicals used in the analysis of compounds delivered to the IPML along with their supplier details.

Equipment	Manufacturer	Product Identifier
Solvent Degasser	Thermo Finnigan	SCM1000
Pump	Thermo Finnigan	P4000
Autosampler	Thermo Finnigan	AS3000
UV detector	Thermo Finnigan	UV2000
LC-MS/MS	Thermo Finnigan	LCQ Classic
HPLC Column	Kromasil	C18 3.5u 150 x 2.0 mm
Scintillation Counter	Packard	Tri-Carb 2900TR

Table 4.2.4 Equipment used in the analysis of compounds delivered to the IPML and the relevant manufacturer details.

Animals

Male pathogen-free FVB/Bl6 mice, which were bred on site as per chapter 3, were used throughout the experiments. The breeding program produced two distinct groups of FVB/Bl6 mice, the first fully expressed wild type levels of mdr1a and mdr1b (mdr1a/b (+/+)) and the second group were knockouts, with no functional expression of these genes (mdr1a/b (-/-)). The mice were housed in temperature and humidity controlled rooms (19-21 ^{o}C and 40-60 % humidity) with a 12 hour dark-light cycle. All mice had access to food and water *ad libitum* and were acclimatised for at least 24 hours following transport from the breeding facility to the experimental laboratories. All animal experiments were performed in adherence to the Animal (Scientific Procedures) Act 1986 and were approved by Cardiff University and GSK, Stevenage.

4.2.2 Analytical Methods

Analytical methods – HPLC-MS/MS

In order to ascertain the absorption profiles of the substrates from the airways of the IPML analytical methods were developed to determine the substrate concentrations within the perfusate reservoir. All substrates, with the exception of digoxin, were analysed by high performance liquid chromatography tandem mass spectrometry (HPLC-MS/MS).

Mass spectrometry is an analytical technique which enables the measurement of a molecules mass/charge ratio (M/Z). This M/Z is utilised in many laboratory techniques to determine the mass

of particles and elucidate chemical structures and elemental and isotopic composition. Tandem mass spectrometry (MS/MS) allows for a greater specificity than regular MS techniques. In MS/MS a specific ion may be trapped utilising the ion trap and collided with helium (He) gas causing it to fragment. As the spectra of the fragments formed are specific to the collision energy and parent molecule they can provide further specificity and filtering over single MS techniques. In certain techniques the fragments themselves can be trapped and collided once more with He gas allowing multiple stages of fragmentation, this can be often be of diagnostic value in the structural determination of complex molecules such as proteins.

A combination of both HPLC and LC-MS/MS techniques enabled the analysis of substrate concentrations in the perfusate samples of the IPML model. Following the injection and subsequent chromatographic separation on a C18 column, the mobile phase (and therefore substrate) is passed through the ion source of the mass spectrometer. The mobile phase which is pumped through the column before substrate elution is discarded due to the presence of large amounts of salt (which do not adhere to the column and elute rapidly) which can damage the mass spectrometer. Following ionisation of the substrate ions are separated according to their M/Z and either fragmented (MS/MS) or passed straight to the detector. The extent of the signal produced by the collisions of the substrate ion or fragment with the detector directly correlates to the amount of ion present; thus allowing the comparison to a standard curve to determine the concentration present in the original perfusate sample.

Before injection onto the C18 column it was necessary to remove the protein from the samples to prevent column degradation. This was achieved by protein precipitation with organic solvent. In the case of samples which would be run with acetonitrile (ACN) and water as the mobile phase ACN was added to the sample at a 2:1 volume to volume ratio. This mixture was then vortexed and allowed to rest for 1 minute. Subsequently the precipitated proteins were separated by centrifugation at 16,000 rcf for 10 mins at 4 ^{o}C. Substrates which were run with methanol (MeOH) as a mobile phase utilised ice-cold MeOH in place of ACN to perform the precipitation in order to prevent changes in column adherence during the chromatography.

In order to carry out the HPLC separation, 10 µL of protein precipitates sample was injected onto a C18 HPLC column and the relevant mobile phase was pumped at 0.2 mL/min either as an isocratic flow or as a gradient (table 4.2.5). The chromatic separation was performed with a column temperature of 30 ^{o}C using the column oven to ensure the temperature remained constant

throughout the analyses. The elution time from the column was substrate specific but mobile phase conditions were altered to ensure elution occurred at least 1 minute after the injection peaks.

Mobile phase from 30 seconds before the elution of a substrate to 1 minute after was directed to the ion source of the mass spectrometer. Substrates which showed insufficient LLQ using LC-MS analysis were analysed using LC-MS/MS which allowed for higher specificity and therefore sensitivity in the analysis, as observed by increases in the peak areas produced by the mass spectrometer. The MS/MS detector settings utilised in the analysis can be seen in table 4.2.6.

In order to obtain concentrations from the peak areas produced by the MS or MS/MS analysis comparisons were made to standard curves. Standard curves for all substrates were prepared in perfusate (3.25 to 200 ng/mL) and were run with a blank perfusate sample before and after; a blank was also included between each animal's samples. Standard curve samples were prepared by protein precipitation in a manner consistent with the IPML samples. Standard curves were prepared and analysed at the beginning of every experimental analysis run.

In order to test for ion suppression the 200 ng/mL standard was injected twice in succession and differences in peak area between the two injections were recorded.

	Mobile Phase		Separation Conditions	Parent (M/Z)	Daughter (M/Z)	Collision Energy (mV)
	A	B				
Acrivastine	MeOH	H_20 + 0.1% FA	50-95% A, gradient	349		
Chloroquine	ACN	H_20 + 0.1% FA	5-95% A, gradient	320		
Colchicine	ACN	H_20 + 0.1% FA	5-95% A, gradient	400		
Domperidone	MeOH	H_20 + 0.1% FA	40% A, isochratic	426	175	35
Eletriptan	ACN	H_20 + 0.1% FA	5-95% A, gradient	383		
Erythromycin	ACN	H_20 + 0.1% FA	60-95% A, gradient	734		
GSK1	ACN	H_20 + 0.1% FA	5-95% A, gradient	572		
GSK2	ACN	H_20 + 0.1% FA	5-95% A, gradient	496		
GSK3	ACN	H_20 + 0.1% FA	5-95% A, gradient	467		
Indacaterol	ACN	H_20 + 0.1% FA	5-95% A, gradient	394		
Mitoxantrone	MeOH	H_20 + 0.1% FA	30-70% A, gradient	445	358	30
Monensin	ACN	H_20 + 0.1% FA	70-100% A, gradient	694	675	30
Puromycin	ACN	H_20 + 0.1% FA	5-95% A, gradient	472		
Rh-123	ACN	H_20 + 0.1% FA	5-95% A, gradient	345		
Salbutamol	ACN	H_20 + 0.1% FA	5-95% A, gradient	240		
Salmeterol	ACN	H_20 + 0.1% FA	5-95% A, gradient	417		
Saquinavir mesylate	ACN	H_20 + 0.1% FA	5-95% A, gradient	670	416	30

Table 4.2.5 Substrate specific conditions used for the analysis by HPLC-MS/MS. A and B indicate the composition of the mobile phase utilised for HPLC. The separation conditions specify the concentrations of each component of the mobile phase used for separation. The parent (M/Z) indicates the isolated mass charge for each substrate during MS analysis. Compounds shown with a daughter M/Z indicate that MS/MS was used for their analysis and the parent was fragmented by the stated collision energy to produce a daughter fragment; this daughter fragment was then analysed to provide concentration data.

Detector	Thermo Finnigan LCQ Classic
Mode	MS or MSMS
Ion Source	ESI (electrospray ionisation)
Ionisation	positive
Source Temperature	450 ^{o}C

Table 4.2.6 MS/MS detector conditions used for all substrates

Analysis of radiolabelled compounds

Perfusate samples (200 µL) were added to translucent scintillation tubes. Scintillation cocktail was added (3 mL) and the samples were measured in a Tri-Carb scintillation counter on dual-counting mode. In the presence of decay the scintillation cocktail emits fluorescence which is detected by the counter, in dual counting mode the fluorescence from both ^{3}[H] and ^{14}[C] decay are measured simultaneously and an output of counts per minute (CPM) is produced. This is converted to decompositions per minute and gives a measure of the total amount of each radiolabel present in the sample. By comparing the DPM of the sample to that of the dose it is possible to calculate the % of dose absorbed to the perfusate at each time point.

4.2.3 Absorption experiments

Absorption of substrates from the airways - dosing

In order to investigate the role of P-gp in the absorption of its substrates from the lung a panel of 18 substrates were administered to the lung. As described in chapter 2 reproducible dosing to the peripheral airways was achieved using a 250 µL stop-lock Hamilton syringe with a 25 µL dose and a 250 µL bolus of air. The syringe was inserted into the trachea until 2 mm before the bifurcation. The contents were then pressurised with the valve closed by depressing the syringe. Upon opening the valve the dose was then ejected and the bolus of air deposited dose equally to all lobes and in to the peripheral airways. See chapter 2 for a more thorough discussion.

All of the doses were administered as solutions in PBS (pH 7.4) containing 0.1 % DMSO. Drug stocks of 10 mg/mL in DMSO were diluted in PBS to form solutions of 50 µM. The relevant amount of

DMSO was added during this dilution to ensure all doses contained 0.5 % DMSO. Table 4.2.7 shows the final amounts of substrate stock, DMSO and PBS added to each dose.

	MW (Da)	Stock Concentration (mg/mL)	Stock added to dose (µL)	DMSO added to dose (µL)	PBS added to dose (µL)
Acrivastine	348	10	1.74	3.26	995
Chloroquine	319	10	1.60	3.41	995
Colchicine	399	10	2.00	3.01	995
Digoxin	780	10	3.90	1.10	995
Domperidone	425	10	2.13	2.88	995
Eletriptan	382	10	1.91	3.09	995
Erythromycin	733	10	3.67	1.34	995
GSK1	571	10	2.85	2.15	995
GSK2	495	10	2.47	2.53	995
GSK3	466	10	2.33	2.67	995
Indacaterol	393	10	1.96	3.04	995
Mitoxantrone	444	10	2.22	2.78	995
Monensin	670	10	3.35	1.65	995
Puromycin	471	10	2.36	2.65	995
Rh-123	344	10	1.72	3.28	995
Salbutamol	239	10	1.20	3.81	995
Salmeterol	416	10	2.08	2.92	995
Saquinavir mesylate	670	10	3.35	1.65	995

Table 4.2.7 The composition of the doses delivered to the airways of the IPML, in all cases the final dose concentration is 50 µM in a solution of PBS containing 0.5% DMSO.

The dose concentration was chosen to match that previously used in investigations with rhodamine 123. In the case of rhodamine 123 a 25 µL dose (50 µM) contained 430 ng of substrate. Assuming a low extent of bioavailability from the lung of 10% of the deposited dose absorbed 43 ng of rhodamine 123 would be absorbed to the perfusate. As the perfusate volume is fixed at 10 mL this level of absorption would result in rhodamine 123 perfusate concentrations of 4.3 ng/mL; this is above the LLQ for rhodamine 123 of 3.25 ng/mL. After the addition of the 25 µL dose to the mouse lungs it is estimated that the total fluid volume of the lungs (epithelial lining fluid (ELF) plus the dose) will be increased to approximately 50 µL (120). This will result in initial rhodamine 123

concentrations within the lung of approximately 25 µM (8.6 µg/mL); a level consistent with studies performed in the isolated rat lung (71,86) and around the reported P-gp K_m for rhodamine 123 (75,121,122).

In order to ensure the integrity of the lung-blood barrier in each experiment was comparable 0.25 µCi of radiolabelled mannitol was included in each dose. For experiments analysed by HPLC-MS/MS this was in the form of 25 pmol of ^{3}[H]-mannitol. As the digoxin used in the IPML experiments was also radiolabelled with ^{3}[H] a different radiolabel was required for the control to distinguish between the two during analysis. To this end 0.25 µCi of ^{14}[C]-mannitol was used as the paracellular control in the digoxin experiments (16.7 pmol). Both forms of radiolabelled mannitol were stored as solutions in ethanol. To add this to the dose the relevant amount was removed and transferred to a pipette, this was allowed to dry overnight in a fume cupboard. The substrate dose could then be added and the mixture vortexed to dissolve the mannitol.

Absorption of substrates from the airways - IPML

To investigate the effect of P-gp upon the pulmonary absorption of a panel of substrates an IPML model was utilised. Substrate doses (as described above) were delivered to the airways of the lungs by forced instillation (as described in chapter 2) of both mdr1a/b (+/+) wild type and mdr1a/b (-/-) knockout mice. The absorption profiles for both groups of mice were determined by changes in the concentration of substrate in the perfusate reservoir throughout the experiment. To this end perfusate samples were removed at 0, 1, 5, 10, 15, 20 and 30 min post dosing and replaced with fresh perfusate at 37^{o}C. Perfusate samples were analysed by either HPLC-MS/MS or scintillation counting as described earlier.

The validation and use of the knockout mice was discussed in chapter 3, where it was shown that the barrier properties of the two groups were not changed by P-gp knockout. Any change in the % of deposited dose absorbed between the two groups presented here was therefore attributed to P-gp expression alone. In all cases the paracellular marker, mannitol, was included in the dose as a radiolabelled compound. The comparison of mannitol absorption profiles between experiments was used to ensure consistent paracellular permeability and barrier integrity both within and between experimental groups.

Absorption of substrates from the airways – power analysis

In order to determine the sample size (number of mice) necessary to provide sufficient statistical power to the investigations a power analysis was carried out using the initial absorption data for rhodamine 123. As is shown in figure 4.2.1 the calculated sample size required for sufficient statistical power (0.95) at a 15 % increase in deposited dose absorbed is n = 6.

In order to reduce the number of mice needed for the study significance was tested at n=4 as described in 4.2.2 *Data analysis*. If the difference in % deposited dose absorbed between the wild type and knockout mice was significant, no further experiments were performed, if there was no significant difference sample size was increased up to n = 6. If no significant difference was observed between the experimental groups at n = 6 it was deemed that P-gp had no effect upon the absorption of the substrate from the IPML.

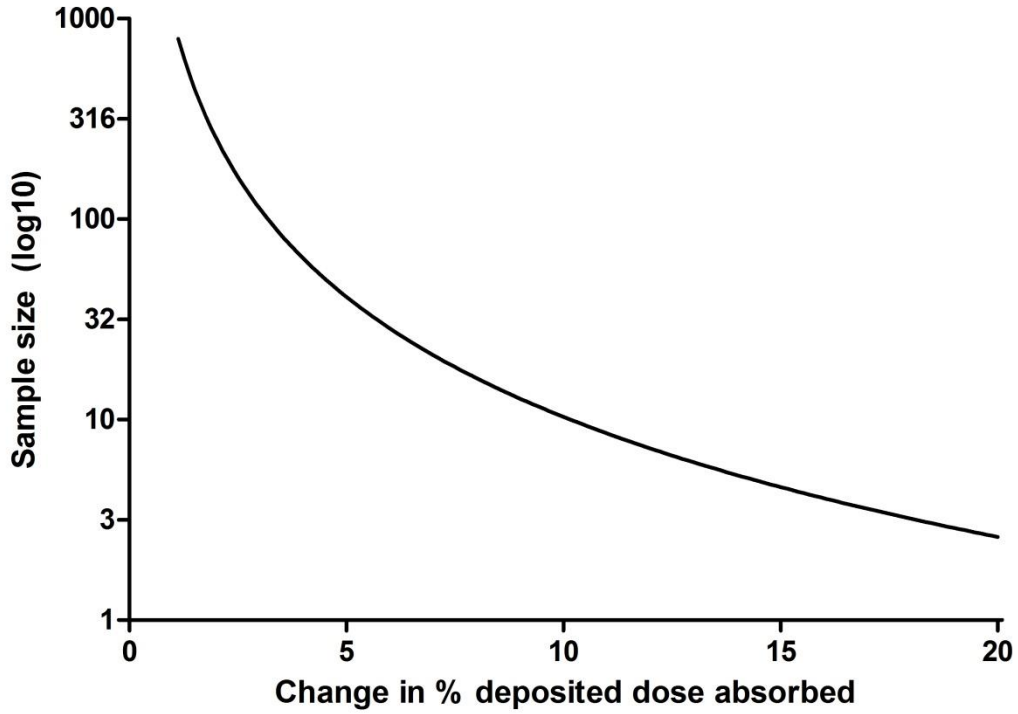

Figure 4.2.1 The sample size required for a statistical power of 0.95 at a range of changes in the % of dose absorbed. Analysis was generated using the mean and variance data for rhodamine 123 absorption studies. The sample size required to generate sufficient power (0.95) to identify a change of 15 % dose absorbed is n = 6.

Data Analysis

In order to understand the effects of P-gp knockdown upon the rate and extent of absorption a compartmental modelling approach was applied to the data. Using WinNonlin values for the rate of absorption (ka) and the bioavailability (F) were calculated according to a single compartment model by applying the following equation:

$$Y = dose * F * (1 - \exp(ka * X))$$

(Where dose can be set to 100%)

Graphs representing the visual fit of the same equation were produced using Graphpad Prism 5 software.

The absorption profiles of the two experimental groups were also compared in a non-compartmental manner using area under the curve analysis (AUC). AUC analysis was performed on the % deposited dose absorbed at all time points using Graphpad Prism 5 software.

To determine the significance of the differences in absorption between the wild type mdr1a/b (+/+) and the knockout mdr1a/b (-/-) mice an independent T-test was performed upon the percentage of deposited dose absorbed at 30 min and the AUC analyses. In all cases significance was accepted as $p< 0.05$.

Correlations between datasets were performed using Microsoft Excel 2010 by calculating the Pearson's moment of correlation. Graphs representing these correlations were generated using Graphpad Prism 5 software.

4.3 Results

4.3.1 HPLC-MS/MS Validation, Precision and Accuracy

The precision of the analysis for all molecules analysed using HPLC-MS/MS was investigated by determining the coefficients of variation (% C_V) for all molecules (n = 4) at opposing ends of the concentration range for analysis, 3.25 and 200 ng/mL. Results are shown Table 4.3.1 and 2 and % C_v values of less than 15 % were deemed acceptable for quantification with regards to precision (123). Accuracy was calculated at the same concentrations by comparing calculated concentrations from the analysis to the nominal concentration expected, an accuracy of ± 20% was deemed acceptable for analysis (123). In all cases the analysis of every molecule was deemed acceptable between the concentration range of 3.25 to 200 ng/mL.

	3.25 ng/mL			
	Mean (ng/mL)	Standard Deviation	Coefficient of Variation (% C_v)	Accuracy
Acrivastine	12.28	0.81	6.58	101.76
Erythromycin	13.36	1.34	10.04	93.59
GSK1	12.07	1.17	9.73	103.54
Mitoxantrone	12.87	0.99	7.68	97.16
Monensin	11.09	1.00	9.01	112.70
Puromycin	11.99	0.65	5.46	104.28
Saquinavir	13.17	1.22	9.30	94.89
Chloroquine	13.41	1.11	8.30	93.20
Colchicine	13.16	1.27	9.61	94.96
Domperidone	11.14	0.81	7.31	112.20
Eletriptan	12.57	0.46	3.63	99.45
GSK2	12.19	0.65	5.37	102.54
GSK3	12.27	0.87	7.06	101.91
Indacaterol	12.05	1.15	9.58	103.69
Rhodamine 123	12.86	0.46	3.57	97.22
Salbutamol	12.97	0.56	4.34	96.41
Salmeterol	13.47	0.32	2.39	92.82

Table 4.3.1 Coefficients of variation for precision of analysis at 3.25 ng/mL

	200 ng/mL			
	Mean (ng/mL)	Standard Deviation	Coefficient of Variation (% C_v)	Accuracy
Acrivastine	240.58	33.19	13.80	83.13
Erythromycin	206.46	15.99	7.74	96.87
GSK1	187.91	27.40	14.58	106.44
Mitoxantrone	203.37	13.65	6.71	98.35
Monensin	192.84	8.45	4.38	103.71
Puromycin	189.24	9.58	5.06	105.69
Saquinavir	187.22	11.10	5.93	106.83
Chloroquine	200.06	19.73	9.86	99.97
Colchicine	211.55	17.69	8.36	94.54
Domperidone	216.92	15.37	7.09	92.20
Eletriptan	187.56	11.65	6.21	106.63
GSK2	185.05	12.96	7.00	108.08
GSK3	199.65	19.65	9.84	100.17
Indacaterol	203.65	8.65	4.25	98.21
Rhodamine 123	223.91	25.00	11.16	89.32
Salbutamol	187.69	24.65	13.14	106.56
Salmeterol	223.33	21.49	9.62	89.56

Table 4.3.2 Coefficients of variation for precision of analysis at 200 ng/mL

4.3.2 Absorption experiments - IPML

The absorption profiles of 18 P-gp substrates were determined in both the wildtype mdr1a/b (+/+) mice and the knockout mdr1a/b (-/-) mice following drug deposition to the airways of the IPML by measuring accumulation in the perfusate reservoir.

As illustrated by figures 4.3.1 to 3, 10 of the 18 substrates tested show a significantly higher percentage of the deposited dose absorbed ($p < 0.05$) when P-gp functionality is attenuated (i.e. in the knockout mice), whilst 8 show no difference in absorption profile between the two experimental groups. This would indicate that P-gp acted to attenuate the absorption of 10 substrates but had no effect on the absorption of the remaining 8.

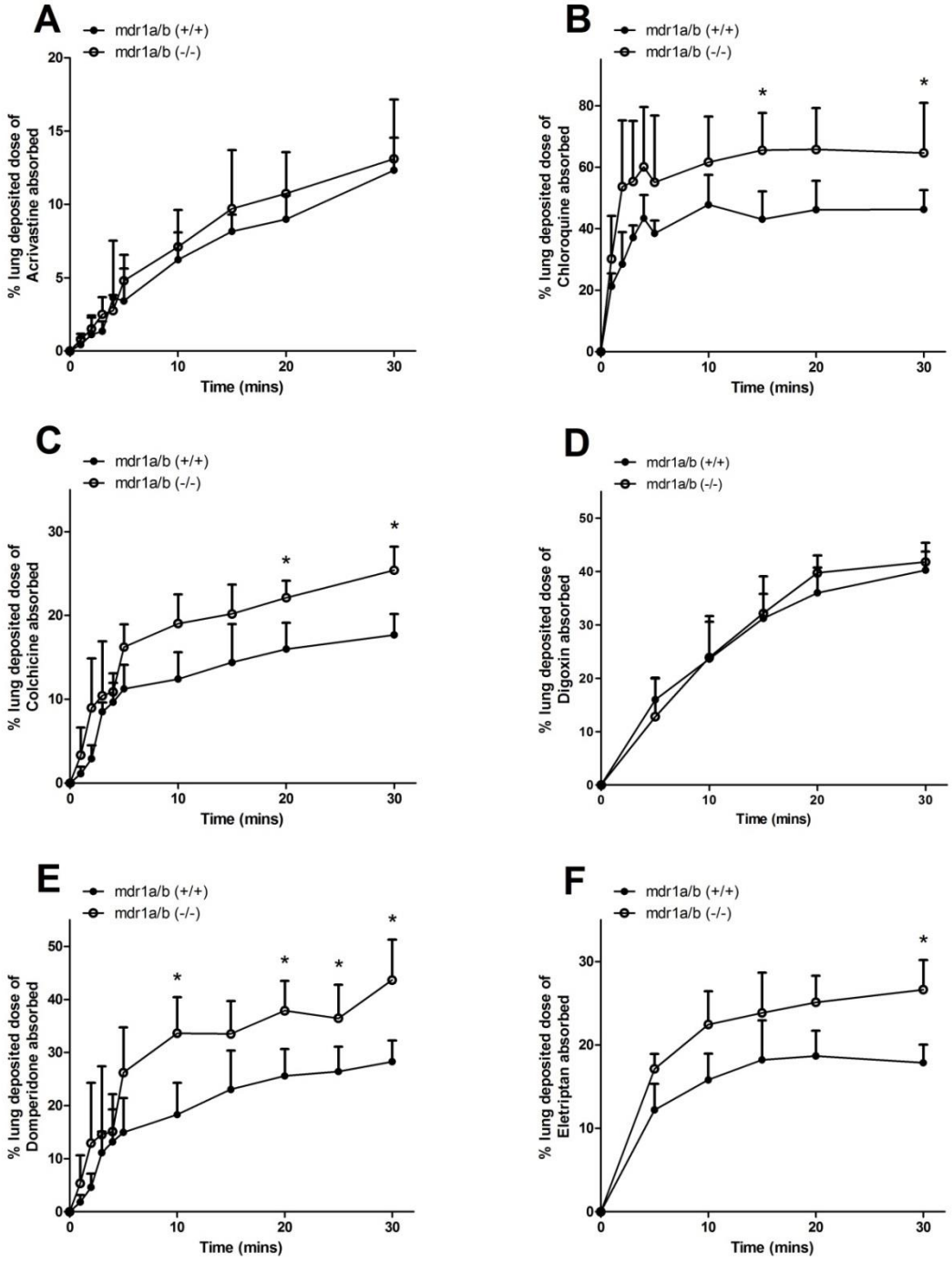

Figure 4.3.1 Absorption profiles from the airways of the IPML in to perfusate for both the wild-type mdr1a/b (+/+) mice and the knockout mdr1a/b (-/-) mice for **[A]** acrivastine (n=4), **[B]** chloroquine (n=4), **[C]** colchicine (n=4), **[D]** digoxin (n=6), **[E]** domperidone (n=4) and **[F]** eletriptan (n=4). In all cases data is presented as the mean ± SD of the percentage of the lung deposited dose absorbed at distinct time points, * indicates a significant difference between the wild-type and knockout mice at that time point.

4.3.2.1 Pulmonary absorption of acrivastine

Following deposition of acrivastine in to the airways of wildtype FVB/B6 mice 12 % of the dose was absorbed within 30 minutes as determined by the increasing perfusate concentrations. In comparison the same experiments in the knockout *mdr1a/b* (-/-) mice showed a total of 13 % of the dose absorbed over the same time frame. As illustrated in figure 4.3.1 and shown in table 4.3.3 this increase in percentage dose absorbed in the knockout mice was not significant ($p>0.05$) at any time with the absorption curves in both the wild type and knockout mice being similar. The lack of an increase in absorption in the absence of functional P-gp suggests that the protein does not play a role in the absorption of acrivastine from the lung in this model.

4.3.2.2 Pulmonary absorption of chloroquine

Following deposition of chloroquine in to the airways of wildtype FVB/B6 mice 46 % of the dose was absorbed within 30 minutes as determined by the increasing perfusate concentrations. In comparison the same experiments in the knockout *mdr1a/b* (-/-) mice showed a total of 65 % dose absorbed over the same time frame. As illustrated in figure 4.3.1 and shown in table 4.3.3 this increase in percentage dose absorbed in the knockout mice was significant ($p<0.05$) at the 15 and 30 minute time points. The increase in absorption in the absence of functional P-gp illustrates a role for the protein in limiting pulmonary absorption of chloroquine.

4.3.2.3 Pulmonary absorption of colchicine

Following deposition of colchicine in to the airways of wildtype FVB/B6 mice 18 % of the dose was absorbed within 30 minutes as determined by the increasing perfusate concentrations. In comparison the same experiments in the knockout *mdr1a/b* (-/-) mice showed a total of 25 % dose absorbed over the same time frame. As illustrated in figure 4.3.1 and shown in table 4.3.3 this increase in percentage dose absorbed in the knockout mice was significant ($p<0.05$) at the 20 and 30 minute time points. The increase in absorption in the absence of functional P-gp illustrates a role for the protein in limiting pulmonary absorption of colchicine.

4.3.2.4 Pulmonary absorption of digoxin

Following deposition of digoxin in to the airways of wildtype FVB/B6 mice 40 % of the dose was absorbed within 30 minutes as determined by the increasing perfusate concentrations. In comparison the same experiments in the knockout *mdr1a/b* (-/-) mice showed a total of 42 % of the dose absorbed over the same time frame. As illustrated in figure 4.3.1 and shown in table 4.3.3 this increase in percentage dose absorbed in the knockout mice was not significant ($p>0.05$) at any time with the absorption curves in both the wild type and knockout mice being similar. The lack of an increase in absorption in the absence of functional P-gp suggests that the protein does not play a role in the absorption of digoxin from the lung in this model.

4.3.2.5 Pulmonary absorption of domperidone

Following deposition of domperidone in to the airways of wildtype FVB/B6 mice 28 % of the dose was absorbed within 30 minutes as determined by the increasing perfusate concentrations. In comparison the same experiments in the knockout *mdr1a/b* (-/-) mice showed a total of 44 % dose absorbed over the same time frame. As illustrated in figure 4.3.1 and shown in table 4.3.3 this increase in percentage dose absorbed in the knockout mice was significant ($p<0.05$) at time points after and including 10 minutes. The increase in absorption in the absence of functional P-gp illustrates a role for the protein in limiting pulmonary absorption of domperidone.

4.3.2.6 Pulmonary absorption of eletriptan

Following deposition of eletriptan in to the airways of wildtype FVB/B6 mice 18 % of the dose was absorbed within 30 minutes as determined by the increasing perfusate concentrations. In comparison the same experiments in the knockout *mdr1a/b* (-/-) mice showed a total of 27 % of the dose absorbed over the same time frame. As illustrated in figure 4.3.1 and shown in table 4.3.3 this increase in percentage dose absorbed in the knockout mice was significant ($p<0.05$) at the 30 minute time point. The increase in absorption in the absence of functional P-gp illustrates a role for the protein in limiting pulmonary absorption of eletriptan.

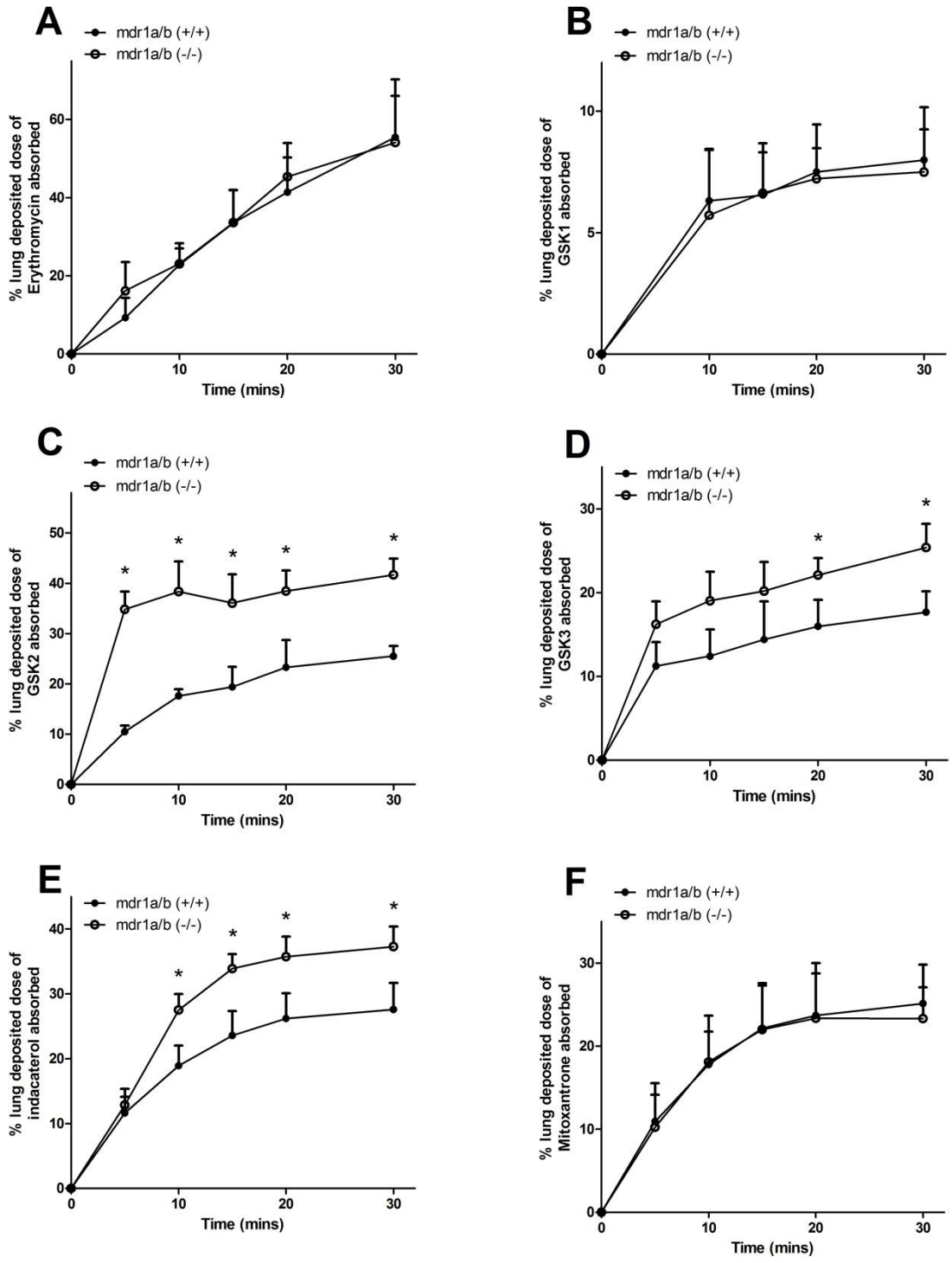

Figure 4.3.2 Absorption profiles from the airways of the IPML in to perfusate for both the wild-type mdr1a/b (+/+) mice and the knockout mdr1a/b (-/-) mice for **[A]** erythromycin (n=5), **[B]** GSK1 (n=5), **[C]** GSK2 (n=4), **[D]** GSK3 (2=6), **[E]** indacaterol (n=4) and **[F]** mitoxantrone (n=4). In all cases data is presented as the mean ± SD of the percentage of the lung deposited dose absorbed at distinct time points, * indicates a significant difference between the wild-type and knockout mice at that time point.

4.3.2.7 Pulmonary absorption of erythromycin

Following deposition of erythromycin in to the airways of wildtype FVB/B6 mice 55 % of the dose was absorbed within 30 minutes as determined by the increasing perfusate concentrations. In comparison the same experiments in the knockout *mdr1a/b* (-/-) mice showed a total of 54 % of the dose absorbed over the same time frame. As illustrated in figure 4.3.2 and shown in table 4.3.3 this increase in percentage dose absorbed in the knockout mice was not significant ($p>0.05$) at any time with the absorption curves in both the wild type and knockout mice being similar. The lack of an increase in absorption in the absence of functional P-gp suggests that the protein does not play a role in the absorption of erythromycin from the lung in this model.

4.3.2.8 Pulmonary absorption of GSK1

Following deposition of GSK1 in to the airways of wildtype FVB/B6 mice 8 % of the dose was absorbed within 30 minutes as determined by the increasing perfusate concentrations. In comparison the same experiments in the knockout *mdr1a/b* (-/-) mice also showed 7 % of the dose absorbed over the same time frame. As illustrated in figure 4.3.2 and shown in table 4.3.3 this increase in percentage dose absorbed in the knockout mice was not significant ($p>0.05$) at any time with the absorption curves in both the wild type and knockout mice being similar. The lack of an increase in absorption in the absence of functional P-gp suggests that the protein does not play a role in the absorption of GSK1 from the lung in this model.

4.3.2.9 Pulmonary absorption of GSK2

Following deposition of GSK2 in to the airways of wildtype FVB/B6 mice 26 % of the dose was absorbed within 30 minutes as determined by the increasing perfusate concentrations. In comparison the same experiments in the knockout *mdr1a/b* (-/-) mice showed a total of 42 % of the dose absorbed over the same time frame. As illustrated in figure 4.3.2 and shown in table 4.3.3 this increase in percentage dose absorbed in the knockout mice was significant ($p<0.05$) at all time points. The increase in absorption in the absence of functional P-gp illustrates a role for the protein in limiting pulmonary absorption of GSK2.

4.3.2.10 Pulmonary absorption of GSK3

Following deposition of GSK3 in to the airways of wildtype FVB/B6 mice 18 % of the dose was absorbed within 30 minutes as determined by the increasing perfusate concentrations. In comparison the same experiments in the knockout *mdr1a/b* (-/-) mice showed a total of 25 % of the dose absorbed over the same time frame. As illustrated in figure 4.3.2 and shown in table 4.3.3 this increase in percentage dose absorbed in the knockout mice was significant ($p<0.05$) at the 20 and 30 minute time points. The increase in absorption in the absence of functional P-gp illustrates a role for the protein in limiting pulmonary absorption of GSK3.

4.3.2.11 Pulmonary absorption of indacaterol

Following deposition of indacaterol in to the airways of wildtype FVB/B6 mice 28 % of the dose was absorbed within 30 minutes as determined by the increasing perfusate concentrations. In comparison the same experiments in the knockout *mdr1a/b* (-/-) mice showed a total of 37 % of the dose absorbed over the same time frame. As illustrated in figure 4.3.2 and shown in table 4.3.3 this increase in percentage dose absorbed in the knockout mice was significant ($p<0.05$) at all of the time points after and including 10 minutes. The increase in absorption in the absence of functional P-gp illustrates a role for the protein in limiting pulmonary absorption of indacaterol.

4.3.2.12 Pulmonary absorption of mitoxantrone

Following deposition of saquinavir in to the airways of wildtype FVB/B6 mice 25 % of the dose was absorbed within 30 minutes as determined by the increasing perfusate concentrations. In comparison the same experiments in the knockout *mdr1a/b* (-/-) mice also showed 23 % of the dose absorbed over the same time frame. As illustrated in figure 4.3.2 and shown in table 4.3.3 this increase in percentage dose absorbed in the knockout mice was not significant ($p>0.05$) at any time with the absorption curves in both the wild type and knockout mice being similar. The lack of an increase in absorption in the absence of functional P-gp suggests that the protein does not play a role in the absorption of mitoxantrone from the lung in this model.

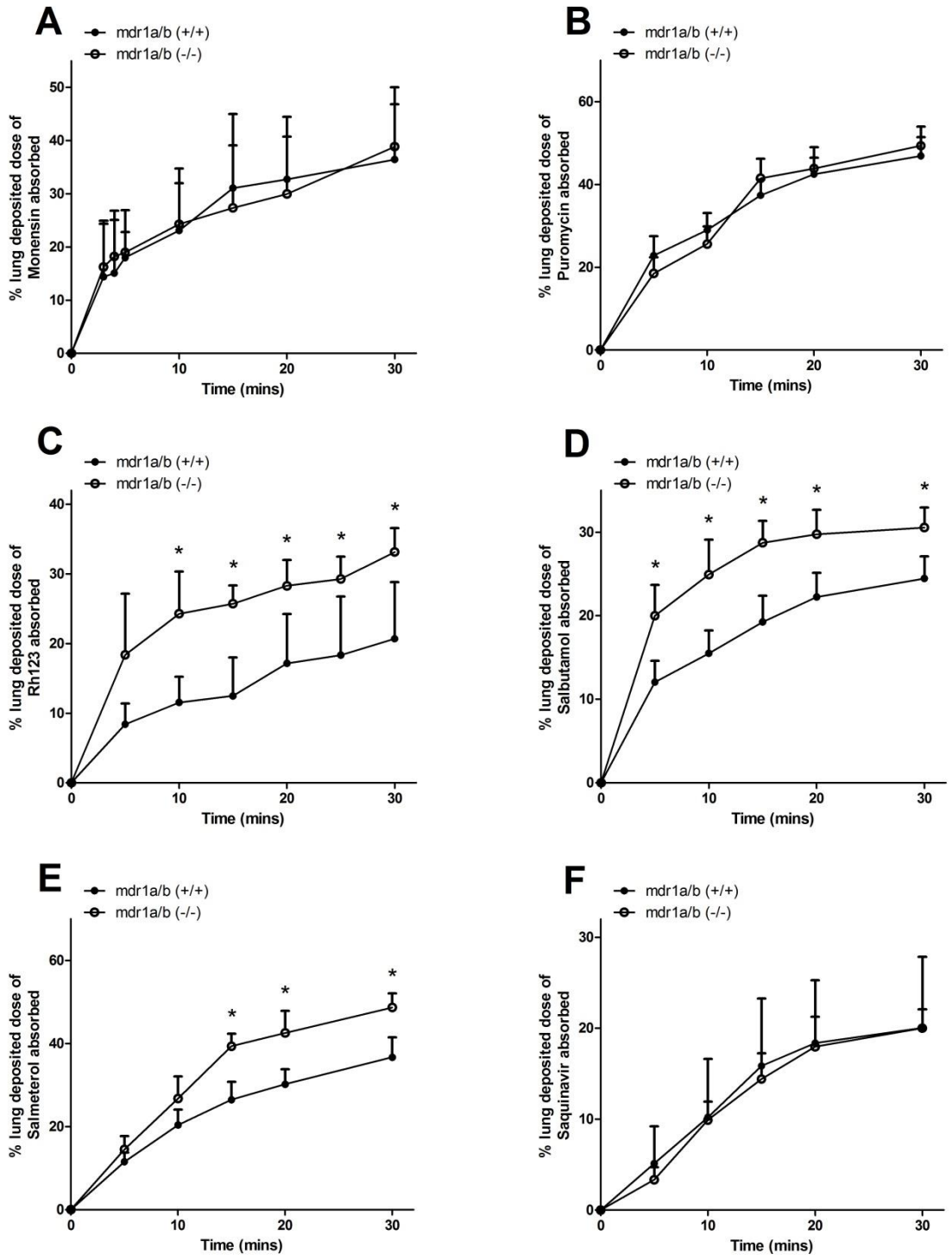

Figure 4.3.3 Absorption profiles from the airways of the IPML in to perfusate for both the wild-type mdr1a/b (+/+) mice and the knockout mdr1a/b (-/-) mice in **[A]** monensin (n=6), **[B]** puromycin (n=6), **[C]** rhodamine 123 (n=6), **[D]** salbutamol (n=4), **[E]** salmeterol (n=4) and **[F]** saquinavir (n=5). In all cases data is presented as the mean ± SD of the percentage of the lung deposited dose absorbed at distinct time points, * indicates a significant difference between the wild-type and knockout mice at that time point.

4.3.2.13 Pulmonary absorption of monensin

Following deposition of monensin in to the airways of wildtype FVB/B6 mice 36 % of the dose was absorbed within 30 minutes as determined by the increasing perfusate concentrations. In comparison the same experiments in the knockout *mdr1a/b* (-/-) mice showed a total of 39 % dose absorbed over the same time frame. As illustrated in figure 4.3.3 and shown in table 4.3.3 this increase in percentage dose absorbed in the knockout mice was not significant ($p>0.05$) at any time with the absorption curves in both the wild type and knockout mice being similar. The lack of an increase in absorption in the absence of functional P-gp suggests that the protein does not play a role in the absorption of monensin from the lung in this model.

4.3.2.14 Pulmonary absorption of puromycin

Following deposition of saquinavir in to the airways of wildtype FVB/B6 mice 47 % of the dose was absorbed within 30 minutes as determined by the increasing perfusate concentrations. In comparison the same experiments in the knockout *mdr1a/b* (-/-) mice also showed 49 % of the dose absorbed over the same time frame. As illustrated in figure 4.3.4 and shown in table 4.3.3 this increase in percentage of the dose absorbed in the knockout mice was not significant ($p>0.05$) at any time with the absorption curves in both the wild type and knockout mice being similar. The lack of an increase in absorption in the absence of functional P-gp suggests that the protein does not play a role in the absorption of puromycin from the lung in this model.

4.3.2.15 Pulmonary absorption of rhodamine 123

Following deposition of rhodamine 123 in to the airways of wildtype FVB/B6 mice 21 % of the dose was absorbed within 30 minutes as determined by the increasing perfusate concentrations. In comparison the same experiments in the knockout *mdr1a/b* (-/-) mice showed a total of 33 % of the dose absorbed over the same time frame. As illustrated in figure 4.3.1 and shown in table 4.3.3 this increase in the percentage of the dose absorbed in the knockout mice was significant ($p<0.05$) at time points after and including 10 minutes. The increased in absorption in the absence of functional P-gp illustrates a role for the protein in limiting pulmonary absorption of rhodamine 123.

4.3.2.16 Pulmonary absorption of salbutamol

Following deposition of salbutamol in to the airways of wildtype FVB/B6 mice 24 % of the dose was absorbed within 30 minutes as determined by the increasing perfusate concentrations. In comparison the same experiments in the knockout *mdr1a/b* (-/-) mice showed a total of 31 % dose of the absorbed over the same time frame. As illustrated in figure 4.3.1 and shown in table 4.3.3 this increase in the percentage of the dose absorbed in the knockout mice was significant ($p<0.05$) at all time points. The increase in absorption in the absence of functional P-gp illustrates a role for the protein in limiting pulmonary absorption of salbutamol.

4.3.2.17 Pulmonary absorption of salmeterol

Following deposition of salmeterol in to the airways of wildtype FVB/B6 mice 37 % of the dose was absorbed within 30 minutes as determined by the increasing perfusate concentrations. In comparison the same experiments in the knockout *mdr1a/b* (-/-) mice showed a total of 49 % of the dose absorbed over the same time frame. As illustrated in figure 4.3.2 and shown in table 4.3.3 this increase in percentage of the dose absorbed in the knockout mice was significant ($p<0.05$) at the 15, 20 and 30 minute time points. The increase in absorption in the absence of functional P-gp illustrates a role for the protein in limiting pulmonary absorption of salmeterol.

4.3.2.18 Pulmonary absorption of saquinavir

Following deposition of saquinavir in to the airways of wildtype FVB/B6 mice 20 % of the dose was absorbed within 30 minutes as determined by the increasing perfusate concentrations. In comparison the same experiments in the knockout *mdr1a/b* (-/-) mice also showed 20 % of the dose absorbed over the same time frame. As illustrated in figure 4.3.3 and shown in table 4.3.3 this increase in percentage dose absorbed in the knockout mice was not significant ($p>0.05$) at any time with the absorption curves in both experiments being similar. The lack of an increase in absorption in the absence of functional P-gp suggests that the protein does not play a role in the absorption of saquinavir from the lung in this model.

	Wildtype		Knockout		P-value
	% Dose Absorbed at 30 minutes	Standard Deviation	% Dose Absorbed at 30 minutes	Standard Deviation	
Acrivastine	12.3	2.2	13.1	4.0	0.742
Digoxin	40.1	5.1	41.8	2.0	0.591
Erythromycin	61.5	14.8	54.1	12.0	0.876
GSK1	8.0	1.3	7.5	2.7	0.747
Mitoxantrone	25.1	4.7	23.3	3.8	0.516
Monensin	40.8	10.4	38.9	11.1	0.731
Puromycin	46.9	4.5	49.3	4.6	0.425
Saquinavir	21.8	8.5	19.9	2.1	0.838
Chloroquine	42.9	6.2	64.6	16.2	0.046
Colchicine	17.7	2.5	25.4	2.8	0.006
Domperidone	28.3	4.0	43.7	7.6	0.008
Eletriptan	17.9	2.2	26.6	3.6	0.006
GSK2	25.5	2.0	41.7	3.2	0.001
GSK3	17.7	2.5	25.4	2.8	0.006
Indacaterol	27.6	4.1	37.3	3.1	0.009
Rhodamine 123	20.7	8.1	33.2	3.4	0.013
Salbutamol	24.5	2.6	30.5	2.4	0.014
Salmeterol	36.7	4.8	48.7	3.4	0.007

Table 4.3.3 The percentage of the total lung deposited dose absorbed within 30 minutes for all 18 P-gp substrates delivered to the airways of the IPML in both wild-type mdr1a/b (+/+) knockout mdr1a/b (-/-) mice. Compounds are split in to those which show no difference in the total percentage of dose absorbed at 30 minutes ($p > 0.05$) and those which show a significant difference ($p < 0.05$). Data is presented as the mean and standard deviation and an unpaired T-test was used to test for differences between the two groups.

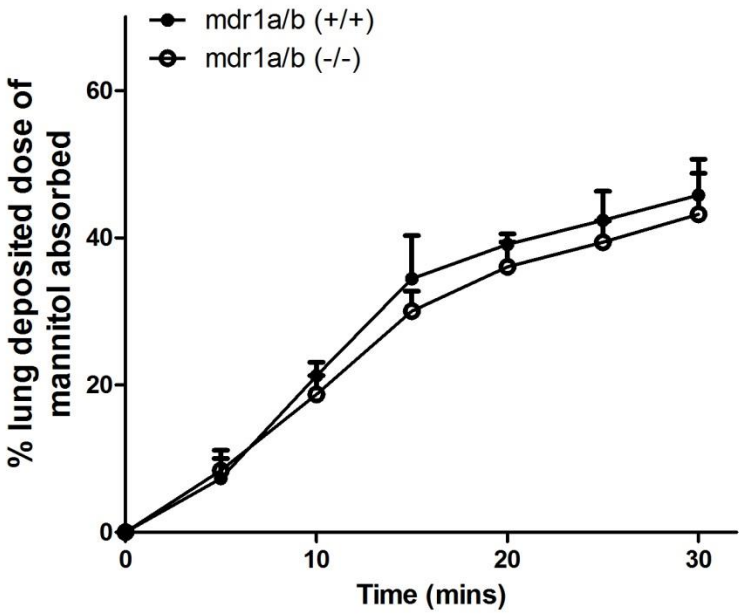

Figure 4.3.4 A representative plot of the absorption of [^{3}H]-mannitol from the airways of the IPML in both the mdr1a/b positive and negative mice. At no time point is a significant difference in the absorption of mannitol observed ($p > 0.05$). Data is presented as mean ± SD, n=12 for both groups.

All 18 substrates were co-dosed with [^{3}H]-mannitol (300 nM), a paracellular marker which is not a substrate for P-gp. Mannitol absorption was utilised as an internal control to ensure that the permeability of the lungs was comparable between the experimental groups. As can be seen in figure 4.3.4 an average of 43 % of the deposited mannitol dose was absorbed within 30 minutes (n=12), data from lungs which showed mannitol absorption within 32-44 % (i.e. one standard deviation from the mean) were deemed acceptable for the study; data from lungs with mannitol absorption outside this range were discarded.

It is the case that, for all 18 substrates, there is no difference in the absorption of the co-dosed mannitol between the wild type mdr1a/b (+/+) mice and the knockout mdr1a/b (-/-) mice. This is indicative of there being no difference in the permeability of the lungs of the wild type and knockout mice except the presence of P-gp, it is therefore assumed that any differences observed in the absorption profiles are as a result of P-gp attenuating the absorption of the substrates.

4.3.3 Pharmacokinetic Analysis

Substrate absorption profiles were analysed in WinNonlin, using a single compartment absorption model (equation in methods) to calculate bioavailability (F) and rate of absorption (K) for each profile (details in materials and methods). Data from the model can be seen in Appendix 1.1. It is apparent the calculations of K proved unreliable for a number of substrates with a very large variance evident in the results (Average % C_v= 52%), despite the model producing fits which, visually, appear to describe the data well. Values for F proved more reliable for all substrates with lower variance in the calculated values, however % covariance was still unacceptably high at an average of 26%. Attempts made to improve the variability seen in values of K and F generated by the model by applying either weighting or two-compartment modelling proved ineffective. Due to the unreliable values of K and F, the model could not be used to describe the absorption of substrates from the IPML.

As the single compartment model could not be used the absorption data was analysed using a non-compartmental model with a focus upon area under the curve (AUC) analysis limited to the timeframe of the experiment i.e. $AUC_{t(0\text{-}30)}$, in order to quantify the absorption profiles in regards to the total % of dose absorbed during the 30 minute experiment. The data obtained from the AUC calculations proved more consistent between experiments, with an average %C_v of 15% across all mice, showing it as a more reliable evaluation of absorption profile than the compartmental model.

Table 4.3.4 shows the AUC data for the 18 P-glycoprotein substrates investigated in both sets of mice. As is clear all 10 substrates which showed significant increases in the % dose absorbed at 30 minutes also showed significantly higher AUC values in the knockout mdr1a/b (-/-) mice.

	Wildtype		Knockout		P-value
	$AUC_{t(0-30)}$ (%.min)	Standard Deviation	$AUC_{t(0-30)}$ (%.min)	Standard Deviation	
Acrivastine	218	49	252	73	0.448
Digoxin	761	128	910	242	0.436
Erythromycin	1020	242	964	89	0.668
GSK1	176	36	168	59	0.809
Mitoxantrone	558	134	543	126	0.865
Monensin	910	301	722	213	0.678
Puromycin	999	78	1004	115	0.939
Saquinavir	342	74	350	56	0.509
Chloroquine	1277	172	1906	541	0.027
Colchicine	398	75	571	53	0.010
Domperidone	613	127	1059	257	0.018
Eletriptan	460	78	638	79	0.019
GSK2	540	62	1043	104	0.001
GSK3	399	80	570	50	0.011
GSK4	605	79	826	60	0.004
Rhodamine 123	376	59	712	71	0.003
Salbutamol	523	64	744	77	0.004
Salmeterol	702	90	965	93	0.006

Table 4.3.4 $AUC_{t(0-30)}$ values for the absorption for all 18 P-glycoprotein substrates tested in the wild-type and knockout mice IPML model. Substrates are split in to those which do not show a difference between the two groups ($p > 0.05$) and those which have significantly higher AUC values in the knockout mice ($p < 0.05$). All AUC data shown is the mean of each individual mouse experiment, presented with SD. An unpaired T-test was used to test for difference between the two groups, $p < 0.05$ taken as significantly different.

Ranking based on pulmonary absorption kinetics

The absorption of substrates from the airways of the knockout mdr1a/b (-/-) mice will be determined by the passive permeability of these molecules across the lung barrier, excluding possible active uptake mechanisms. As illustrated by table 4.3.5 the knockout $AUC_{t(0-30)}$ of the 8 molecules which do not show attenuation of absorption by P-gp is lower (average $AUC_{t(0-30)}$ = 614) than the 10 which were significantly affected (average $AUC_{t(0-30)}$ = 903) although this difference is not significant (p= 0.11).

The lack of significance between the knockout $AUC_{t(0-30)}$ of the affected and unaffected is reflected in the correlation between the knockout $AUC_{t(0-30)}$ and the ratio between the knockout and wild-type $AUC_{t(0-30)}$. This ratio shows the net effect of P-gp attenuation on absorption by calculating the percentage of the knockout $AUC_{t(0-30)}$ observed in the wild type animals; 100% indicates the two experimental groups possess identical $AUC_{t(0-30)}$, higher values indicate increased $AUC_{t(0-30)}$ for the knockout lungs in comparison to wild type. As illustrated in figure 4.3.4B the correlation between this ratio and the passive absorption from the lung (observed as knockout $AUC_{t(0-30)}$) is slightly positive but weak (r = 0.36) indicative of no true relationship between the variables. In the presence of P-gp (in the wild type mice) this weak correlation is completely abolished (r = -0.15).

	Wild type AUC (%.min)	Knockout AUC (%.min)	Ratio of knockout / wild type AUC (%)
Monensin	910	722	79
Erythromycin	1020	964	95
GSK1	176	168	95
Mitoxantrone	558	543	97
Puromycin	999	1004	100
Saquinavir	342	350	102
Acrivastine	218	252	116
Digoxin	761	910	120
GSK4	605	826	136
Salmeterol	702	965	138
Eletriptan	460	638	139
Salbutamol	523	744	142
GSK3	399	570	143
Colchicine	398	571	143
Chloroquine	1277	1906	149
Domperidone	613	1059	173
Rhodamine 123	376	712	189
GSK2	540	1043	193

Table 4.3.5 AUC values for the absorption profiles in the IPML in both the wild-type mdr1a/b (+/+) and knockout mdr1a/b (-/-) mice compared to the ratio of knockout to wild type AUC expressed as a percentage, substrates are ranked according to this ratio. AUC values are presented as means (SD is available in Table 4.3.4).

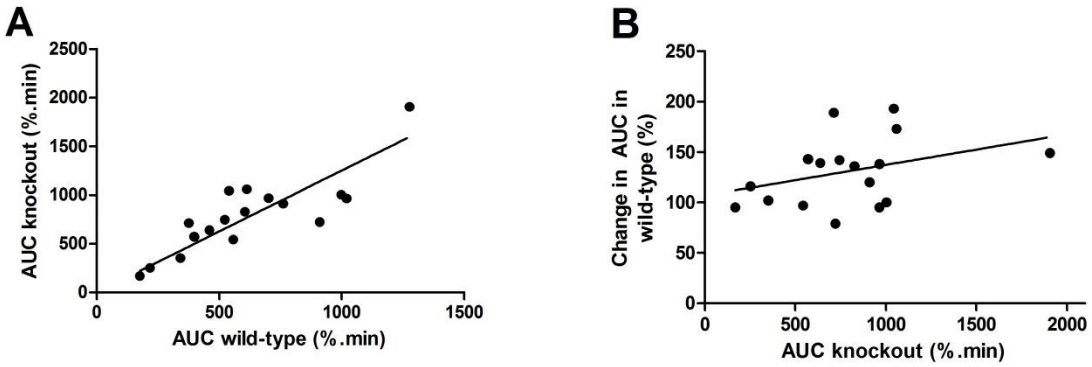

Figure 4.3.4 Correlations showing the relationships between **[A]** average AUC values from the IPML in the wild-type mdr1a/b (+/+) and knockout mdr1a/b (-/-) mice, **[B]** the average AUC in the knockout mdr1a/b (-/-) mice and the % change in AUC between the wild-type and knockout mice. All points represent average values with lines representing the line of best fit calculated by linear regression.

4.4. Discussion

P-glycoprotein (P-gp) has become one of the most intensely studied drug transporters since its discovery nearly 40 years ago (124). The protein's role in the PK/PD of a wide range of drugs is well documented with a functional role established at a large number of barriers including, but not exclusive to, the intestine, blood-brain barrier, kidney and liver. As described in detail in Chapter 3 it is now generally accepted that P-gp is expressed within the respiratory system (5), and specifically within the parenchyma of the lung. A number of immunohistochemical studies have been undertaken to identify more specifically the expression profile of P-gp within the lung and staining has been observed in both the bronchial and alveolar epithelium as well as in alveolar macrophages and endothelial tissue (110)(112)(111)(113).

In addition to these studies of expression there are examples of a functional role for P-gp in the lung. Using primary cell cultures form both human (115) and rat (110) lungs it has been shown that, at least in an *in vitro* situation, pulmonary P-gp expression does result in the efflux of substrates from cells expressed at the lung/blood barrier. In both studies polarised transport of known P-gp substrates was abolished by the addition of a selective P-gp chemical inhibitor, providing confirmation of the functional role of P-gp in these primary cell studies.

Despite the transporter being amongst the most well studied and characterised, there have been few studies investigating the effects of P-gp in an intact lung. In 2003 a study by the group of Kuhlmann *et al* investigated the accumulation of idarubicin in the lungs of rats after dosing via the circulation (118). The study showed that accumulation of the known P-gp substrate from the perfusate to the lung was increased with the addition of a P-gp inhibitor. This would imply that in the lung P-gp acts as an efflux pump minimising drug uptake into the lung, i.e. serving as a barrier for drug movement from blood to the lung tissue, , a finding which was supported by similar work in rabbit lungs a year later by a separate group (73) using rhodamine 6G as the model P-gp substrate. This finding has yet to be confirmed by another laboratory and is not supported by systemic pharmacokinetic studies, if indeed P-gp was acting in the blood to lung direction it would follow that we would observe reduced equilibrium partitioning in the lungs of P-gp deficient mice for P-gp substrates, a number of studies have shown this is not the case (125). Indeed the majority of literature evidence supports a role for P-gp acting basolaterally to apically in a large range of cell types in a number of tissues including but not limited to; hepatocytes, kidney proximal tubules, intestinal epithelial cells and the capillary endothelial cells of the blood-brain barrier (126)(111).

Within the lung itself P-gp has been localised to the apical surface of type I alveolar epithelial cells of both human and rat (115)(110) and polarised transport of the P-gp substrate etoposide has been shown in the basal to apical direction in isolated primary alveolar epithelial cells (110) as well as in the pulmonary Calu-3 cell line (127).

Two substrates tested as part of this study, rhodamine 123 and digoxin, have previously been the subject of studies to investigate the effect of pulmonary P-gp upon lung airway to blood absorption. However, the data from these studies appears contradictory in terms of the conclusions drawn about a role for pulmonary P-gp. Original work with rhodamine 123 utilised an isolated perfused rat lung and chemical inhibition with GF120918, a potent and selective P-gp inhibitor. The work showed a significant role for pulmonary efflux in the absorption of this well characterised substrate (22) characterised by increases in the rate and extent of rhodamine 123 absorption from the lung in the presence of the chemical inhibitor. Similar isolated perfused lung studies, however, have failed to show P-gp to attenuate the pulmonary absorption of digoxin. Specifically, in the latter work with digoxin it was observed that mice possessing a spontaneous deleterious mutation in mdr1a, i.e. CF1 mice only expressing mdr1b, showed no difference in the lung airway to circulation absorption profile compared to that of wild type mdr1a/b (+/+) CF1 mice (23). This study comes with the caveat that these spontaneous mutants still express mdr1b; which is expressed to a far greater extent, relative to mdr1a, in the lung than at other barriers (5). It is possible that that the lack of effect observed upon digoxin absorption could be due to residual mdr1b expression present in both experimental groups of mice. However, a later study by the same group makes this explanation unlikely; they performed a chemical inhibition study in rats, similar to that of the rhodamine 123 study, and again showed that inhibition of P-gp function did not alter the absorption of digoxin from the lung (24).

To address the apparent anomaly in the literature, studies in chapter 2 looked at the effect of chemical P-gp inhibition, utilising GF120918, on the absorption of both rhodamine 123 and digoxin as part of a multi species study (71). The absorption of rhodamine 123 and digoxin was assessed by chemical inhibition studies in both the isolated rat and mouse lung models. The results were similar to those found in the disparate literature studies, i.e. P-gp appears to have a significant role in attenuating the pulmonary absorption of rhodamine 123 but no effect on the absorption of digoxin. The 2013 study expanded upon the P-gp substrates studied with an additional investigation of the absorption of loperamide and saquinavir; the effect of P-gp upon the pulmonary absorption of these two substrates had not previously been investigated in an intact lung model. The results show

similar discordance to rhodamine 123 and digoxin, i.e. loperamide absorption was more rapid and extensive in the presence of GF120918 (i.e. affected by P-gp) whilst the absorption of erythromycin was unaffected by the inhibitor, i.e. unaffected by P-gp function. This indicated that discordances in the pulmonary effects of P-gp are seen across multiple, structurally diverse substrates.

It is possible that the apparent discrepancy seen between the absorption of substrates from the lung in the chemical inhibition studies is due to a non-P-gp mediated effect of the inhibitor; for example, if GF120918 was responsible for an off target effect, such as displacement of rhodamine 123 from intraluminal binding sites. The chemical and structural differences between the GF120918 (a highly lipophilic carboxamide) and rhodamine 123 and loperamide (both lipophilic amines) do, however, make competition for binding sites unlikely. The data presented here confirms that the chemical inhibitor is not the cause of discordance by utilising a genetic knockout and therefore removing the need for co-administration of GF120918. After dosing of rhodamine 123 to the airways of both mdr1a/b (+/+) and mdr1a/b (-/-) mice it is apparent that the absorption is attenuated in the wild-type controls in comparison to the knockout mice, as observed by a lower percentage of the deposited dose absorbed and a lower AUC (tables 4.3.3 and 4). This observation, similar to the chemical inhibition studies discussed earlier, provides evidence of a functional role for P-gp in attenuating the absorption of rhodamine 123.

Previous studies have shown the lack of mdr1a/b in mice to have no significant biological effect (93); with the exception of increased levels of CYP3A proteins (128). If an increase in cytochrome levels were resulting in a difference in absorption from the lung it would be predicted to decrease absorption by increasing the rate of metabolism, an effect contrary to that observed here where an increase in absorption from the knockout mice was observed. It is unlikely the increased absorption of select P-gp substrates in lungs of the knockout mice is due to a general increase in the permeability of the lungs as a result of the genetic knockout of mda1a/1b. The similarity in the barrier permeability properties between the wild type and knockout mice is supported by permeability data for the absorption of the paracellular probe, mannitol. This molecule is not a P-gp substrate, and was included as a constituent of the dose in all studies reported in this thesis. It was found that there was no difference in mannitol absorption between the wild type and knockout mice. This is indicative of comparable physiologic permeability between the experimental mice groups except for transport pathways involving a P-gp mechanism. It should also be re-emphasised that the very fact that different P-gp substrates appear to be affected to a greater or lesser (inc. no effect) extent with P-gp knockout implies involvement of a specific underlying mechanism. Further,

using the genetic knockout mice we show a lack of effect of P-gp functionality upon the absorption of digoxin from the airways in the IPML model, a finding consistent with the previous literature utilising chemical inhibition. The similarity between the absorption profiles of both the mdr1a/b (+/+) wild type and mdr1a/b (-/-) knockouts provides additional evidence that the lungs of the P-gp deficient mice do not show a generally increased permeability.

The above data on the discordance between the absorption of rhodamine 123 and digoxin using both chemical and genetic inhibition in two separate species, confirmed the discrepancy seen in the literature to be a real biological phenomenon. However, the mechanism underlying the difference between the absorption of the two substrates is not clear. In order to gain an improved understanding of the structure-activity relationship (SAR) involved we undertook studies with a larger panel of substrates to identify how the physicochemical properties of the molecules may drive differences in the absorption from the lung in comparison to the intestine.

The 18 substrates within the panel (including rhodamine 123 and digoxin) represent a diverse spectrum of physicochemical properties. The panel included six inhaled drugs representing molecules that have already gained approval for pulmonary delivery (i.e. salbutamol, salmeterol and indacaterol) or were currently in development (GSK1 – 3) as respiratory therapeutics. Their inclusion provides a close-to-practice context to the SAR profiling (129). The remainder of the 18 member panel are non-inhaled P-gp substrates chosen for their diversity in physicochemical characteristics. All molecules in the panel show P-gp mediated efflux from the intestine and cell culture models (130,131)(GSK data, unpublished)

The absorption data for all IPML experiments were analysed initially using a single compartment pharmacokinetic (PK) model to identify values for the bioavailability (F) and absorption rate constant (K) (graphs showing the fit of the non-linear regression are in Appendix 1). This compartmental modelling has been used previously in defining absorptive PK parameters in rat IPL experiments (22). However, it is clear that for this current dataset in the IPML the calculations of K proved unreliable in a number of substrates with very large and unacceptable variance in the results (average % C_v= 52.2%). This is due to both the large standard deviations in the early time points of some absorption profiles where the drug levels in perfusate were below or around the limit of quantification, as well as the sampling strategy which included too few early time points to adequately explain the initial absorption phase. This is despite the compartmental model producing visually good fits to the data, as can be seen in Appendix 1. The values for F proved more reliable due to the greater dependence

for this parameter on the later time points; however the percentage covariance at 25.6 % was still too high to prove reliable for analysis. This was not improved by implementing various weighting schemes ($1/_{Cobs}$, $1/Cobs^2$ or the $C_{predicted}$ equivalents) or the use of a more complicated two compartmental model. As the compartmental modelling approach could not be used to analyse the IPML absorption data a non-compartmental approach was utilised using area under the curve (AUC) analysis to describe the data. Due to the short duration of the experiments it is assumed that metabolism and chemical degradation, and that other mechanisms of loss, e.g. binding to plastic tubing are negligible. With these assumptions the AUC of the absorption profiles when limited to the first 30 minutes of experiment will be dependent upon the rate at which drugs are absorbed from the airways; note the perfusate reservoir is an accumulating 'compartment' solely. Indeed for the substrates tested where reliable analysis of early time points was observed, the AUC data correlates well with the absorption rate constant (K) calculated by compartmental models.

Of the six inhaled drugs only one, GSK1, showed no difference in absorption between the wild-type and mdr1a/b (-/-), i.e. appears unaffected by P-gp, this substrate was also absorbed to the lowest extent of any of the molecules tested (Tables 4.3.3-4), a finding consistent with data observed in previous isolated rat lug models (GSK data, personal communication). The five remaining inhaled drugs, including the three currently marketed beta-adrenoreceptor agonists, all showed increases in absorption in the knockout mdr1a/b (-/-) mice in comparison to the wild-type; this is the first evidence of P-gp acting to attenuate the absorption of these molecules from an intact lung, although P-gp has been observed to attenuate the absorption of salbutamol following oral dosing (132). All three beta-adrenoreceptor agonists have previously been identified as P-gp substrates: salbutamol in the rat intestine study mentioned above and salmeterol by MDCK-MDR1 bidirectional assays (133) in which polarised transport was abolished by co-dosing with verapamil (a known P-gp inhibitor); data for the affinity of indacaterol to P-gp is from internal GSK studies (GSK data, personal communication) and is reaffirmed again in this current work.

Previous studies in the literature have reported on the absorption of salbutamol following both inhaled and oral dosing. In the intestine it has been observed that following oral dosing the absorption of salbutamol is poor, with a low extent of bioavailability and peak plasma concentrations at two to four hours post dosing (134). More recent work has identified the effect of P-gp efflux to contribute to this poor intestinal absorption. A study by Valenzuela *et al.* showed that the intestinal absorption of salbutamol was saturable and increased 2-3 fold by co-dosing with verapamil (a molecule often used as a competitive P-gp inhibitor) (131,135). Although in this current

work we see attenuation of the pulmonary absorption of salbutamol by P-gp following inhaled dosing, it would seem that the net effect of P-gp on the pharmacokinetics of salbutamol in the lung is less pronounced than that observed by Valenzuela in the intestine. Indeed even in the presence of P-gp lung absorption of salbutamol is shown to remain both rapid and high with peak plasma levels observed as soon as 12 minutes after dosing (136).

It is unclear how these observed changes in the PK of inhaled drugs will affect, if at all, local pulmonary PD. Current inhaled therapies are generally limited to molecules acting locally within the lung (with the noted exception of inhaled anaesthetics) and therefore improvements in therapeutic outcome are observed with increases in pulmonary bioavailability, i.e. the rate and extent at which drugs reach the sites of action within the lung. Current improvements for local pulmonary bioavailability are mainly due to improvements in the delivery device resulting in increased deposition within the lungs as opposed to the oropharynx from where they are swallowed leading to systemic exposure (137–139). Lung retention (and therefore pulmonary bioavailability) is also improved by the use of drugs able to form lipid conjugates, such as corticosteroids with a hydroxyl group in the 21 position (140). The lipid-drug conjugates are not active but also not absorbed from the lung (141). As the ester bond formed in their creation is reversible this results in them acting as a slow-release reservoir within the lung tissue (142). An example of this is the absorption of budesonide, 20 minutes post inhalation 80% of the budesonide remaining in the lungs is conjugated, increasing the lipophilicity of the drug up to 10,000 fold and therefore causing tissue retention (143).

It is possible that P-gp could be used in a similar manner to reduce the rate of absorption from the lung and increase lung retention. For example, the attenuation of the absorption of ten substrates in the panel (including the three inhaled beta-adrenoreceptor agonists) is most simply described by P-gp efflux from the apical membrane of the alveolar epithelial cells in to the lumen of the airways. The result of this is slower absorption rates across the epithelia following inhaled dosing and therefore increased luminal residence time of the drug. For drugs with sites of action in the airways of the lung (such as anti-infectives) this could result in improved drug exposure and increases in the time spent above minimal effective concentrations following inhaled dosing. Currently, anti-infectives for pulmonary infections are commonly dosed either orally or intravenously and the PK-PD in relation to the clearance of lung infections has been well studied following these dosing strategies (144–146). However, despite the lack of literature upon the PK and PD of anti-infectives following inhaled dosing it would seem apparent that direct dosing of the lung via an inhaled dose would result in increased local concentrations of drug within the lung, lower efficacious doses and reduced

systemic exposure and side-effects, in a manner consistent with that observed for the corticosteroids. This being the case, P-gp efflux within the lung could be utilised to improve exposure times by developing drugs which are also pulmonary P-gp substrates. This would likely have the added bonus of reducing intestinal absorption and therefore reducing negative systemic effects caused by absorption after swallowing.

For drugs with sites of action downstream of epithelial absorption (such as the beta-adrenoreceptor agonists in the panel) P-gp appears to be acting to both slow and decrease the extent of exposure of the drug to the binding sites, potentially limiting their efficacy. However, it must be said that inferring PD relationships from measurements of drug perfusate concentrations may be poorly predictive. It has been argued that the measurements of PK using systemic bioavailability markers (such as plasma or blood levels) may not be predictive of PD for these locally acting lung molecules (147). Considerations on why systemic drug concentrations may generally not be predictive for pulmonary PK-PD of drugs with local sites of action include: plasma drug concentrations that will be downstream of those in the lung tissue itself and potentially dependent upon multi-phasic pulmonary absorption processes; drug disposition in the lung influenced by depot effects and non-absorptive processes; local lung efficacy potentially driven by drug concentrations exclusively in the lung, or by a combination of lung and plasma drug concentrations.

With effects of P-gp activity upon the PK of over half the substrates within the panel the question arises as to why this discordance occurs – a question that will be repeatedly challenged throughout this thesis, both experimentally and philosophically. The current understanding is that the efficiency of the efflux for a given P-gp substrate is dependent not only upon the substrate's affinity to the transporter but also by its transmembrane movement rate. Molecules which show higher rates of transmembrane movement tend to show a lower net effect of P-gp mediated efflux (130,148) This has been observed *in vivo* in the intestine where substrates with high passive permeability (such as verapamil) are not affected to a significant extent by P-gp, whereas the absorption of those (such as digoxin) which show slower absorption rates are significantly attenuated by P-gp efflux. However, this relationship does not appear to explain the differential impact of P-gp functionality for the pulmonary absorption data of our panel.

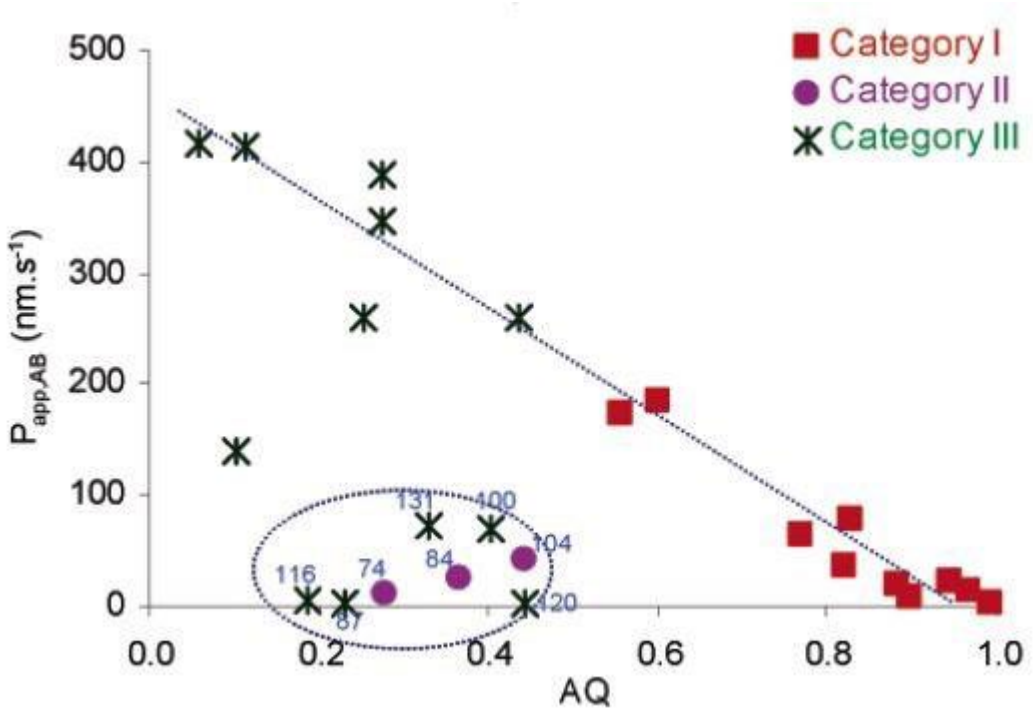

FIGURE 4.4.1 A graph showing the inverse linear relationship observed between the intestinal permeability of the molecule ($P_{appA.B}$) and the net effect of P-gp on intestinal transport (AQ). The substrates are split in to 3 categories in descending order of the effect of P-gp observed in *in* vitro studies, i.e. category 1 showed the highest effect of efflux. The graph is adapted from work by Varma *et al.* (130).

We found a positive correlation (Figure 4.3.4 B) between molecule absorption from the lungs of the P-gp knockout mice (a measure of the molecules' passive absorption) and the ratio of knockout to wild type absorption (a measure of the attenuation by P-gp of pulmonary absorption), a finding which contrasts to the negative relationship we would have predicted based upon intestinal data from the literature. As is seen in figure 4.4.1 previous literature studies would suggest that in the intestine we would expect to see less of an impact of P-gp for those molecules which show the greater passive absorption capacity. This would corroborate discordant physiologic determinants between P-gp attenuation of absorption in the lung and intestine and would evoke additional factors in the lung not entirely explainable by a substrate's transmembrane movement rate or membrane residence time. The difference may instead be due to structural differences between the two barriers such as the relative prevalence of the paracellular pathway in the lung in comparison to the intestine (149), or differences in P-gp binding kinetics between the substrates and their interplay with the different P-gp expression levels between the two barriers, both investigated more fully in later chapters. Further, it is not explained by saturation of the P-gp transporter itself. For example some of the substrates unaffected by P-gp in the lung, e.g. digoxin, were delivered as a radiolabelled

dose of only 16 pmol (i.e. 315 nM in the ELF based upon an ELF volume of 25µL) and therefore far below the concentrations required for saturation; one of the molecules affected by P-gp in the lung, for example rhodamine 123, would similarly be predicted to have achieved ELF levels of approximately 25 µM. This is discussed further in chapter 5 where the binding kinetics of the substrates is explored more fully.

Taken together the comparison in absorption profiles between the knockout and control mice for the 18 substrate panel confirms the discordance seen in the earlier literature and expands upon the observations across a diverse range of compounds. In total 10 of the substrates exhibited enhanced absorption in the absence of P-gp, including five which are either currently marketed inhaled drugs or in development, whilst eight were unaffected by its presence, including one inhaled drug development candidate. This makes clear that the attenuation of pulmonary absorption by P-gp is a necessary consideration during the development of inhaled drugs. However, as is shown by the absorption of salbutamol the attenuation by P-gp is likely to be quantitatively less than that observed in the intestine, and still allows for considerable absorption. The effect on the PK-PD of an inhaled drug may be dependent upon its site of action and there is a potential for utilising efflux to increase the exposure time of drugs acting locally in the airways.

Subsequent to the absorption studies it was discovered that the absorption of acrivastine was influenced by active uptake processes in the intestine (150). The presence of an active component in the uptake of acrivastine provides a route of uptake which avoids interaction with P-gp and providing a possible explanation for the lack of pulmonary efflux seen with this substrate. Due to the confounding nature of acrivastine absorption it was removed from the panel for future experiments.

The presence of eight substrates within the dataset which do not show P-gp mediated attenuated absorption from the lung (despite previous literature suggesting they are effluxed in the intestine) highlights the difference in the functional impact of P-gp at these two barriers. The 18 substrates presented here can now form the backbone of a study of the mechanism of this discordance whilst also providing the first evidence of an effect of P-gp upon the absorption of drugs which are currently delivered to the lung.

Chapter 5

Ussing chamber permeability and P-gp binding kinetics

5.1 Introduction

5.1.1 Intestinal P-gp expression

Intestinal P-gp has been shown to affect the bioavailability of a wide range of P-gp substrates following oral dosing. The prevalence of the oral route as a dosing strategy has meant intestinal P-gp is one of the most important and extensively studied areas of research for the interplay between transporter proteins and pharmacokinetics.

Spatial expression of P-gp within the intestine

There are many examples in the literature of P-gp substrates with observed oral bioavailabilities far below those predicted by their passive permeability. The expression of P-gp has been localised to the apical membranes of the columnar epithelial cells which constitute the majority of the surface area of the intestine (151). The localisation of P-gp to the apical surface of the intestines was achieved using a mouse monoclonal antibody (MRK16) in normal human tissue. The presence of P-gp on the apical surface of epithelial cells is corroborated by a similar study in the *in vitro* Caco-2 cell line. Using the same monoclonal antibody P-gp was observed on the apical membrane of the Caco-2 cells (152).

The localisation of P-gp on the apical surface of intestinal epithelia cells results in the expulsion of substrates from the cells in to the lumen of the intestine and therefore explains the poor bioavailability of many substrates following oral dosing. Attenuation of absorption by P-gp in the intestines is not consistent throughout their length; there is a body of literature suggesting that P-gp expression generally increases towards the distal end of the intestine.

Gene expression in the intestine

There is a body of evidence for an uneven intestinal P-gp expression generated by measuring the concentration of mRNA in the segments of the guts of both rats and humans. In 1996, Fricker *et al*. provided an early analysis of the intestinal expression of P-gp in three segments of human intestines (i.e. stomach, jejunum and colon) (153). The results showed a general increase in P-gp expression towards the distal intestines with levels in the colon>jejunum>stomach. The functional effect of this

trend in P-gp expression was assessed by its effect on the absorption of cyclosporine A. The inverse correlation of the absorption of this P-gp substrate with the levels of P-gp expression is striking with absorption in the stomach>jejunum>colon.

The increase in mRNA concentrations towards the distal intestine by the early studies has been refined by a number of groups in both rat and human intestines, two species which appear to show similar intestinal distributions of P-gp. The literature would suggest that the highest expression levels of P-gp are found in the ileum, indeed in the study by Brady *et al.* the expression levels of mdr1a in the rat ileum were the highest of all organs investigated, higher than those in the brain, liver or kidneys (109). High levels have also been observed in the jejunum (in particular the distal jejunum) and the colon with considerably lower expression in the duodenum (5,154–157). It appears the pattern of P-gp expression is one where the expression levels are increased with proximity to the ileum, i.e. ileum>jejunum/colon>duodenum.

Protein expression in the intestine

As well as the studies of mRNA levels within the segments of the small intestine there have been several immunohistochemical (IHC) studies which investigate the spatial expression of P-gp within the intestines of both rats and humans. All of the studies identified P-gp expression within the intestines in a manner consistent with the distribution of P-gp mRNA.

In 2003 Mouly and Paine performed a Western blot analysis of a series of mucosal scrapings from human intestine (158). They found P-gp expression generally increased from the proximal to distal terminus of the small intestine in all 4 of the individual intestines studied, i.e. ileum>jejunum>duodenum. Interestingly, the group also identified significant inter-individual variation with regards to the extent of P-gp expression in the intestines highlighting the possible importance of P-gp expression and its influence on the inter-individual variations observed in oral bioavailability of a number of drugs in humans.

A similar study by the group of Berggren *et al.* provides further evidence for the distribution pattern of P-gp protein observed by Mouly and Paine (155). The group identified an increase in protein concentration by Western blot that correlated with proximity to the ileum, that is to say expression levels in the ileum>colon>jejunum.

In an attempt to improve the resolution of the understanding of the spacial distribution of P-gp in the intestines a more recent study investigated the levels of protein present throughout the entire length of the intestine with smaller segments (159). The group of MacLean *et al.* divided the intestine of rats into successive 3 cm segments along its entire length. The levels of P-gp present in the homogenates of each of these was then analysed by Western blot analysis, figure 5.1.1. The increased resolution afforded by the use of the many small successive segments clearly illustrates the concentration of high levels of P-gp expression at the terminal jejunum and ileum with a considerably lower expression in the duodenum, terminal jejunum and colon. Variability in the location of the cuts used to divide the intestinal segments in the earlier analysis (for example if a section of ileum was included in the colon segment or if the proximal jejunum was used instead of the distal) may explain differences seen in the P-gp distribution patterns seen in the early experiments

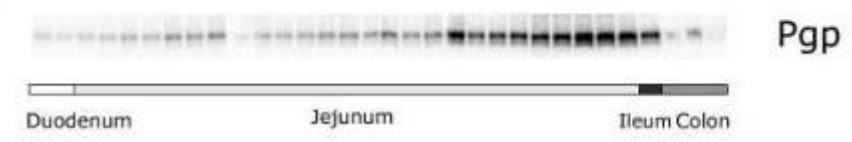

Figure 5.1.1 The expression levels of P-gp (mdr1a) across the entire length of the rat small intestine. Increased expression of P-gp was observed at the distal end of the jejunum. Figure adapted from MacLean *et al.* (159).

Functional evidence of the P-gp spatial distribution

The spatial distribution of P-gp identified in the genetic and protein investigations discussed above has been shown to result in variance in the absorption of P-gp substrates in the different segments of the intestine. For example, the absorption of tacrolimus from rat ileum segments is enhanced by the addition of a P-gp inhibitor (160) suggesting that the absorption of tacrolimus from the ileum is attenuated by P-gp. Conversely, the addition of the inhibitor to absorption studies in the jejunum segments did not enhance tacrolimus absorption. The lack of significant P-gp efflux witnessed in the jejunum can be explained by the lower levels the transporter protein present in this gut segment.

In a similar study Valenzuela *et al.* observed an active and saturable process which resulted in the attenuation of salbutamol from an *in situ* perfused rat small intestine (161). The group investigated the active process seen in the whole intestine by the separate isolation of the proximal, distal and colon segments of the rat intestines. Absorption studies were conducted in the separate segments in the presence and absence of verapamil (a known P-gp inhibitor). The addition of verapamil was shown to have no influence on the absorption of salbutamol from the proximal (duodenum) and colon segments but resulted in a significant increase in absorption in the proximal segment (jejunum and ileum). The group then compared the results from the absorption experiments to mRNA levels of P-gp in each of the segments and showed they correlated well with P-gp expression levels (132).

The functional implications of the P-gp distribution in the intestine have also been shown for the absorption of rhodamine 123. In a manner consistent with the absorption experiments of salbutamol and tacrolimus the absorption of rhodamine 123 has been shown to be attenuated in the ileum. This is despite no efflux observed in the duodenum of the same animals (162).

5.1.2 Balancing intestinal P-gp efflux and passive permeability

There is now a large body of work in the literature confirming a role for P-gp in limiting the oral absorption of a wide range of drugs. In spite of this there are a number of drugs which have been shown to be uninfluenced by the transporter following oral dosing despite being highlighted as substrates by various *in vitro* assays (163). It is apparent that the P-gp efflux mechanism and the passive permeability of a substrate operate in an opposite direction to influence the overall absorption and both influence overall bioavailability. This indicates that the permeability of substrates across the intestine is determined by the passive influx rate minus the P-gp efflux rate. Therefore it can be assumed that the lack of an effect of P-gp on the absorption of a subset of substrates is the result of high passive permeability masking a relatively minimal efflux by P-gp.

Mechanism of the interplay between P-gp efflux and passive permeability

Substrates for P-gp tend to be amphipathic and hydrophobic in nature and therefore interact extensively with membrane compartments. This results in a high concentration of substrate in the outer leaflet of the epithelial membrane acting as a drug pool for absorption with a relatively low concentration of substrate in the cytoplasm (164). Any substrate transported from the "pool" in the extracellular membrane will be immediately replaced by free substrate from the intraluminal medium.

Transmembrane movement of these hydrophobic substrate-type drugs has been shown to occur via distinct flip-flop events and not by a gradual diffusion process across the lipid core (165). The frequency of these flip-flop events is the rate limiting step in the transmembrane absorption of these drugs with a wide range of frequencies observed. For example the transmembrane movement of rhodamine 123 has been shown to occur by flip-flop events with an average frequency of 3 minutes, i.e. on average a rhodamine 123 molecule will inhabit the external membrane for 3 minutes before a flip-flop events results in absorption to the inner leaflet (166). Other molecules (such as verapamil and doxorubicin) possess much faster flip-flop rates (165).

The result of these flip-flop events is a relatively high concentration in the inner membrane leaflet and a concentration gradient to the cytoplasm. Due to the hydrophobic nature of the substrates the absorption in to the cytoplasm is via the adsorption to molecular sinks such as anthracyclines. The concentration present in these molecular sinks is in constant equilibrium with the inner membrane leaflet.

The crystal structure of P-gp has shown that this drug transporter recruits substrates directly from the inner leaflet (167). After association with a substrate P-gp functions as a flippase transferring the molecule to the outer leaflet of the membrane (168).

If the rate of the flippase activity of P-gp transporting substrates from the inner leaflet to the external is higher than the passive flip-flop rate of absorption then P-gp will function to exclude the substrate from the cell. The result of this is a lower cytoplasmic concentration of substrate in P-gp expressing cells and therefore a decreased rate of release from the basal membrane due to the lower diffusion gradient.

Conversely, as the flip-flop rate of the substrates is increased the net effect of P-gp is decreased to a negligible point as the absorption from the substrate pool in the outer leaflet becomes considerably faster than P-gp mediated efflux. In this instance the effect of P-gp does not influence the

intracellular concentrations of substrate and therefore does not slow the absorption across the intestinal barrier. P-gp substrates which show rapid flip-flop rates and whose absorption is subsequently unaffected by P-gp, for example verapamil, have been shown to be good P-gp inhibitors.

The importance of a substrate's passive permeability upon the net effect of P-gp absorption stresses the important of substrate characteristics which affect passive permeability. It is possible the discordance seen in the effect of P-gp upon the absorption of the panel of substrates from the IPML may not decrease the functional significance of P-gp within the lung. Rather it may be highlighting the intricate relationship between the passive absorption of a molecules and P-gp efflux.

5.1.3 Experimental objectives

In chapter 4 the absorption of a panel of substrates was investigated in the IPML and discordance was observed in the effect of P-gp upon their absorption. A subset of the molecules showed enhanced absorption in the absence of functional P-gp whereas another showed no difference in either its presence or absence. In the intestine there is a body of literature supporting a similar discordance in relation to the passive permeability of a substrate.

This chapter aims to investigate the absorption of the panel of substrates from the intestines of wild type and mdr1a/b (-/-) mice in order to draw comparisons between the effects of P-gp upon their absorption at both barriers. This should provide evidence towards the underlying mechanism responsible for the discordant effects of P-gp observed in the absorption of the panel from the lung.

Further the specific binding kinetics of the substrates within the panel to P-gp will be investigated. This will allow the determination of whether the discordance seen in the lung is due to substrate specific interactions with the transporter, i.e. saturation.

5.2 Materials and Methods

5.2.1 Ussing Chamber studies of intestinal absorption

Ussing chamber equipment

Tissue diffusion chambers; product 66-0036 (Harvard Apparatus, MA, USA)

Vertical diffusion chamber system with heating block and gas manifold; product 66-0048 (Harvard Apparatus, MA, USA)

NaviCyte Ag/AgCl electrodes; product 66-0023 (Harvard Apparatus, MA, USA)

Epithelial voltage clamp; product EC-800 (Harvard Apparatus, MA, USA)

Physiological buffer – materials

D-glucose anhydrous; $C_6H_{12}O_6$, (Fisher Scientific, Loughborough, UK, G/0450/60)

Potassium chloride; KCl, (Fisher Scientific, Loughborough, UK, Cat: P/4280/53)

Magnesium sulphate heptahydrate; $MgSO_4.7H_2O$, (Fisher Scientific, Loughborough, UK, Cat: M/0600/53)

Sodium bicarbonate; $NaHCO_3$, (Fisher Scientific, Loughborough, UK, Cat: S/4200/60)

Calcium chloride dihydrate; $CaCl_2.2H_2O$, (Fisher Scientific, Loughborough, UK, Cat: C/1500/50)

Sodium chloride; NaCl, (Fisher Scientific, Loughborough, UK, Cat: S/3105/63)

Potassium dihydrogen phosphate; KH_2PO_4, (Fisher Scientific, Loughborough, UK, Cat: P/4800/53)

Physiological buffer – method

The buffer used throughout the Ussing chamber experiments was a protein-free Krebs-Henseleit (pH 7.4) (KH), similar to that used in the IPRL experiments. The buffer was made by the same protocol as that for the IPRL perfusate with the omission of bovine serum albumin. Buffer was made at least 12 hours before an experiment (overnight) and used no later than 48 hours after production.

Animals

Male pathogen-free FVB/Bl6 mice, which were bred on site as per chapter 3, were used throughout the experiments. The breeding program produced two distinct groups of FVB/Bl6 mice, the first fully expressed wild type levels of mdr1a and mdr1b (mdr1a/b (+/+)) and the second group were knockouts, with no functional expression of these genes (mdr1a/b (-/-)). The mice were housed in temperature and humidity controlled rooms (19-21 ^{o}C and 40-60 % humidity) with a 12 hour dark-light cycle. All mice had access to food and water *ad libitum* and were acclimatised for at least 24 hours following transport from the breeding facility to the experimental laboratories. All animal experiments were performed in adherence to the Animal (Scientific Procedures) Act 1986 and were approved by Cardiff University and GSK, Stevenage.

Doses

The P-gp substrates used for dosing to the Ussing chapter studies are the same as those utilised in the IPML model in chapter 4. Digoxin was delivered as a ^{3}[H]-radiolabelled dose, all others were administered as non-radiolabelled compound.

The final dose concentrations used in the Ussing chambers was chosen to match those used in the IPML model (50 µM for non-radiolabelled substrates and 0.25 Ci and 16.7 pmol or 600 nM for radiolabelled digoxin). As a 5-fold dilution of the dose occurred during the dosing of Ussing chamber experiments initial doses were made at 250 µM for non-radiolabelled drugs and 3000 nM for ^{3}[H]-digoxin. Non-radiolabelled doses were prepared from 10 mg/mL stocks in DMSO by dilution in KH buffer. The relevant volume of DMSO was added during the dilution to result in a final DMSO concentration of 0.5 %.

Radiolabelled doses of digoxin were prepared by drying the relevant volume of ^{3}[H]-digoxin (stored as a solution in ethanol) overnight. After evaporation of the ethanol, KH and DMSO were added to result in a final dose composition similar to that of the previous doses.

Preparation

Before surgery the circulating water bath attached to the diffusion chamber system is started in order to equilibrate the system at 37 ^{o}C.

Surgery and experimental setup

In order to reduce the animal usage during the experiments intestinal segments were obtained from the mice sacrificed for the IPML experiments. During the setup of the IPML there is an equilibration period for the lungs during which the intestines are removed by sharp incision and bathed in ice cold KH.

During the interval of the 5-10 minute time points of the IPML the intestinal segments are suspended in the Ussing chambers. The entire length of the small intestine is held by tweezers and the third (by length) nearest to the colon is removed by sharp incision. This distal third is then flushed with cold KH to remove faeces. The cleaned intestinal segment is then cut in to 3 x 1 cm long segments avoiding any visible Peyer's patches.

The 1 cm segments are then opened longitudinally and fixed to the Navicyte diffusion chambers by the four pins around the opening. The intestinal segments are fixed so the epithelial surface of the intestine is facing the dosing compartment. The diffusion chambers are then assembled and secured using the retaining ring before being inserted in to the heated diffusion chamber system. Five mL of warmed KH (37 ^{o}C) was added to each side of the diffusion chambers in alternate 1 mL intervals. It has been suggested that the addition of a large volume to one side of the chamber whilst the other is empty may result in damage to the intestinal segment. The gas supply to the 3 diffusion chambers is then attached and the intestinal segments allowed to equilibrate in the device for 10 minutes.

Following equilibration, a measurement of the transepithelial electrical resistance (TEER) was recorded. To record TEER the gas supply was temporarily removed and the 2x voltage and 2x current electrodes were placed in the chambers. The TEER of the intestinal segment was then determined according to Ohm's law using the epithelial voltage clamp. TEER measurements were taken hourly during the experiment and also at the termination of the experiment to determine membrane integrity throughout. After the measurements of TEER were conducted the gas supply was reconnected to the chambers.

Dosing of the Ussing chambers was achieved by replacing 1 mL of KH in the dosing chamber with 1 mL of KH + dose (as described above). The solution in the dosing chamber was mixed by the action of the gas supply, this creates a circulation of buffer in both the donor and receiver compartments.

At intervals the solution in the receiver compartment was sampled (sampling was performed at 0, 30, 60, 90, 120 and 180 min) by removing 1 mL of the buffer. The buffer was immediately replaced with fresh KH (37 ^{o}C).

Buffer samples were then analysed by either HPLC-MS/MS or liquid scintillation as described in chapter 4. The results of the 3 intestinal segments from each animal were averaged and a total of 4 wild type and 4 mdr1a/b (-/-) mice were used for each substrate in the panel.

In all experiments viability of the tissue throughout the experiment was assessed by the decrease in TEER. A terminal TEER value of 80 % or more of that observed at the beginning of the experiment was taken to indicate viability throughout the experiment in accordance with previous literature (169).

The absorptive apparent permeability coefficients (P_{app}) for the transport across the intestinal segments were then calculated according to Eq.1.

$P_{app} = (dQ/dt)/(A*C_0)$ (1)

Where dQ/dt is the rate of transport observed across the 180 minute experiment, A is the surface area of the intestinal segment exposed in the experiment (0.12 cm^2) and C_0 is the initial donor concentration of the drug.

5.2.2 *In-vitro* assessment of P-gp binding kinetics

Materials

Gentest ATPase Assay Kit; product 459006 (Corning, Germany)

Human P-gp membranes; product 453228 (Corning, Germany)

Murine mdr1a membranes; product 453252 (Corning, Germany)

Murine mdr1b membranes; product 453250 (Corning, Germany)

Method

The Corning ATPase assay kit was utilised to investigate the specific binding kinetics of the panel of substrates to human and murine P-gp. The kit measures the accumulation of P^i produced in the breakdown of ATP to ADP as a measure of P-gp activation.

The kit was used in accordance with the manufacturer's protocol for the evaluation of K_m and V_{MAX}. In summary, test compounds were serially diluted across a concentration range of 0-900 µM (resulting in a final assay concentration of 0-300 µM) in assay buffer. The test compound

concentration range was added 4 rows of a 96-well plate (columns 3-12) (20 µL per well). Columns 1 and 2 contained a phosphate standard curve of 0-150 mM.

The first two rows of the test compounds were incubated with 20 µL of a P-gp membrane solution (90 µL of 5 mg/ml membranes, 13.5 µL of H_2O and 346.5 µL of assay buffer). The remaining two rows were incubated with 20 µL of a similar solution but with the inclusion of the P-gp inhibitor sodium orthovanadate (NaOV) (90 µL of 5 mg/ml membranes, 13.5 µL of NaOV and 346.5 µL of assay buffer). The 96-well plate was incubated at 37^{o}C for 5 minutes.

	STANDARD (mM)		CTRL	SERIAL DILUTIONS OF TEST COMPOUNDS (µM)								
	1	2	3	4	5	6	7	8	9	10	11	12	
A	150	150	Ctrl 1	300	150	75	37.5	18.75	9.375	4.68	2.34	1.17	Test compound 1
B	120	120	Ctrl 1	300	150	75	37.5	18.75	9.375	4.68	2.34	1.17	
C	90	90	Ctrl 2	300	150	75	37.5	18.75	9.375	4.68	2.34	1.17	Test compound 1 +NaOV
D	60	60	Ctrl 2	300	150	75	37.5	18.75	9.375	4.68	2.34	1.17	
E	30	30	Ctrl 1	300	150	75	37.5	18.75	9.375	4.68	2.34	1.17	Test compound 2
F	9	9	Ctrl 1	300	150	75	37.5	18.75	9.375	4.68	2.34	1.17	
G	3	3	Ctrl 2	300	150	75	37.5	18.75	9.375	4.68	2.34	1.17	Test compound 2 +NaOV
H	0	0	Ctrl 2	300	150	75	37.5	18.75	9.375	4.68	2.34	1.17	

Figure 5.2.2 The summarised layout of the 96-well plates prior to the 30 minute incubation step. Layout is copied from the Quickstart guide for the assay kit.

After incubation, 20 µL of the ATP stock solution (10 mM) was added to each of the test compound wells to initiate P-gp activity. The plate was then incubated with gentle shaking at 37 ^{o}C for 30 minutes.

After the secondary incubation, the assay was stopped by the addition of 30 µL of the Assay Stop Solution (SDS) and the colorimetric reagent was added. A final 37 ^{o}C incubation of 20 minutes was then performed to allow the colour change to occur. The assay was then analysed by quantifying the colour change as the absorbance of each well on a spectrophotometer at 800 nm.

The absorbance of the two sets of duplicates was averaged and the absorbance of the NaOV control was subtracted to measure the vanadate sensitive phosphate release. The corrected absorbance readings were then compared to the P^{i} standard curve to determine the concentration of phosphate

in each well. As these had been corrected to account for non-P-gp related breakdown of ATP the concentration of P^i in the well was a measure of P-gp activity.

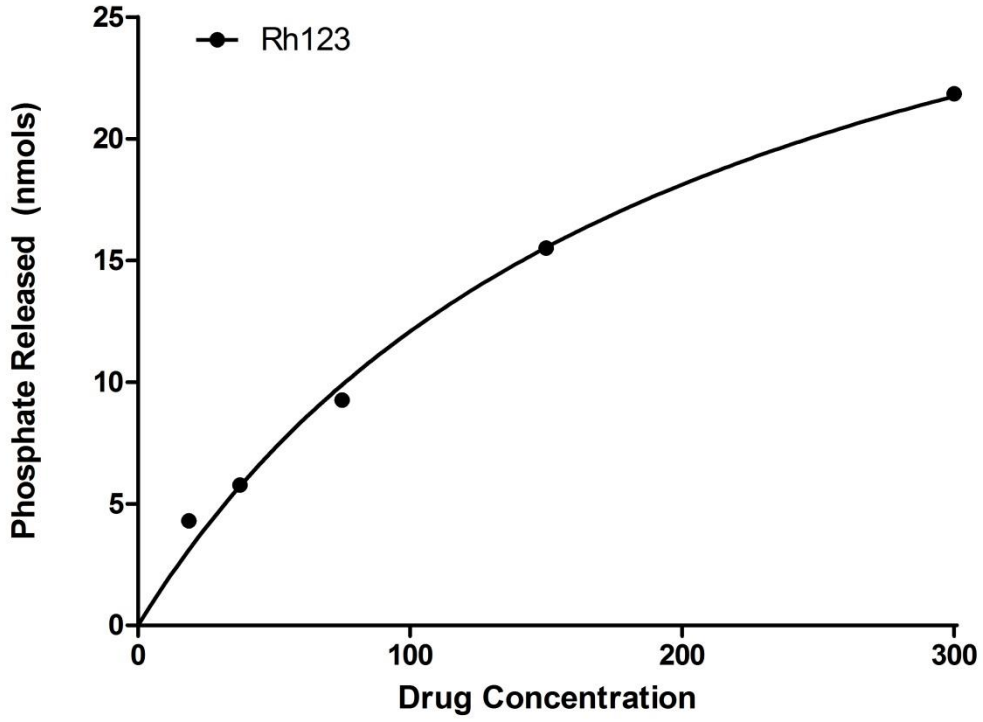

Figure 5.2.3 A representative graph of the non-linear Michaelis-Menten fit applied to the ATPase data for rhodamine 123 for the calculation of K_m and V_{MAX}.

The amount of phosphate released at each test compound concentration was used to calculate the enzyme binding kinetics. Graphs were generated in GraphPad Prism and analysed using Michaelis-Menten kinetics to determine the K_m and V_{MAX} for each substrate in the panel. An example of the Michaelis-Menten fit to the ATPase data is shown in figure 5.2.3.

5.3 Results

5.3.1 Ussing chamber studies of intestinal absorption

Tissue viability

In the Ussing chamber absorption experiments tissue viability was assessed using the transepithelial electrical resistance (TEER) values of the intestinal segment. At the beginning of the experiments initial TEER values averaged 82 ± 23 $\Omega.cm^2$, tissue segments which presented a TEER value lower than 40 $\Omega.cm^2$ were considered poorly viable and discarded. This TEER value cut-off is in agreement with previous Ussing studies in mouse intestines (170,171). In a similar manner any experiment which showed a 15 % or greater decrease in TEER during the timeframe of the experiment was discarded.

Using a 15 % decrease in TEER as a marker for loss of tissue viability early experiments showed that tissue in the Ussing chambers was viable for a minimum of 3.5 hours after suspension of the intestinal segment in the chamber. As absorption experiments were performed over a 3 hour time frame no intestinal segment showed a 15 % drop in TEER during an absorption experiment.

General permeability – influence of P-gp knockout

In a manner consistent with that seen in the IPML model, the loss of functional P-gp in the mdr1a/b (-/-) mice did not result in a change in the general barrier properties of the intestine as measured by TEER. Across all experiments there was no significant difference in the TEER values observed in the wild type or mdr1a/b (-/-) mice (TEER = 83 ± 21 and 79 ±19 $\Omega.cm^2$, respectively).

Intestinal absorption of the substrate panel – effect of P-gp knockout

In order to elucidate the role of P-gp in the intestinal absorption of the panel of substrates the absorption of each was investigated in an Ussing chamber model. Comparative studies in the FVB/B6 wild type and mdr1a/b (-/-) mouse intestinal segments were conducted to define the extent of the attenuation of absorption by P-gp in this model.

		Wild type mice			Mdr1a/b (-/-) mice			Fold-difference	P-value
1	acrivastine	91.67	±	28.67	143.23	±	28.84	1.56	0.044
2	digoxin	60.42	±	14.63	209.38	±	29.39	3.47	0.0001
3	erythromycin	30.21	±	11.47	136.98	±	45.37	4.53	0.004
4	GSK1	31.25	±	12.50	105.73	±	32.29	3.38	0.005
5	mitoxantrone	46.88	±	10.55	136.98	±	26.92	2.92	0.001
6	monensin	109.38	±	17.80	190.63	±	24.09	1.74	0.002
7	puromycin	58.33	±	23.81	149.48	±	23.28	2.56	0.002
8	saquinavir	15.63	±	6.91	157.29	±	35.21	10.07	0.0002
9	chloroquine	149.48	±	23.28	233.85	±	41.82	1.56	0.012
10	colchicine	69.27	±	31.47	149.48	±	31.84	2.16	0.012
11	domperidone	107.81	±	17.71	254.17	±	80.38	2.36	0.012
12	eletriptan	48.96	±	25.09	110.42	±	21.65	2.26	0.010
13	GSK2	81.77	±	23.28	175.0	±	29.1	7.59	0.002
14	GSK3	122.40	±	22.53	153.13	±	22.47	1.25	0.102
15	indacaterol	152.08	±	27.85	292.19	±	43.98	1.92	0.002
16	rh123	90.63	±	18.12	225.52	±	22.40	2.49	0.0001
17	salbutamol	105.73	±	23.03	148.96	±	21.62	1.41	0.034
18	salmeterol	158.33	±	21.58	183.33	±	23.75	1.16	0.170

Table 5.3.1 The apparent permeability of the panel of substrates (P_{app}) observed in the Ussing chamber model using intestinal segments of both the wild type and mdr1a/b (-/-) mice. Data are presented as mean ± S.D, n=4.

Permeability data from the Ussing chamber absorption experiments shows significantly increased permeability in the mdr1a/b (-/-) intestines for 16 of the 18 substrates in the panel. The permeability of salmeterol and GSK3 showed no significant difference between the two mice strains, table 5.3.1. The data suggests that P-gp in the intestine attenuates the absorption of the panel of substrates with the exception of salmeterol and GSK3. In all experiments the general permeability of the lung was identical between the two groups of mice as evidenced by the measurements of TEER during the experiments.

It is of note that the absorption of the two substrates which do not show P-gp mediated attenuation of absorption in the intestine is affected in the lung, i.e. both salmeterol and GSK3 show increased pulmonary absorption in the knockout mice.

Comparison of intestinal and lung permeability

In order to investigate the mechanism behind the discordance seen in the pulmonary absorption of the panel of substrates their permeability in the lung and intestine was compared.

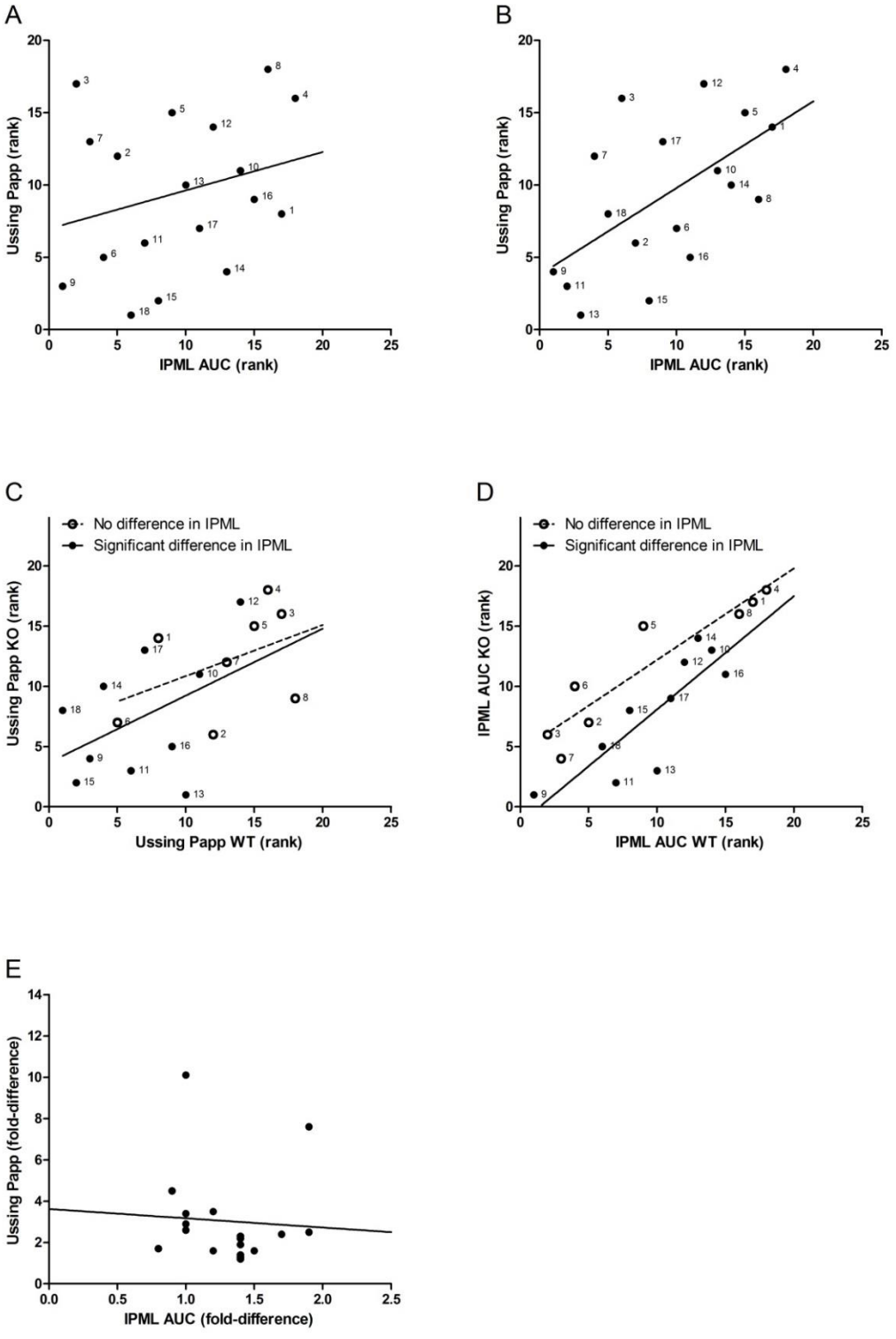

Figure 5.3.1 Legend on following page.

Correlations between the IPML model and the Ussing intestinal segments. Scatter plots illustrating correlations between IPML model and the Ussing intestinal absorption model in terms of the ranked absorption (A-D) or absolute absorption (E) parameters for the 18 molecules investigated. All correlations were undertaken using a linear regression model shown graphically by the solid or dashed lines. (A-B) Correlation between the ranked AUC data from the IPML model and the ranked P_{app} data from the Ussing intestinal model: (A) in wild type animals (P-glycoprotein positive) where linear regression shows a weak correlation (r^2= 0.07, P= 0.29); (B) in mdr1a/b (-/-) (P-glycoprotein negative) animals where the correlation is stronger and significantly non-zero (r^2= 0.36, P= 0.009). (C-D) Correlation between the ranked absorption parameters in wild type animals and the relevant mdr1a/b (-/-) knockouts with the substrates split in two groups based upon whether significant efflux was evident (solid line) or not evident (dashed line) in the IPML; (C) correlation in the ranks in the Ussing intestinal absorption model between wild type and knockout mice (r^2= 0.19 P= 0.27 efflux evident in IPML ; r^2= 0.20 P= 0.19 efflux not evident in IPML). (D) correlation in the ranks in the IPML absorption model between wildtype and knockout mice (r^2= 0.86 P= 0.0009 efflux evident in IPML ; r^2= 0.71 P= 0.002 efflux not evident in IPML). (E) Correlation between the fold-difference in absorption between the wild type and mdr1a/b (-/-) knockout mice in the IPML and Ussing intestinal absorption models (r^2= 0.004, P= 0.80). Compound numbers used in the graph refer to the order of compounds in table 5.3.1.

It is apparent that in the absence of P-gp (in the knockout mice) the permeability of the substrates in the lung and intestine is correlated and significantly non-zero (r^2= 0.36, P= 0.009). In the presence of P-gp this correlation in the permeability of the barriers is lost (r^2= 0.07, P= 0.29) (figure 5.3.1A-B). If P-gp affected the absorption of the panel to a similar extent at both barriers the correlation would have been maintained in the wild type mice, its loss shows the discordant effect of P-gp upon the absorption of the substrates at the two barriers.

This discordance is highlighted when the correlations are split in two groups based upon whether significant efflux was observed in the IPML (figure 5.3.1C-D). In the comparison of the IPML permeability in wild type and knockout lungs the split is expectedly clear and the two groups distinct. When the same criteria are used to split the correlation of the permeability in the intestine the distinction is lost. The effect of P-gp on the intestinal absorption of the substrates which showed a significant efflux in the IPML is not distinct from those which were unaffected in the lung. This suggests that increased P-gp efflux in the lung is not predictive of increased efflux in the intestine and *vice versa*. Indeed there is no correlation between the magnitude of the effect of P-gp in the lung and the intestine (figure 5.3.1D).

5.3.2 In vitro P-gp binding kinetics

As previously discussed, the net effect of P-gp upon the absorption of its substrates is dependent upon the passive permeability of the substrate and its affinity to P-gp. An *in vitro* ATPase assay was used to quantify the affinity of the substrate panel to P-gp and investigate the relationship between P-gp binding kinetics and efflux in the lung and intestine and determine if differences in binding kinetics explained the discordance seen in the IPML.

The binding kinetics of the substrates were investigated in human P-gp and both forms of mouse P-gp (mdr1a and mdr1b). With the exception of digoxin the calculated K_m values for both mdr1a and mdr1b are similar to those obtained for human P-gp suggesting similar substrate affinity between the different proteins. None of the 16 substrates showed more than a 3-fold positive or negative change in K_m between the human and mouse forms of P-gp. However, the K_m for digoxin was considerably lower for human P-gp than either mouse P-gp (there was a 17-fold increase in mdr1a over human P-gp and a 13-fold increase in mdr1b). This suggests that digoxin possesses a higher affinity for human P-gp than either of the mouse proteins.

When the panel is split in two groups dependent upon the effect of P-gp upon the absorption from the IPML there is no significant difference in the P-gp binding kinetics of the two groups for any of the three proteins (table 5.3.3).

	Human (MDR1)		Mouse (mdr1a)		Mouse (mdr1b)	
	V_{MAX} (μM/min)	K_m (μM)	V_{MAX} (μM /min)	K_m (μM)	V_{MAX} (μM /min)	K_m (μM)
Digoxin	19.7	1.7	26.7	29.3	44.1	22.5
Erythromycin	19.3	116.1	28.4	64.2	48.5	78.7
GSK1	63.4	2.8	81.0	1.5	62.0	5.9
Mitoxantrone	32.2	4.6	27.5	9.1	35.0	6.4
Monensin	15.6	14.8	27.6	22.0	42.3	30.6
Puromycin	19.6	12.1	16.5	18.9	31.5	14.0
Saquinavir	41.3	24.9	39.5	31.7	47.1	32.0
Chloroquine	3.1	13.2	12.5	8.6	17.0	11.5
Colchicine	16.6	15.4	22.7	9.1	28.4	7.7
Domperidone	37.7	122.6	21.7	74.0	32.2	52.0
Eletriptan	42.2	91.5	32.6	45.6	76.1	58.1
GSK2	79.3	21.0	89.1	12.0	63.2	19.8
GSK3	19.2	34.3	15.3	45.1	22.7	31.5
GSK4	81.1	16.6	119.5	34.2	131.9	18.8
Rh123	36.3	2.2	35.2	6.0	29.7	2.2
Salbutamol	45.6	9.5	52.3	8.7	49.1	6.1
Salmeterol	24.4	15.3	27.5	12.7	38.2	14.8

Table 5.3.2 The enzyme binding kinetics obtained from the *in vitro* ATPase model using the Michaelis-Menten model. Substrates are split based upon whether efflux was observed in the IPML, the top seven molecules showed absorption from the IPML which was unaffected by P-gp, the lower ten showed increased pulmonary absorption in mdr1a/b (-/-) mice.

	Human (MDR1)	Mouse (mdr1a)	Mouse (mdr1b)
No difference in the IPML	25.3 ± 17.3	25.2 ± 21.2	44.4 ± 25.1
Significant difference in the IPML	38.5 ± 25.5	42.8 ± 35.0	48.8 ± 34.5

Table 5.3.3 Average K_m values for the binding kinetics of the panel when split in two groups dependent upon the effect of P-gp upon pulmonary absorption in the IPML. Data are presented as mean ± S.D.

The lack of a difference between the binding kinetics of the affected and unaffected groups provides evidence that the lack of efflux seen in seven of the substrates was not due to saturation of P-gp. The data presented here would suggest that if saturation of P-gp had occurred for the group which showed no effect of P-gp upon pulmonary absorption it would also have been present in the group whose absorption was attenuated. It is therefore assumed that the discordance in the pulmonary absorption of the two groups is not due to the saturation of P-gp.

5.4 Discussion

The use of an Ussing chamber provides a powerful and well validated tool for the investigation of intestinal absorption. The method was originally developed by Hans H. Ussing in the 1960's to measure the active transport of NaCl and has since been adapted and well utilised for the study of active transport processes.

Although originally developed as a technique for measuring electrochemical processes and solute transport the technique has now been well used for the study of the effects of P-gp on intestinal absorption. In 2002 Stephens *et al.* used an Ussing chamber model to investigate the effects of P-gp upon the absorption of digoxin, paclitaxel and etoposide from the ileum of mdr1a (-/-) mice (171). The validation of the model for use with the P-gp deficient mice showed that the absence of P-gp did not affect the permeability of the intestine. The absorption of the paracellular markers mannitol and propranolol were unchanged between the knockout and wild type mice and the two strains also showed indistinguishable TEER values throughout the experiments. This is a finding in agreement with the observations here which also suggest the mdr1a/b (-/-) mice do not show altered barrier properties. The group then compared the absorption of all three substrates in both A:B and B:A in both strains of mice. The results for digoxin and paclitaxel showed that in the wild type mice the absorption across the intestine was polarised (efflux ratios of 10 and 17, respectively) and the polarisation was lost in the knockout mice. This is strong evidence to support both the role of P-gp in the efflux of these substrates in the intestine and the suitability of the Ussing chamber model for identifying efflux at this barrier. The results for etoposide showed reduced but not eliminated polarised transport in the knockout mice. As the residual efflux of etoposide was subsequently abolished by an inhibitor of MRP it was concluded that the molecule was effluxed by both transporters in the intestine.

The Ussing model has also been used to identify the role of P-gp on intestinal absorption using chemical inhibition. P-gp inhibition has been shown to increase the permeability of a range of substrates in the intestine (170,172).

The model utilised here for the study of intestinal P-gp has been adapted from those utilised previously in the literature. Many Ussing chamber preparations of intestine require the stripping of the smooth muscle layer to identify absorption processes at the epithelia. For mouse intestines this process requires specialised equipment and a highly skilled operator due to the size of the barrier

(169). The study discussed above which investigated intestinal absorption in P-gp deficient mice utilised unstrapped intestinal segments. Data from this group provides evidence that the stripping is not necessary for mouse intestines as it was shown that unstrapped mouse intestines produce absorption data which is in agreement with data generated from stripped rat intestines (171). The intestines utilised in this chapter were not stripped of the smooth muscle layer.

As discussed in the introduction, the expression of P-gp is not even throughout the small intestine, rather it is concentrated around the distal jejunum and ileum. Therefore experiments conducted here used intestinal segments from the distal third of the small intestines. Due to the necessity of obtaining triplicate 1 cm intestinal segments from each mouse it was not possible to utilise only the ileum in the experiments. By utilising the most distal third of the small intestine we attempted to conduct our experiments with the intestinal region most relevant for P-gp efflux.

In order to investigate the discordance observed in the effects of P-gp upon the absorption of the panel of substrates from the IPML it is important to establish whether this discordance is lung specific. The substrates selected for the panel had all been shown to possess decreased oral bioavailability in the presence of P-gp (130) and here we corroborate this by determining the effect of intestinal P-gp on the absorption of the whole panel in a single experiment.

Permeability data from the Ussing chamber model implicated P-gp in the absorption of 15 of the 17 substrates in the panel. These 15 substrates all showed enhanced permeability in the knockout mdr1a/b (-/-) mice in comparison to wild type. Conversely, the absorption of salmeterol and GSK3 showed no difference between the two mice strains suggesting that P-gp did not affect the intestinal absorption of these substrates. It is of note that both salmeterol and GSK3 showed P-gp attenuated absorption from the IPML.

It is clear that the discordant effects of P-gp observed in the IPML are not replicated at the intestinal barrier. The 7 molecules which showed no attenuation of absorption by P-gp in the lung all showed increased intestinal permeability in the mdr1a/b (-/-) mice.

In the absence of P-gp (i.e. in the knockout mice) a correlation is observed between the absorption of the panel at both barriers, those molecules most highly absorbed from the IPML are more likely to be highly absorbed in the intestine. This correlation is lost in the presence of P-gp. If the effects of intestinal P-gp on the absorption of the panel mirrored those observed in pulmonary absorption we

would expect to have seen this correlation maintained. The loss of the correlation suggests that the factors which determine the net effect of P-gp efflux in the intestine are distinct from those in the lung.

This is corroborated by directly comparing the net effect of P-gp (measured as fold-difference in AUC between wild type and knockout mice) at both barriers. If it was the case that the net effect of P-gp was determined by the same parameters at both barriers, we would see a strong positive correlation between the net effect of P-gp in the lung and in the intestine. Instead there is no correlation observed (r^2= 0.004) showing that a high extent of efflux from the intestine is not predictive of efflux from the lung.

It is generally accepted that P-gp expression is lower in the lung than in the intestine (5,109) and it is therefore possible that a concentration of substrate which allows efflux in the intestine could saturate P-gp in the lung. It is therefore feasible that the subset of substrates from the panel which show no efflux from the lung do so because they saturate pulmonary P-gp. The evaluation of the binding kinetics of the panel of substrates with mdr1a and mdr1b could be seen to support this. The dose delivered to the mouse lung for all substrates except digoxin would result in approximately 25 µM of the drug in the ELF, for many of the substrates presented here the calculated K_m values are below this concentration. However, saturation is unlikely to explain the discordance observed in the pulmonary absorption of the panel. One of the molecules which showed no effect of P-gp upon its pulmonary absorption (digoxin) was delivered as a radiolabelled dose at nanomolar concentrations, approximately 100-fold lower than K_m. Saturation cannot be responsible for the lack of efflux seen with digoxin.

Saturation is also unlikely to explain the lack of pulmonary efflux in the remaining six molecules. It is obvious that the 10 substrates which showed efflux in the IPML did not saturate P-gp. As the six remaining un-effluxed substrates were dosed at the same concentrations as these ten, saturation would only occur if they had higher affinity to P-gp. This is not observed in the enzyme binding kinetics determined here. Here we show that there is no difference in the enzyme binding kinetics of both groups of substrates (those which show pulmonary efflux and those which do not) in either mdr1a or mdr1b.

As discussed in the introduction, the net effect of P-gp efflux upon the absorption of a substrate is a complex process influenced by both the passive permeability of the substrate and the efficiency of P-

gp at excluding it from the cell. In the intestine this is shown to result in a situation where the oral bioavailability of substrates which show moderate or low passive absorption across the intestine is limited by P-gp. Conversely, there is a set of P-gp substrates which show high passive absorption and decrease the effect of P-gp efflux to a negligible level. Due to the nature of P-gp substrates those with high intestinal passive absorption tend to be molecules which show rapid absorption across membranes, i.e. have a high transmembrane movement rate. The physicochemical factors which predict high transmembrane movement rates are discussed more fully in chapter 6.

It seems feasible that the discordance between the effects of pulmonary and intestinal P-gp could be due to differences in the passive permeability of the substrates at both barriers. In particular a prominent difference between the two barriers is the permeability of the paracellular pathway (149).

The paracellular pathway in the lung is generally accepted to be more permeable to the absorption of a range of hydrophilic compounds than that of the intestine. Work compiling a number of *in vivo* studies from the literature has shown that an inverse linear relationship between the MW and clearance rate of a range of hydrophilic compounds form the lung (173). The fact that the clearance rate from the lung is determined by the MW of a molecule implies that it is a passive diffusion process.

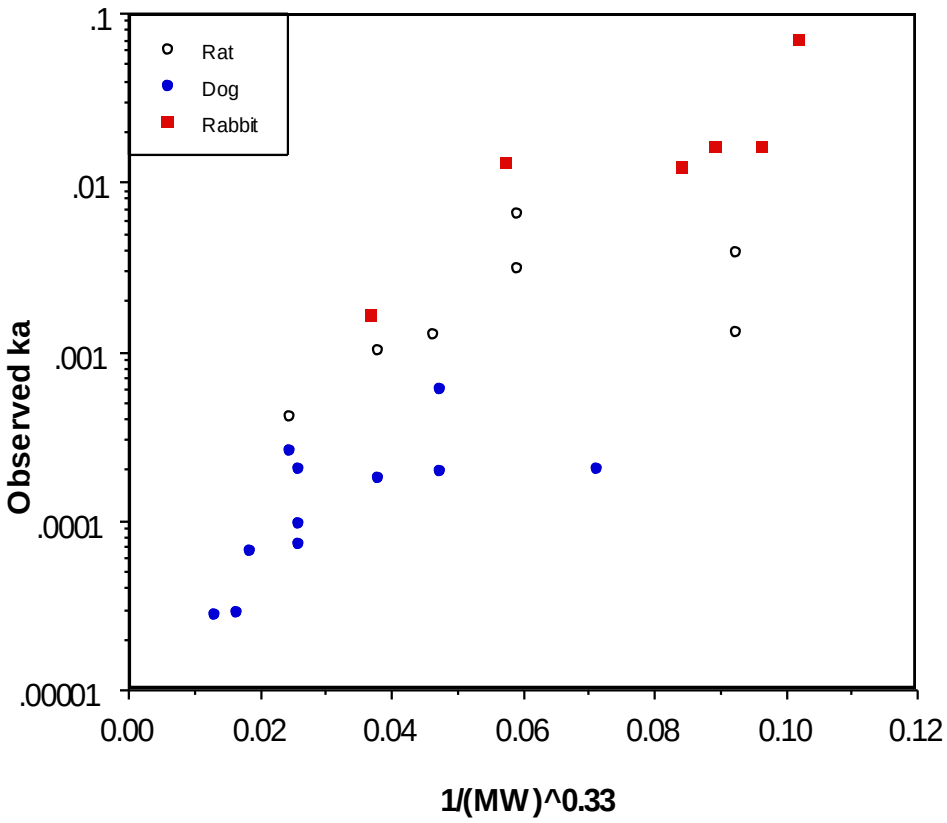

Figure 5.4.1 A graph adapted from (174) showing the linear relationship between the observed rate of absorption from the airways (ka) and their MW. MW is expressed as $1/MW^{0.33}$, a numerator which describes the diffusion coefficients of the molecules according to the Stokes' equation. Data are adapted from (173,175,176)

Similar studies have shown the same prevalence of the pulmonary paracellular pathway for the absorption of a range of molecules. In all cases a linear relationship is observed between the rate of absorption from the lung and the size of the molecule (figure 5.4.1) (174). The compilation of literature data provides strong evidence for a restrictive diffusion process through an aqueous matrix in the lung, i.e. evidence for paracellular permeability of a range of molecules. Indeed it has been shown that the absorption of a range of cardiac glycosides from the lungs of rats was increased with reductions in lipophilicity (177).

As the efficiency of P-gp mediated attenuation of absorption is dependent upon both the affinity of a substrate to P-gp and the substrates passive permeability characteristics it would seem likely that an increase in paracellular permeability could result in changes in the net effects of P-gp. It is possible that the lack of effect of P-gp on the pulmonary absorption of a group of substrates within the panel is due to the increased paracellular permeability of the lung. Here we have shown that the

absorption of these substrates across a barrier with more restrictive paracellular transport (the intestine) is attenuated by P-gp.

In order to investigate the contribution of the paracellular pathway further the membrane binding characteristics and physicochemical properties of the substrates in the panel will be investigated. The data generated will enable the development of a hypothesis into the mechanism of the discordance seen in the absorption of substrates from the lung and provide an insight in to why it appears distinct from the intestinal effects of P-gp.

Chapter 6

Membrane binding affinity and physicochemical parameters

6.1 Introduction

The primary mechanism for the transmembrane movement of most low molecular weight drugs is passive transport. As discussed in chapter 5, the first step in the transport of a drug across a lipid membrane is interaction with the outer membrane leaflet. The affinity of a molecule to bind with the lipid membrane therefore modulates the transmembrane movement rate. This initial binding step of a drug with the lipid membrane is determined by the physicochemical properties of the molecule. Due to the importance of membrane affinity in a wide range of pharmacological functions there have been numerous approaches developed to investigate the relationship between a molecule and membrane.

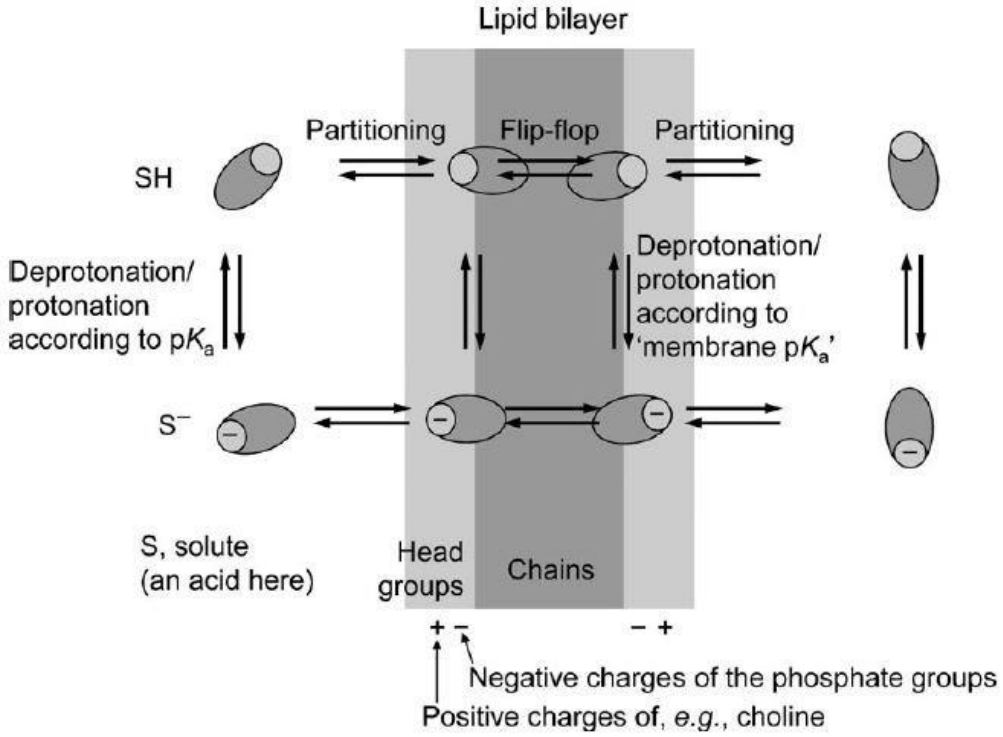

Figure 6.1.1 A schematic representation of the flip-flop absorption process of drug like compounds. Figure was adapted from (178)

6.1.1 Physicochemical characteristics for predicting membrane interaction

Physicochemical prediction of membrane binding

In its simplest form the interaction of a molecule with a lipid membrane is determined by the physicochemical features determining its lipophilicity. Increases in lipophilicity and therefore membrane interaction are associated with low H-bonding potential, PSA and an increase in rotatable bond counts (179).

Molecules with the ability to form numerous hydrogen bonds have been shown to interact preferably with water rather than the polar head groups of a lipid membrane, it is suggested this is due to the abundance of water molecules present in this membrane region in comparison to lipid molecules. The hydrogen bonds formed with water must be broken before these molecules can interact with the lipid membrane. The result is a higher energy burden on interaction with the lipid membrane and therefore a lower membrane affinity. Similar relationships between membrane and affinity and PSA may be describing the same hydrogen bonding interactions, the two physicochemical parameters are generally well correlated.

Simple measurements of hydrogen bond donor and acceptor counts do not fully explain the degree of this interaction, as the strength of the interaction is not determined solely by the number of hydrogen bonds but also by their strength. To account for differences in the strength of the hydrogen bonds acidity and basicity can be determined according to the Abraham solvation model.

The Abraham solvation model which describes linear free energy relationship of solute partitioning in condensed phase has been used previously to successfully predict the partition coefficients of a range of molecules at the intestinal, skin and plasma-to-milk barriers (180,181)It is described by the equation –

$$SP = c + e.E + s.S + a.A + b.B + v.V$$

Where SP is solute partitioning, E is the excess molar fraction, S refers to the polarisability, A and B are measures of the hydrogen bond acidity and basicity and V is the McGowan volume. Upper case letters refer to the descriptors of the solute, lower case letters refer to the descriptors of the barrier.

Although the solvation model is well utilised for prediction of solute partitioning it is also possible to use it to work out the strength of hydrogen bond acidity / basicity and polarisability of a molecule. This is achieved by calculating the solute partitioning coefficient experimentally in a range of solvents with known Abraham descriptors. The Abraham descriptors of the solute can then be determined.

6.1.2 Experimental methods for predicting membrane interaction

Octanol/water partitioning

One of the most common methods used to estimate the affinity of a molecule for a lipid membrane is that of the octanol-water partition coefficient (LogP). Despite its abundant and frequent use, it has been suggested that LogP is a poor descriptor of membrane interactions for many drugs. This is the result of the lack of hydrogen-bonding in the octanol-water partitioning resuting in a poor model of the amphitropic mammalian membranes. Predictions of membrane interactions involving polar or charged molecules are particularly poor as LogP fails to take in to account the effect of electrostatic interactions of the charged molecules due to the simplicity of the isotropic medium used in its calculation (182).

A study by El Tayar *et al.* highlights the issues involved with utilising LogP as a measure of membrane partitioning. The group showed a significant correlation between the micelle-water partition coefficient ($LogP_{MW}$) and the activity of a range of antiplatelet agents. However, the same study showed no correlation between the $LogP_{OCT}$ values and activity of the agents in the same study.

The use of LogD attempts to expand upon the use of LogP by accounting for the presence of ionic species in its calculation. As such LogD relies on the pH of the medium and pKa of the molecule to account for the ionic species.

Historically, logP was determined experimentally by measuring the fractions of a drug present in water and octanol following equilibrium of a shake-flask experiment (183). Recently, it is more common for the parameter to be computationally determined using a fragment based additive approach to generate a calculated or cLogP (184).

Reversed-phase chromatography

Reversed-phase chromatographic techniques such as HPLC and thin layer chromatography (TLC) are frequently used to simulate octanol-water partitioning as measurements of lipophilicity. When compared to the conventional methods of determining LogP they provide a more robust, high throughput system which has been shown to produce more reproducible results. There is evidence in the literature supporting the relationships between lipophilicity measurements generated in this manner in comparison to octanol-water partitioning (185).

The lipophilicity measurement determined by these techniques is derived from the retention time of the molecules in relation to the solvent front. It is described as Log*k* and can be compared to the Log*k* of molecules with a known LogP in order to estimate the lipophilicity of the molecule as a linear relationship exists between the two parameters. The standardisation of the chromatographic conditions used in the production of Log*k* values have helped to establish good correlation with values for LogP and LogD. Generally, the experiments utilise C18 columns as a stationary phase and measure the retention time of substrates with a mobile phase of varying ratios of methanol or acetonitrile in water.

Liposome partitioning

Unlike the isocratic systems described above, partitioning in to liposomes is considered a more direct model of membrane interaction and may therefore prove more relevant to studies of drug-membrane interaction. The liposomes themselves are generally composed of phospholipids, frequently phosphatidylcholine, which spontaneously form lipid bilayers trapping small amounts of media in the interior of the liposome. Liposome models have been described with a huge variation in the number of bilayer sheets from simple vesicles with a single sheet to large multilamellar vesicles with hundreds of layers (186).

Unlike octanol-water partitioning the surface of the liposomes possesses a dipole field determined by the polar headgroups. The result of this is the increased partitioning of charged molecules to liposomes in comparison to the isocratic techniques discussed above. This more closely mimics the situation *in vivo* as electrostatic interactions at the membrane surface have been shown to be important for binding and partitioning of charged molecules.

Determination of the liposome-water partition coefficient relies on the equilibration of a drug solution with a suspension of liposomes. The liposomes must then be removed from the suspension

and the fraction present in the lipid phase calculated. The production of liposomes is associated with difficulties in relation to their stability and reproducibility of formation. These difficulties have resulted in limited use of liposome partitioning as an alternative to octanol partitioning although there are examples of the successful use of the technique in the literature.

One such example utilised the liposome-water partition to examine the effect of the membrane affinity of rhodamine dyes on their P-gp efflux (148). The study utilised liposomes composed of phosphatidylcholine (PC) and phosphatidylglycerol (PG) to investigate the transmembrane movement rate of seven rhodamine dyes. Due to the the generally lipophilic nature of all P-gp substrates an equilibrium is reached rapidly between the outer membrane and the aqueous media upon addition of rhodamine dyes to multilamellar vesicle (MLV) suspensions. Dye uptake to the subsequent inner layers is then determined principally by the transmembrane movement rate of the dye as it has to traverse the first membrane to reach the second. It is therefore assumed that with the exception of the rapid initial binding to the outer membrane the amount of rhodamine dye associated with the liposomes at a given time point (its binding rate) is determined solely by the transmembrane movement rate of the molecule.

The study compared the data generated for the transmembrane movement rates of the rhodamine dyes and their P-gp efflux ratios. It was found that, independent of the affinity to P-gp, the efflux ratio was inversely proportional to the transmembrane movement rate of the dye. This was early evidence of the effect of increasing passive permeability in order to reduce the effects of P-gp mediated efflux.

Immobilised artificial membrane (IAM) chromatography

The frequent criticisms of the use of isocratic systems such as octanol-water partitioning as measurements of membrane partitioning has led to the development of IAM chromatography. This model attempts to combine the relevance of the more complex liposome partitioning experiments with the ease of reverse phase chromatography (187,188). In IAM chromatography a stationary phase of fixed PC is used to simulate the outer membrane leaflet. The mobile phase used is generally either PBS to simulate physiologic conditions or for the elution of more strongly retained molecules acetonitrile:water solutions. If solutions of acetonitrile are used multiple retention times in various acetonitrile compositions (commonly 10, 20 and 30 %) are generated in order to extrapolate a retention time in pure water. Mobile phases containing methanol should be avoided as there is evidence of damage to the fixed PC in the presence of methanol.

Despite offering the same simplicity as the reverse phase HPLC techniques described previously, studies have shown the IAM is capable of generating data which correlates well with liposome absorption studies (189). A number of studies have shown improvements in membrane partitioning prediction using IAM techniques as opposed to isotropic techniques such as octanol-water partitioning. It has been shown that the antihaemolytic activity of a series of drugs was described significantly better by LogK values determined using an IAM column as opposed to simple isotropic techniques (190). Similarly, it has been shown that the IAM columns are better descriptors of lipophilic and polar interactions for a series of dihydropyridines (191).

Studies utilising IAM chromatography have been able to correlate performance in the IAM with measurable *in vivo* membrane transport processes such as brain penetration (192). The retention factors for a set of 26 drugs for which literature brain penetration data was available were determined using an IAM column. Correlations between the $Logk_{IAM}$ and brain penetration highlighted the predictive capability of the model for the assessment of membrane transport. Similarly, the prediction of oral absorption has been achieved for a set of 37 compounds from the literature (193) with a strong coefficient of determination of 0.9. The IAM was shown to be a more predictive tool than octanol-water partitioning in the same experiments.

6.1.3 Experimental Objectives

In previous chapters we have shown a discordant effect of P-gp upon the pulmonary absorption of a panel of substrates in a manner that is distinct from that observed previously in the intestine. Previous studies have shown that the net effect of P-gp upon absorption is due to a relationship between the exclusion of the substrate from the cell by P-gp and its passive absorption rate.

Here we hypothesise that the differences seen in the effects of P-gp between the lung and intestine are due to the increased permeability via the enhanced paracellular pathway of the lung. To investigate this we measure the membrane binding and affinity of the substrate panel using both IAM chromatography and liposome partitioning. The physicochemical parameters of the panel will be established and used to explain the lack of pulmonary efflux seen in a subset of the panel as well as make predictions about the prevalence of the predicted pulmonary P-gp efflux within the drugs currently administered via inhalation.

6.2 Materials and Methods

6.2.1 IAM chromatography

Materials

Chemical	Descriptor	Product Code	Supplier
Acetonitrile	HPLC Grade	10407440	Fisher Scientific, Loughborough, UK
Dimethyl Sulfoxide	n/a	10080110	Fisher Scientific, Loughborough, UK

Table 6.2.1 Chemicals and solvents used in the analysis of compounds delivered to the IPML along with their supplier details.

Equipment	Manufacturer	Product Identifier
Solvent Degasser	Thermo Finnigan	SCM1000
Pump	Thermo Finnigan	P4000
Autosampler	Thermo Finnigan	AS3000
UV detector	Thermo Finnigan	UV2000
IAM Column	Regis Technologies	IAM.PC.DD2, 10cm x 4.6 mm ID

Table 4.2.4 Equipment used in the analysis of compounds delivered to the IPML and the relevant manufacturer details.

Method

Drug solutions of 100 µg/mL were prepared in 50:50 acetonitrile:water prior to chromatographic separation. The analysis of the retention time of drugs on the IAM column was achieved by injecting 10 µL of the drug solution on to the column and eluting with mobile phase which was pumped through the column at 1 mL/min as an isocratic gradient in all experiments. The retention time of all substrates was calculated in three mobile phase compositions, 10 % acetonitrile in water, 20 % acetonitrile in water and 30 % acetonitrile in water.

Using the multiple gradients of acetonitrile concentrations the retention times were extrapolated by linear regression to determine the theoretical retention time in 100 % water. This was then used to calculate $LogK_{IAM}$ according to the equation –

$$LogK_{IAM} = \log[(T_r - T_0)/T_0]$$

Where T_r and T_0 are the retention time of the substrate in 100 % water and the retention time of an unretained compound / the solvent front (75 seconds in all experiments).

6.2.2 Liposome partitioning

Liposome formation - Method

The formation of multi lamellar vesicles was performed as detailed by Eytan (148). Solutions of 8 mg phosphatidylcholine and 2 mg phosphatidylglycerol in 10 mL chloroform were dried whilst rotating under vacuum to produce a lipid film. Vacuum was maintained for an hour after all visible liquid had evaporated to ensure no residual chloroform was present. Mutlilamellar vesicles (MLV) were then formed by the addition of 1 mL of 25 mM HEPES-Tris buffer (pH 7.5) and gentle shaking for 4 hours. The suspension was then centrifuged at 6000 rcf for 15 minutes to pellet the vesicles and the supernatant was removed. The MLVs were then resuspended in 10 mL of PBS (pH 7.4) and stored at 4 ^{o}C under nitrogen gas overnight before partition experiments were performed.

Freeze drying of the resultant suspension showed average lipid yields of 46 ± 8 % in the MLV formation, a value consistent with the Eytan study. This yield generates a MLV suspension containing approximately 10 - 15 μM of phospholipid. This was consistent across all paritition experiments as they were all performed on a single batch of MLVs.

Partition experiments

MLV suspensions were removed from 4 ^{o}C and diluted 1000-fold in PBS (pH 7.4). Aliquots of the resultant suspension (1 mL) were transferred to microcentrifuge tubes. All substrates were tested in triplicate with 3 microcentrifuge tubes per substrate. 10 μL of a 100 μg/mL dose was administered to all liposome suspensions resulting in a drug concentration of 1 μg/mL in the aqueous compartment at the beginning of the experiment.

Suspensions were then incubated at 37 ^{o}C with shaking for 4 hours to allow the equilibration of the dose in the lipid and aqueous fractions. The liposomes were then pelleted and 100 μL of supernatant removed for analysis.

The concentration of the dose present in the supernatant was determined by either LC-MS/MS or liquid scintillation in the manner described in chapter 4. It was assumed that all dose not in solution in the aqueous supernatant had partitioned in to the liposomes.

Partitioning in to the liposomes was determined according to the following equation –

$$\text{Liposome partition co-efficient} = (C_0\text{-}C_S) / C_0$$

Where C_0 is the drug concentration present at the beginning of the experiment (1 µg/mL) and C_s is the concentration present in the supernatant at the end of equilibration.

6.2.3 Computer generated physicochemical properties

Determining primary physicochemical properties

Values for cLogP, cLogD, H-bond donors, H-bond acceptors, rotatable bond count, molecular volume and molecular weight were determined using the online ACD/Labs software with the SMILES string of each substrate as the input.

Connolly accessible surface area and polar surface area (PSA) were calculated in the ChemBio3D Ultra 11.0 software (Cambridgesoft, UK) from the chemical structures of the substrates.

Determining Abraham solvation parameters

As mentioned in the introduction it is possible to determine the Abraham solvation parameters experimentally by comparisons of a substrates partition coefficients in standard solvents. A more high-throughput approach was utilised here by utilising a fragment based approach (GSK in house software). This is achieved by the software breaking the chemical structure in to small simple fragments. These are then screened against a large database containing the Abraham solvation parameters for many such fragments. The solvation parameters of the fragments can then be used to determine the solvation parameters of the parent molecule in a simple additive manner.

Calculation of Abraham descriptors in this was has been shown to produce good correlations with values determined experimentally (194).

6.3 Results

6.3.1 IAM chromatography

In order to gain an insight in to the membrane interactions of the panel of substrates, a number of studies were carried out in order to assess membrane affinity. The first of these utilised an HPLC column with a PC stationary phase to assess the extent of the interactions of each drug with this phospholipid. Drugs which interact less with PC showed a decreased retention time on the column and therefore possess lower $LogK_{IAM}$ values.

	IAM Aqueous Retention Time (secs)	Liposome Partition Coefficient
digoxin	0.9	0.3
erythromycin	0.9	0.46
GSK1	1.1	0.65
mitoxantrone	1.1	0.59
monensin	1.3	0.68
puromycin	1.3	0.62
saquinavir	1.2	0.45
chloroquine	1.4	0.95
colchicine	1.3	0.86
domperidone	1.3	0.92
eletriptan	1.5	0.94
GSK2	1.3	0.86
GSK3	1.4	0.97
GSK4	1.2	0.92
rh123	1.3	0.82
salbutamol	1.5	0.88
salmeterol	1.6	0.8

Table 6.3.1 Data showing the data for both the IAM and liposome membrane affinity experiments. Increases in either determinant are associated with increased membrane association. Data are split according to the observed effect of P-gp upon their pulmonary absorption, substrates in the upper section were unaffected by pulmonary P-gp and those in the lower showed significant P-gp efflux in the lung.

All of the substrates were retained on the IAM suggesting they are all capable of membrane interaction. Compounds which are hydrophilic and do not interact with membranes (such as sucrose) show no retention on IAM columns and are eluted with the solvent front.

There is a significant difference between the $LogK_{IAM}$ of the molecules affected by P-gp in the lung and those which are not (mean= 1.39 and 1.22, respectively, p = 0.002). This suggests the strength of the membrane interactions of these two groups is distinct with a higher affinity for membranes observed in the P-gp effected group of substrates.

6.3.2 Liposome partitioning

Data for the partitioning of the substrates into liposomes acts to corroborate the difference observed in the IAM model of membrane partitioning. The significantly increased membrane affinity of the substrates effected by P-gp in the lung compared to those which are not is also observed in the liposome partitioning coefficient (mean = 0.89 and 0.54, respectively, $p = 2 \times 10^{-6}$).

A strong correlation is observed between the data generated by IAM chromatography and liposome partitioning ($r^2 = 0.74$). This is in agreement with the literature studies which have seen strong predicitons of membrane interaction from the IAM column. The calculated basic physicochemical parameters and Abraham descriptors are shown in tables 6.3.1 and 6.3.2, respectively. The table is split in to two groups with the substrates in the upper section showing no effect of P-gp upon their pulmonary absorption from the IPML whilst the absorption of those in the lower section was significantly attenuated.

6.3.3 Physicochemical properties

When the physicochemical properties of the two groups were compared it was observed that they formed two distinct physicochemical profiles. The group of substrates which was affected by P-gp expression in the lung possessed significantly lower hydrogen bond acidity and basicity (as measure by Abraham solvation parameters and simple H-bond counts) (p = 0.12 for Abraham acidity and 2.8×10^{-5} for Abraham basicity). The polarisability and PSA of this group was also significantly lower (p = 0.02 and 5.5×10^{-7}, respectively)

As these are physicochemical properties which have been shown to influence membrane affinity it suggests that the increase seen in the membrane affinity for this group is due to these physicochemical distinctions. Indeed Abrahams acidity, basicity and polarisability all show strong negative correlations to the liposome binding coefficient (r^2= -0.73, -0.91 and -0.66, respectively).

	cLogD (7.4)	cLogP	H bond donor (acidity)	H bond acceptor (basicity)	H bond total	Rotatable bond count	Polar Surface Area	MW
Digoxin	0.90	0.90	6	14	20	13	203.00	780
Erythromycin	1.20	1.90	5	14	19	12	194.00	733
GSK1		3.75	10	3	13	7	130.48	571
Mitoxantrone	1.00	1.55	8	10	18	16	163.00	444
Monensin	0.96	4.01	4	11	15	13	153.00	670
Puromycin	0.97	1.30	5	12	17	11	164.00	471
Saquinavir mesylate	3.60	4.03	6	11	17	14	167.00	670
Chloroquine	1.59	4.41	1	3	4	8	28.00	319
Colchicine	1.07	1.07	1	7	8	5	87.00	399
Domperidone	2.93	4.05	2	7	9	5	79.00	425
Eletriptan	0.23	2.98	1	4	5	6	53.00	382
GSK2		3.28	7	2	9	6	99.50	495
GSK3		3.11	3	0	3	9	33.02	466
Indacaterol		-1.71	5	1	6	4	59.06	393
Rhodamine 123	4.01	4.01	4	5	9	5	90.00	344
Salbutamol	-1.44	0.69	4	4	8	8	73.00	239
Salmeterol	1.15	3.07	4	5	9	19	82.00	416

Table 6.3.2 The calculated physicochemical parameters for the panel of P-gp substrates. The substrates are split in to two groups depending on the effect of P-gp on their pulmonary absorption, the upper section are unaffected and the lower are affected.

	Abraham Acidity (>0.75)	Abraham Basicity (>3)	Abraham Volume	Abrhaham Polarizability (>3)	Abraham Molar Refractive Index
Digoxin	1.72	4.62	5.75	5.34	3.20
Erythromycin	1.02	4.71	5.77	3.55	1.97
GSK1	1.08	2.67	3.83	5.28	3.83
Mitoxantrone	0.52	2.88	3.29	2.06	3.31
Monensin	1.45	3.55	5.24	2.44	1.61
Puromycin	0.51	3.56	3.42	3.58	3.38
Saquinavir mesylate	1.61	4.68	5.89	6.30	4.25
Chloroquine	0.20	1.59	2.63	1.73	1.91
Colchicine	0.37	1.96	2.99	2.96	2.11
Domperidone	0.65	2.23	3.06	3.09	3.81
Eletriptan	0.00	1.84	2.93	3.17	2.74
GSK2	0.83	2.56	3.76	3.78	3.76
GSK3	0.00	0.80	3.88	2.36	3.88
Indacaterol	0.54	2.06	3.09	2.54	3.09
Rhodamine 123	0.50	1.21	2.56	2.90	3.27
Salbutamol	1.08	1.91	1.98	1.41	1.41
Salmeterol	1.08	2.11	3.49	2.11	2.07

Table 6.3.3 The calculated Abraham solvation parameters for the panel of P-gp substrates. The substrates are split in to two groups depending on the effect of P-gp on their pulmonary absorption, the upper section are unaffected and the lower are affected.

6. Discussion

The interaction of a molecule with a plasma membrane is determined by the physicochemical properties of both the molecule and the membrane. It has been suggested that systems such as the octanol-water coefficient are poorly predictive of this interaction due to the over simplicity of the model (195). Models such as octanol-water partitioning do not possess the electrostatic interactions present on the surface of phospholipid membranes due to the dipole charges of the phospho-headgroups. These electrostatic interactions with the solute are important for determining the energy cost involved with solute-membrane binding. The lack of the dipole charges in octanol-water partition coefficient models significantly reduces their usefulness in the analysis of charged compounds.

Here we present data from two models which have been shown to be predictive of membrane binding in a biological situation, IAM chromatography and liposome binding. The data from these two experiments clearly highlights discordance in the membrane affinity of the substrate panel. In both membrane models the substrates which show a significant effect of P-gp efflux are shown to possess higher membrane affinities. This is reflected in similar differences in the physicochemical properties which have been shown to influence the process of membrane binding. That is to say that the substrates which show positive efflux from the lung possess significantly decreased PSA, H-bond acceptors, H-bond donors, MW, Abraham acidity, Abraham basicity and Abraham polarisability.

In order to validate the use of physicochemical descriptors as predictors of membrane interactions the Abraham solvation parameters were correlated with the results of the liposome partitioning experiments. The results show that increases in Abraham acidity, basicity and polarisability are all well correlated with decreases in the membrane affinity of a molecule. This is shown by the strong negative correlations obtained of r^2= -0.73, -0.91 and -0.66, respectively. This is in agreement with the literature where it has been shown that Abraham descriptors are good predictors of binding to biological membranes (196)

For lipophilic drugs such as P-gp substrates it has been shown that their mechanism of transport across a phospholipid bilayer is one of a distinct flip-flop type event, discussed in detail previously. Whilst the rate limiting factor of a single molecule's transport has been shown to be the flip-flop itself (165) increases in membrane affinity will increase the concentration of drug present in the outer leaflet of the membrane which acts as the donor compartment for this reaction.

It would therefore be predicted that increases in membrane affinity would result in increases in passive permeability across the lung. By taking the pulmonary absorption of the substrate panel from the IPML with the lungs of P-gp deficient mice as a measure for the passive permeability at this barrier it is possible to compare the effect of membrane affinity on passive pulmonary absorption. In the lungs there is no observed correlation between the two parameters (r^2= 0.23). This is perhaps indicative of the increased absorption of the lung to hydrophilic compounds due to the increased prevalence of the paracellular pathway.

The relationship witnessed here between the membrane affinity of a substrate and the net effect of efflux is not the same as those observed in the intestine (130). In the intestine enhancements in membrane affinity have been shown to lead to decreases in P-gp efflux. The opposite relationship is observed here where it is shown that the substrates which show significant efflux by P-gp are also those which show the highest membrane affinity.

We propose this is reflective of the differences in the permeability of the two barriers via the paracellular route. This hypothesis is explained in detail in the next chapter but simply, substrates which show a lower membrane affinity will fraction less to the membrane compartment in the lung. This will lead to a higher concentration of drug in the aqueous compartment. Free drug in the aqueous compartment is available for passive absorption via the paracellular pathway and as this is more prevalent in the lung we would expect a higher level of absorption via this pathway for these substrates than that of the intestine. The absorption of an increased proportion of the low-membrane bound drugs via the paracellular pathway results in their avoidance of P-gp efflux and a lower net effect of pulmonary P-gp up in their absorption from the lung.

Chapter 7

General Discussion

7. General Discussion

Previously in the thesis (chapter 4) it was demonstrated that the absorption of a panel of known P-gp substrates showed discordance in the effects of P-gp upon their pulmonary absorption. A subset (ten) of the substrates showed significantly higher extents of absorption from the lung in the P-gp knockout mice, suggesting pulmonary P-gp acted to attenuate the absorption of these molecules from the IPML. The remaining molecules (seven) were absorbed to a similar extent in both the wild type and knockout mice, suggesting pulmonary P-gp does not affect their absorption.

By investigating the P-gp binding kinetics of the panel it was shown that the discordance seen in the effects of pulmonary P-gp are not explained by differences in P-gp affinity between the two groups. Previous studies, mainly in the intestine, have highlighted the importance in the relationship between passive permeability and P-gp efflux.

P-gp substrates are mainly lipophilic or amphipathic molecules (1) and their absorption through the intestine is therefore mainly transcellular. This is due to the route of uptake of a drug across a biological barrier being determined by its physicochemical properties. Molecules which exhibit a lower polarity (and subsequent increased lipophilicity) show high transcellular permeability due to increased membrane affinity (197). The extent of partitioning in to membranes (and subsequent transcellular diffusion) of these substrates has been shown to decrease with increases in H-bonding potential and polarity (198).

The extent of membrane binding and transmembrane movement rate is an important determinants in the net effect of P-gp on substrate absorption. As discussed in detail earlier in the thesis molecules which show high passive permeability have been shown to have a lower net effect of P-gp efflux (the mechanism behind this is discussed in chapter 5). This effect has been observed in both *in vitro* cell lines and in the oral bioavailability of a range of molecules.

An early study by Lentz utilised the Caco-2 cell line to compare the efflux ratio observed in this cell line with a molecules passive permeability (199). The group showed that the substrates with high passive permeability across the barrier showed no efflux by P-gp with absorptive and secretory transport rates being equal. A similar effect is observed using oral bioavailability data to show the effect of P-gp on the intestinal absorption of its substrates. A study by Varma *et al* compared the effects of P-gp in limiting oral absorption of a large set of substrates to their passive transport rates.

The results confirm those seen in the *in vitro* studies with substrates which possess high passive absorption overcoming the effects of P-gp and showing no measurable efflux in the intestine.

In order to investigate whether a similar effect can describe the discordance seen within the pulmonary effects of P-gp in the panel of substrates tested in the IPML we conducted investigations in to the membrane affinity of these substrates. In order to accurately predict the affinity of the substrates to a biological membrane we investigated the affinity of the substrates to multi lamellar vesicles (MLVs) and an IAM column. As discussed in the introduction there is literature support that both of these models predict plasma membrane interactions in a biological situation. As both models measure the affinity of a molecule to phosphatidylcholine (an abundant phospholipid in membranes) it is perhaps unsurprising that the data generated by both models is remarkably similar.

Both models show that when the membrane binding affinity of the substrate panel is compared, a significant difference is observed between the membrane affinity of the substrates which show pulmonary efflux and those which do not; the set of substrates which show positive efflux from the lung show significantly higher membrane affinity in both the IAM and MLV experiments.

This data seems at odds with the previous literature where an increase in membrane affinity is observed to decrease P-gp efflux. It is proposed that this difference in the relationship between P-gp and passive permeability between the two barriers is due to differences in their physical properties, and in particular the prevalence of the paracellular pathway in the lung which has been shown to be more permeable than that of the intestine (173). As the membrane affinity of a molecule decreases the fraction remaining in the aqueous absorption compartment will increase. This will in turn lead to a greater availability of the molecule to absorption via the paracellular pathway, a route which avoids P-gp mediated efflux.

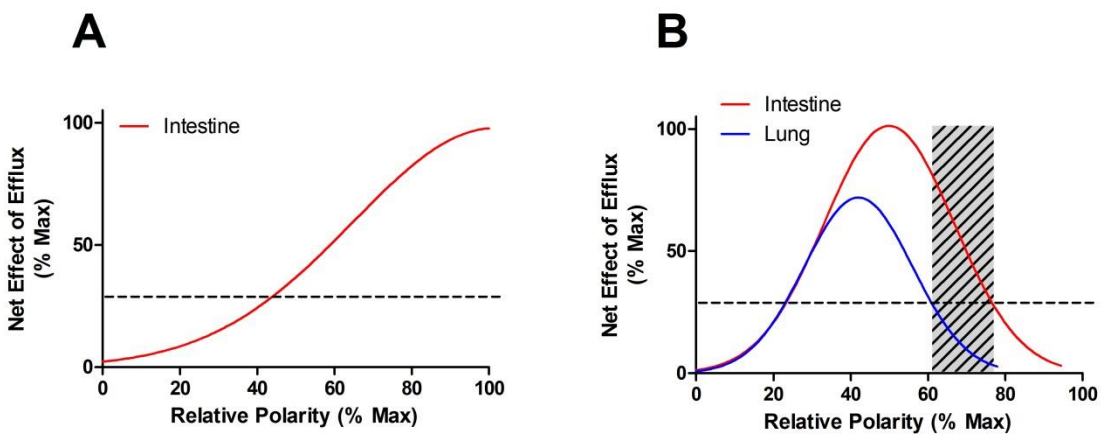

Figure 6.4.1 Graphical representations of the effect of polarity upon the net effect of P-gp efflux observed at the intestinal and pulmonary barrier. [A] The currently accepted hypothesis with an increase in polarity leading to increased efflux. [B] The hypothesis suggested by the IPML absorption data where both extremes of polarity result in decreased efflux. The dashed line indicates an arbitrary level below which efflux is below the limit of quantification.

The hypothesis proposed here is represented in Figure 6.4.1B. We suggest that at low polarity (and therefore high membrane affinity) the passive permeability of a molecule is almost exclusively by the transcellular route. The substrate is therefore absorbed by a pathway that exposes it to P-gp. During this process it is suggested the relationship between the passive permeability of a substrate and the net effect of P-gp efflux is as described in the literature.

In addition to the current model it is now hypothesised that as polarity increases past a set point (and membrane affinity decreases) the portion of the drug absorbed via the paracellular pathway increases. As this pathway results in absorption of the drug without exposure to P-gp the result is a decrease in the net effect of observable efflux.

In the intestine this process may be unimportant as the paracellular pathway is much tighter than that of the lung. This will mean the polarity required for a significant fraction of the drug to be absorbed via the paracellular route, and bypass P-gp, will be higher. This is likely to exclude P-gp substrates from absorption via this route as they tend to be lipophilic molecules as discussed previously.

The result of this prediction is a set of molecules with decreased membrane affinity which escape P-gp efflux in the lung, the hatched area of figure 6.4.1B. We hypothesise that the substrates which showed no effect of P-gp upon their pulmonary absorption lie in this chemical space.

The possible contribution of pulmonary P-gp to the absorption of substrates in the lung appears to be defined by a more complicated physicochemical relationship than that observed in the intestine. As a result P-gp is likely to attenuate the pulmonary absorption of only a subset of intestinal P-gp substrates.

To quantify this the Abraham descriptors for the panel of substrates were established and showed that the membrane binding differences are explained by significant differences in the hydrogen bond acidity and basicity as well as the polarisability of the substrates. Using these descriptors we challenged a database of the physicochemical properties of 131 known P-gp substrates. Of the 131 substrates 98 (75 %) were seen to possess the physicochemical properties which we have shown to predict pulmonary efflux. If the same analysis is performed on only the currently approved inhaled drugs (129) we show that 70% (7 of 10) would be predicted to show pulmonary efflux, this includes salbutamol, salmeterol and indacaterol for which pulmonary efflux was shown experimentally earlier in the thesis.

Chapter 8

Appendix

4.3.3 PK Analysis – F and K

As illustrated in table 4.3.1 the absorption data for all IPML experiments was analysed using a single compartment model to identify values for the bioavailability (F) and rate of absorption (K). These pharmacokinetic parameters were then compared between wildtype and knockout mouse groups using an unpaired t-test to test for significant differences attributable to P-gp knockout. In all cases where the percentage absorbed at individual time points showed a significant difference a significant difference ($p < 0.05$) was also observed in the calculation of bioavailability. The converse is also true with the substrates showing no difference in percentage absorbed at each time point also showing no significant difference in bioavailability.

The same relationship is not reflected in the rates of absorption (K) with only one substrate, salbutamol, showing a significantly ($p < 0.05$) increased absorption in the knockout mice. All other substrates show no significant difference in absorption rates despite an overall trend for higher rates in the knockout animals (on average molecules were absorbed 130% more rapidly from knockout mouse lungs). The lack of significance in the rates appears to be due to high variability in the early time points and in some instances the complete lack of early time points due to the concentrations present in the perfusate being below the level of detection for analysis.

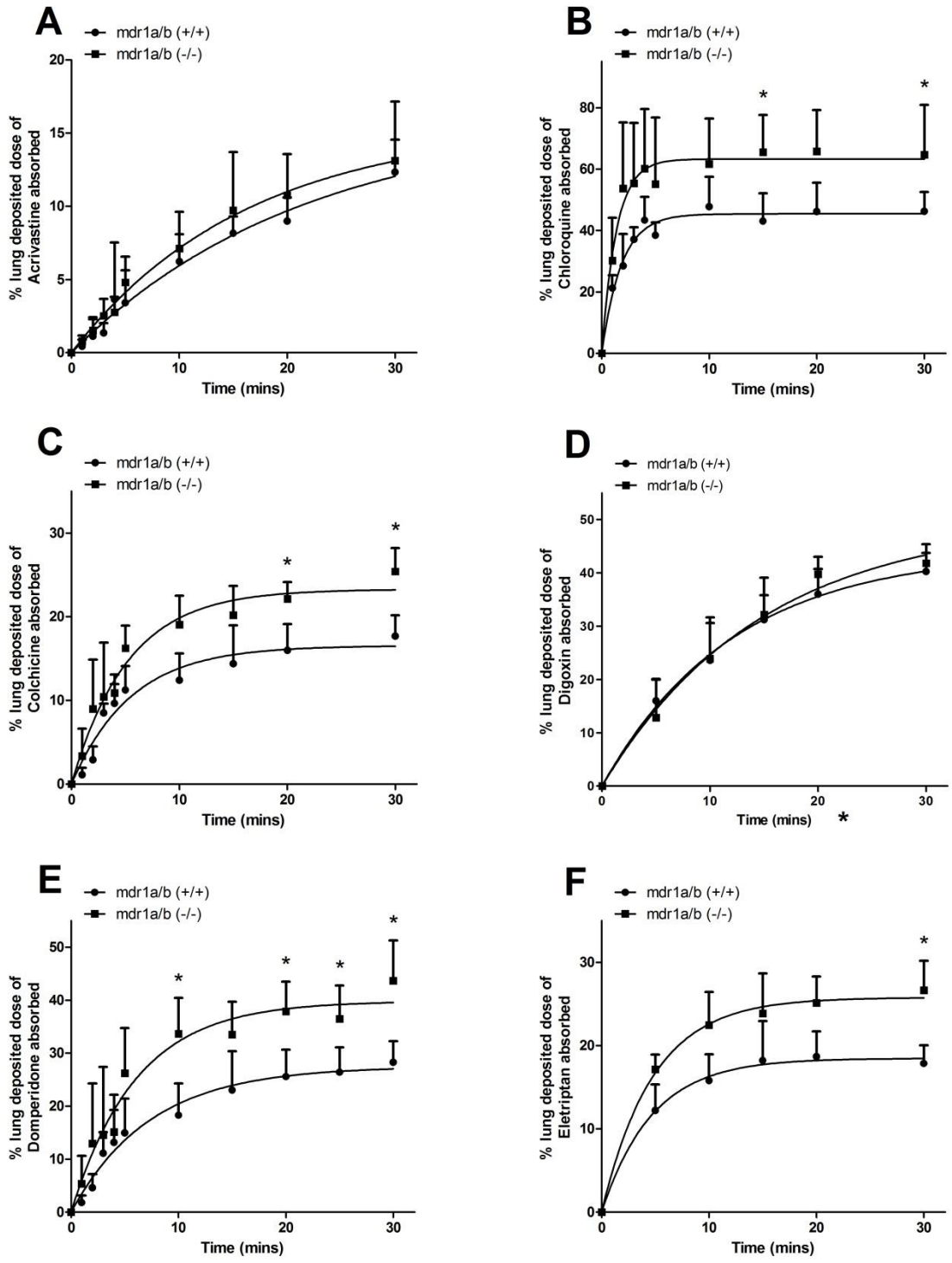

Figure 8.1.1 Absorption profiles from the airways of the IPML in to perfusate for both the wild-type mdr1a/b (+/+) mice and the knockout mdr1a/b (-/-) mice for **[A]** acrivastine (n=4), **[B]** chloroquine (n=4), **[C]** colchicine (n=4), **[D]** digoxin (n=6), **[E]** domperidone (n=4) and **[F]** eletriptan (n=4). In all cases data is presented as the mean ± SD of the percentage of the lung deposited dose absorbed at distinct time points, * indicates a significant difference between the wild-type and knockout mice at that time point. Non-linear regression is performed using the equation described in chapter 4.

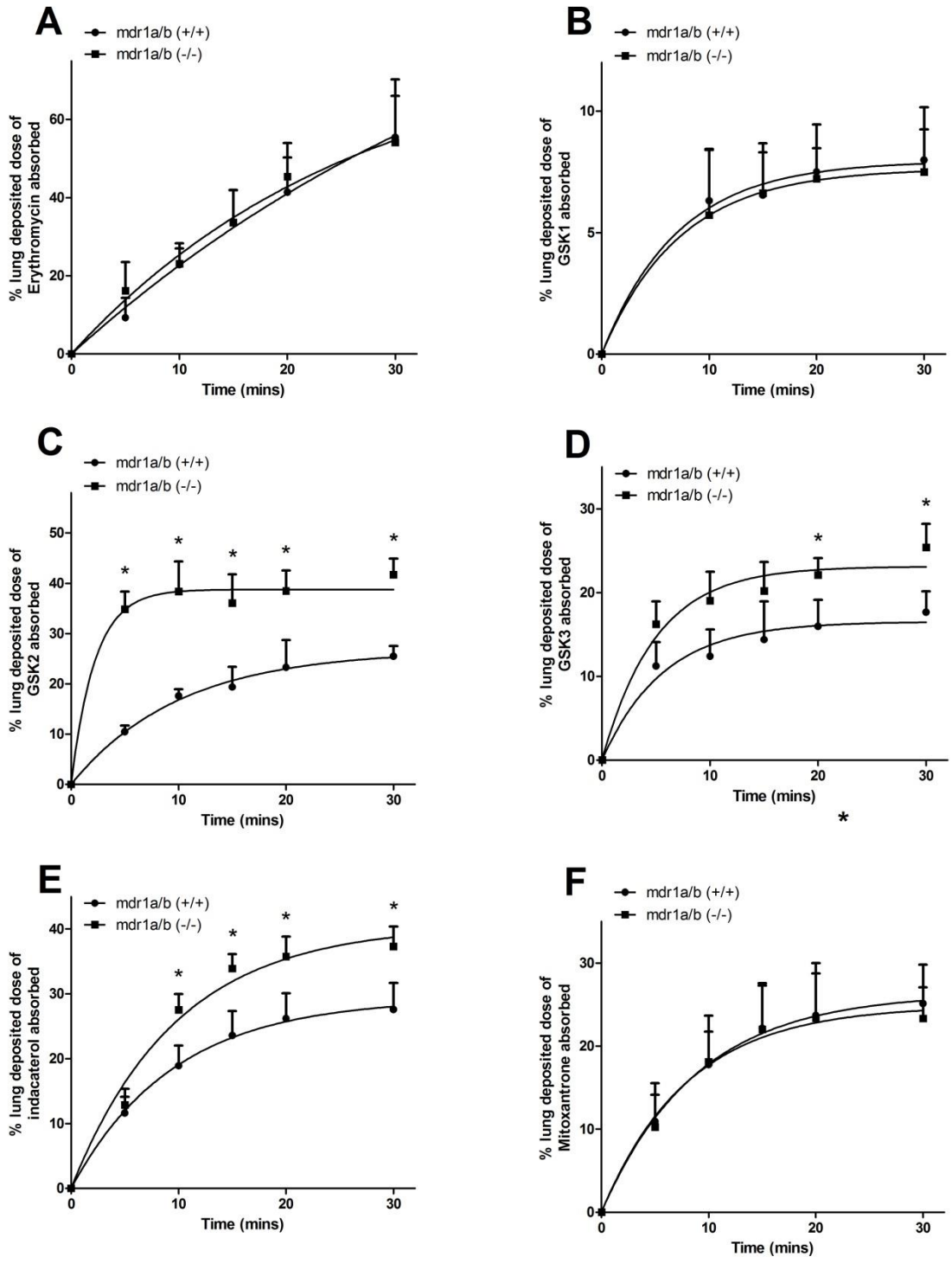

Figure 4.3.2 Absorption profiles from the airways of the IPML in to perfusate for both the wild-type mdr1a/b (+/+) mice and the knockout mdr1a/b (-/-) mice for **[A]** erythromycin (n=5), **[B]** GSK1 (n=5), **[C]** GSK2 (n=4), **[D]** GSK3 (2=6), **[E]** indacaterol (n=4) and **[F]** mitoxantrone (n=4). In all cases data is presented as the mean ± SD of the percentage of the lung deposited dose absorbed at distinct time points, * indicates a significant difference between the wild-type and knockout mice at that time point. Non-linear regression is performed using the equation described in chapter 4.

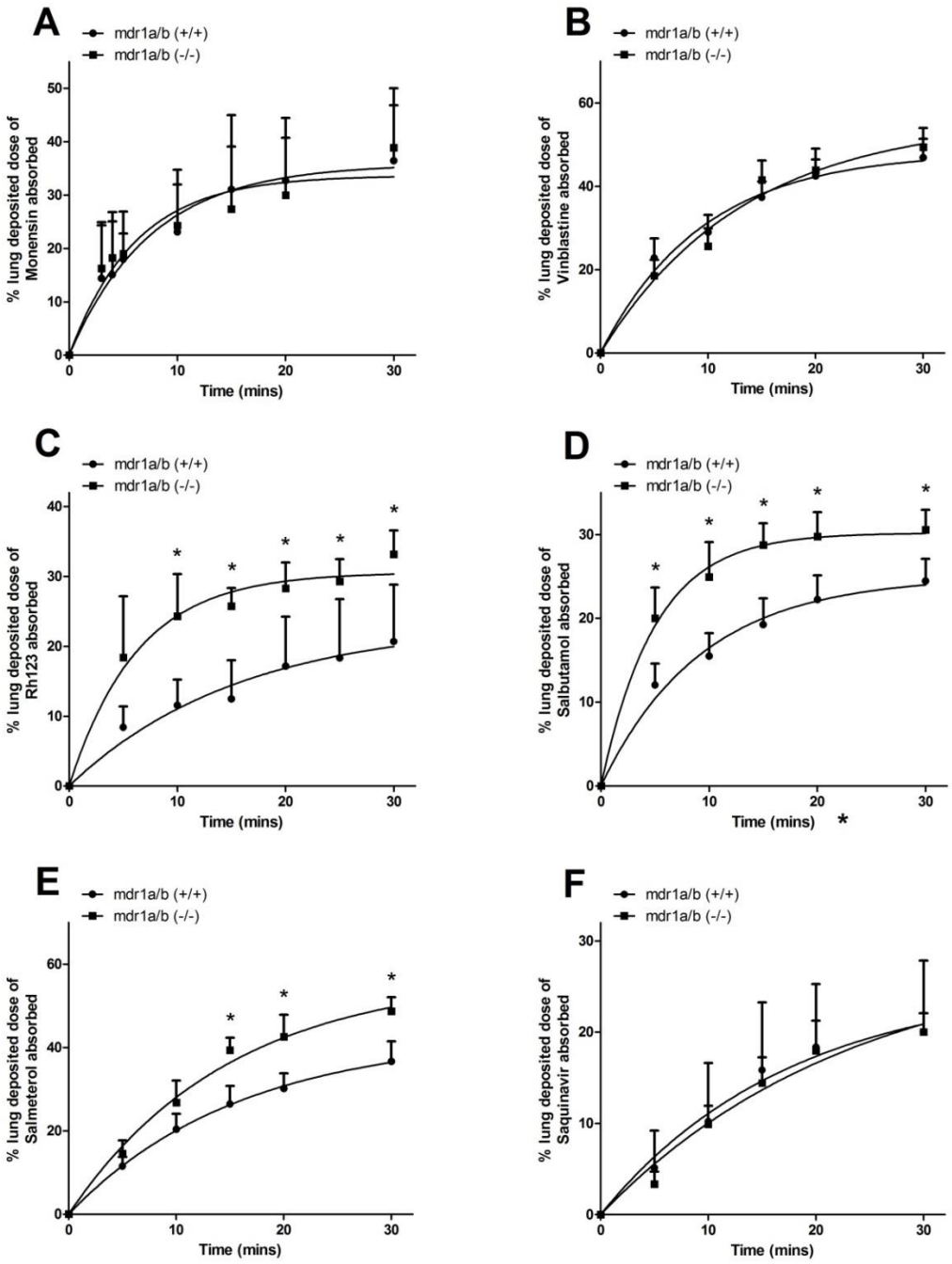

Figure 4.3.3 Absorption profiles from the airways of the IPML in to perfusate for both the wild-type mdr1a/b (+/+) mice and the knockout mdr1a/b (-/-) mice in **[A]** monensin (n=6), **[B]** puromycin (n=6), **[C]** rhodamine 123 (n=6), **[D]** salbutamol (n=4), **[E]** salmeterol (n=4) and **[F]** saquinavir (n=5). In all cases data is presented as the mean ± SD of the percentage of the lung deposited dose absorbed at distinct time points, * indicates a significant difference between the wild-type and knockout mice at that time point. Non-linear regression is performed using the equation described in chapter 4.

References

1. Aller SG, Yu J, Ward A, Weng Y, Chittaboina S, Zhuo R, et al. Structure of P-glycoprotein reveals a molecular basis for poly-specific drug binding. Science (80-) [Internet]. 2009/03/28 ed. 2009;323(5922):1718–22.

2. Raub TJ. P-glycoprotein recognition of substrates and circumvention through rational drug design. Mol Pharm [Internet]. 2006;3(1):3–25.

3. Stouch TR, Gudmundsson O. Progress in understanding the structure-activity relationships of P-glycoprotein. Adv Drug Deliv Rev [Internet]. 2002/03/30 ed. 2002;54(3):315–28.

4. Pajeva IK, Wiese M. Pharmacophore model of drugs involved in P-glycoprotein multidrug resistance: explanation of structural variety (hypothesis). J Med Chem [Internet]. 2002/12/13 ed. 2002;45(26):5671–86.

5. Bleasby K, Castle JC, Roberts CJ, Cheng C, Bailey WJ, Sina JF, et al. Expression profiles of 50 xenobiotic transporter genes in humans and pre-clinical species: a resource for investigations into drug disposition. Xenobiotica [Internet]. 2006/11/23 ed. 2006;36(10-11):963–88.

6. Sakamoto A, Matsumaru T, Yamamura N, Uchida Y, Tachikawa M, Ohtsuki S, et al. Quantitative expression of human drug transporter proteins in lung tissues: analysis of regional, gender, and interindividual differences by liquid chromatography-tandem mass spectrometry. J Pharm Sci [Internet]. 2013;102:3395–406.

7. Sakamoto A, Matsumaru T, Yamamura N, Suzuki S, Uchida Y, Tachikawa M, et al. Drug Transporter Protein Quantification of Immortalized Human Lung Cell Lines Derived from Tracheobronchial Epithelial Cells (Calu-3 and BEAS2-B), Bronchiolar-Alveolar Cells (NCI-H292 and NCI-H441), and Alveolar Type II-like Cells (A549) by Liquid Chromat. J Pharm Sci [Internet]. 2015

8. Endter S, Francombe D, Ehrhardt C, Gumbleton M. RT-PCR analysis of ABC, SLC and SLCO drug transporters in human lung epithelial cell models. J Pharm Pharmacol [Internet]. 2009/05/02 ed. 2009;61(5):583–91.

9. Fetsch PA, Abati A, Litman T, Morisaki K, Honjo Y, Mittal K, et al. Localization of the ABCG2 mitoxantrone resistance-associated protein in normal tissues. Cancer Lett [Internet]. 2005/07/02 ed. 2006;235(1):84–92.

10. Scheffer GL, Pijnenborg a CLM, Smit EF, Müller M, Postma DS, Timens W, et al. Multidrug resistance related molecules in human and murine lung. J Clin Pathol [Internet]. 2002 May;55(5):332–9.

11. Langmann T, Mauerer R, Zahn A, Moehle C, Probst M, Stremmel W, et al. Real-Time Reverse Transcription-PCR Expression Profiling of the Complete Human ATP-Binding Cassette Transporter Superfamily in Various Tissues. 2003;238:230–8.

12. Flens MJ, Zaman GJ, van der Valk P, Izquierdo MA, Schroeijers AB, Scheffer GL, et al. Tissue distribution of the multidrug resistance protein. Am J Pathol [Internet]. 1996/04/01 ed. 1996;148(4):1237–47.

13. Brechot JM, Hurbain I, Fajac A, Daty N, Bernaudin JF. Different pattern of MRP localization in ciliated and basal cells from human bronchial epithelium. J Histochem Cytochem [Internet]. 1998/05/09 ed. 1998;46(4):513–7.

14. Lehmann T, Kohler C, Weidauer E, Taege C, Foth H. Expression of MRP1 and related transporters in human lung cells in culture. Toxicology [Internet]. 2001/09/15 ed. 2001;167(1):59–72.

15. Lips K, Volk C, Schmitt B, Pfeil U, Arndt P, Miska D, et al. Polyspecific cation transporters mediate luminal release of acetylcholine from bronchial epithelium. Am J Respir Cell Mol Biol. 2005;33:79–88.

16. Lips K, Luhrmann A, Tschernig T, Stoeger T, Alessandrini F, Grau V, et al. Down-regulation of the nonneuronal acetylcholine synthesis and release machinery in acute allergic airway inflammation of rat and mouse. Life Sci. 2007;80:2263–9.

17. Tamai I, Ohashi R, Nezu JI, Sai Y, Kobayashi D, Oku a, et al. Molecular and functional characterization of organic cation/carnitine transporter family in mice. J Biol Chem [Internet]. 2000 Dec 22 [cited 2012 Mar 16];275(51):40064–72.

18. Horvath G, Schmid N, Fragoso MA, Schmid A, Conner GE, Salathe M, et al. Epithelial organic cation transporters ensure pH-dependent drug absorption in the airway. Am J Respir Cell Mol Biol [Internet]. 2006/08/19 ed. 2007;36(1):53–60.

19. Kummer W, Wiegand S, Akinci S, Schinkel AH, Wess J, Koepsell H, et al. Role of acetylcholine and muscarinic receptors in serotonin-induced bronchoconstriction in the mouse. J Mol Neurosci [Internet]. 2006/12/29 ed. 2006;30(1-2):67–8.

20. Bosquillon C. Drug transporters in the lung--do they play a role in the biopharmaceutics of inhaled drugs? J Pharm Sci [Internet]. 2009/12/02 ed. 2010;99(5):2240–55.

21. Tamai I, Nezu J, Uchino H, Sai Y, Oku a, Shimane M, et al. Molecular identification and characterization of novel members of the human organic anion transporter (OATP) family. Biochem Biophys Res Commun [Internet]. 2000 Jun 24;273(1):251–60.

22. Francombe D, Taylor G, Taylor S, Somers G, Edwards C, Gumbleton M. Functional role of P-gp efflux in limiting pulmonary drug absorption within an intact lung: application of an isolated perfused rat lung model. Proc Resp Drug Deliv 2008. 2008:461–4.

23. Manford F, Riffo-Vasquez Y, Spina D, Page CP, Hutt AJ, Moore V, et al. Lack of difference in pulmonary absorption of digoxin, a P-glycoprotein substrate, in mdr1a-deficient and mdr1a-competent mice. J Pharm Pharmacol [Internet]. 2008/09/25 ed. 2008;60(10):1305–10.

24. Madlova M, Bosquillon C, Asker D, Dolezal P, Forbes B. In-vitro respiratory drug absorption models possess nominal functional P-glycoprotein activity. J Pharm Pharmacol [Internet]. 2009/02/19 ed. 2009;61(3):293–301.

25. Gumbleton M, Al-Jayyoussi G, Crandon-Lewis A, Francombe D, Kreitmeyr K, Morris CJ, et al. Spatial expression and functionality of drug transporters in the intact lung: objectives for further research. Adv Drug Deliv Rev [Internet]. 2010/09/28 ed. 2011;63(1-2):110–8.

26. Eytan GD. Mechanism of multidrug resistance in relation to passive membrane permeation. Biomed Pharmacother [Internet]. 2005/03/30 ed. 2005;59(3):90–7.

27. Knowlton FP, Starling E. The influence of variations in temperature and bloodpressure on the performance of the isolated mammalian heart. J Physiol. 1912;44(3):206–19.

28. Newell M. The Direct Influence of Gradual Variations of Temperature upon the Rate of Beat of the Dog's Heart. Philos Trans R Soc London. 1883;174.

29. Delaunois A. Improvements in an isolated perfused lung technique. Arch Int Pharmacodyn Ther. 1956;107(1):90–2.

30. Ryrfeldt A, Nilsson E. Uptake and biotransformation of ibuterol and terbutaline in isolated perfused rat and guinea pig lungs. Biochem Pharmacol [Internet]. 1978 Feb 1;27(3):301–5.

31. Ryrfeldt A, Persson G, Nilsson E. Pulmonary disposition of the potent glucocorticoid budesonide, evaluated in an isolated perfused rat lung model. Biochem Pharmacol. 1989;38(1):17–22.

32. Byron PR, Niven RW. A novel dosing method for drug administration to the airways of the isolated perfused rat lung. J Pharm Sci. 1988;77(8):693–5.

33. Byron PR, Roberts NS, Clark AR. An isolated perfused rat lung preparation for the study of aerosolized drug deposition and absorption. J Pharm Sci. 1986;75(2):168–71.

34. Niven RW, Byron PR. Solute absorption from the airways of the isolated rat lung. I. The use of absorption data to quantify drug dissolution or release in the respiratory tract. Pharm Res. 1988;5(9):574–9.

35. Byron PR. Solute absorption from the airways of the isolated rat lung. IV. Mechanisms of absorption of fluorophore-labeled poly-alpha,beta-[N(2-hydroxyethyl)-DLaspartamide]. Pharm Res. 1994;11(2):221–5.

36. Byron PR. Solute absorption from the airways of the isolated rat lung. II. Effect of surfactants on absorption of fluorescein. Pharm Res. 1990;7(1):8–13.

37. Niven R, Rypacek F, Byron PR. Solute absorption from the airways of the isolated rat lung. III. Absorption of several peptidase-resistant, synthetic polypeptides: poly-(2- hydroxyethyl)-aspartamides. Pharm Res. 1990;7(10):990–4.

38. Tronde A, Norden B, Jeppsson AB, Brunmark P, Nilsson E, Lennernas H, et al. Drug absorption from the isolated perfused rat lung--correlations with drug physicochemical properties and epithelial permeability. J Drug Target [Internet]. 2003/07/11 ed. 2003;11(1):61–74.

39. Keserü B, Barbosa-Sicard E, Popp R, Fisslthaler B, Dietrich A, Gudermann T, et al. Epoxyeicosatrienoic acids and the soluble epoxide hydrolase are determinants of pulmonary artery pressure and the acute hypoxic pulmonary vasoconstrictor response. FASEB J. 2008;22(12):4306–15.

40. Fuchs B, Rupp M, Ghofrani HA, Schermuly RT, Seeger W, Grimminger F, et al. Diacylglycerol regulates acute hypoxic pulmonary vasoconstriction via TRPC6. Respir Res. 2011;12:20.

41. Yoo HY, Zeifman A, Ko EA, Smith KA, Chen J, Machado RF, et al. Optimization of isolated perfused/ventilated mouse lung to study hypoxic pulmonary vasoconstriction. Pulm Circ [Internet]. 2013;3:396–405.

42. Roth M, Rupp M, Hofmann S, Mittal M, Fuchs B, Sommer N, et al. Heme oxygenase-2 and large-conductance Ca2+-activated K + channels: Lung vascular effects of hypoxia. Am J Respir Crit Care Med. 2009;180(4):353–64.

43. Bernal PJ, Leelavanichkul K, Bauer E, Cao R, Wilson A, Wasserloos KJ, et al. Nitric Oxide-Mediated Zinc release Contributes to Hypoxic regulation of pulmonary vascular tone. Circ Res. 2008;102(12):1575–83.

44. Patton JS, Byron PR. Inhaling medicines: delivering drugs to the body through the lungs. Nat Rev Drug Discov [Internet]. 2007 Jan [cited 2012 Mar 16];6(1):67–74.

45. Empey DW. Diseases of the respiratory system. Introduction: structure and function of the lungs. Br Med J. 1978;1(6113):631–3.

46. Stone KC, Mercer RR, Gehr P, Stockstill B, Crapo JD. Allometric relationships of cell numbers and size in the mammalian lung. Am J Respir Cell Mol Biol [Internet]. 1992 Feb;6(2):235–43.

47. Plopper CG. Structure and function of the lung. In: Respiratory system. Jones TC, Dungworth, D. L., and Mohr, U. E, editors. Berlin, Sprinter Verlag; 1996. 135-150.

48. Patton S. Mechanisms of macromolecule absorption by the lungs. Adv Drug Deliv Rev. 1996;19(95):3–36.

49. Crapo JD, Barry BE, Gehr P, Bachofen M, Weibel ER. Cell number and cell characteristics of the normal human lung. Am Rev Respir Dis [Internet]. 1982/08/01 ed. 1982;126(2):332–7.

50. Hedrich H. The Laboratory Mouse (Handbook of Experimental Animals). Hedrich H, editor. Elsevier Academic Press, New York; 2012.

51. James F, Stephen W B, Muriel T D, Newcomer CE, Quimby FW, Smith AL, editors. The Mouse in Biomedical Research, Volume III: Normative Biology, Husbandry, and Models. Second. American College of Laboratory Animal Medicine; 2007.

52. Harkness JE, Turner P V, VandeWoude S, Wheler CL, editors. Biology and Medicine of Rabbits and Rodents. Wiley-Blackwell; 2010.

53. VERLOOP MC. On the arteriae bronchiales and their anastomosing with the arteria pulmonalis in some rodents; a micro-anatomical study. Acta Anat (Basel). 1949;7(1-2):1–32.

54. Staub NC. Basic Respiratory Physiology. Staub NC, editor. Churchill Livingstone Inc, New York; 1991.

55. Chediak AD, Wanner A. The circulation of the airways: anatomy, physiology and potential role in drug delivery to the respiratory tract. Adv Drug Deliv Rev. 1990;5(1-2):11–8.

56. Kröll F, Karlsson JA, Persson CG. Tracheobronchial microvessels perfused via the pulmonary artery in guinea-pig isolated lungs. Acta Physiol Scand. 1987;129(3):445–6.

57. Hartley CJ, Michael LH, Entman ML. Noninvasive measurement of ascending aortic blood velocity in mice. Am J Physiol. 1995;268(1 Pt 2):H499–505.

58. Mehendale HM, Angevine LS, Ohmiya Y. The isolated perfused lung--a critical evaluation. Toxicology. 1981;21(1):1–36.

59. Tronde A. The Isolated Perfused Lung for Drug Absorption Studies. 2007. Thesis.

60. Joucher F, Mazmanian G-M, German-Fattal M. Endothelial cell early activation induced by allogeneic lymphocytes in isolated perfused mouse lung. Transplantation. 2002;74(10):1461–9.

61. Joucher F, Mazmanian G-M, German-Fattal M. E-selectin early overexpression induced by allogeneic activation in isolated mouse lung. Transplantation. 2004;78(9):1283–9.

62. Von Bethmann AN, Brasch F, Nusing R, Vogt K, Volk HD, Muller KM, et al. Hyperventilation induces release of cytokines from perfused mouse lung. Am J Respir Crit Care Med [Internet]. 1998/01/28 ed. 1998;157(1):263–72.

63. Held HD, Uhlig S. Mechanisms of endotoxin-induced airway and pulmonary vascular hyperreactivity in mice. Am J Respir Crit Care Med. 2000;162(4 I):1547–52.

64. Sabbagh F, Lecerf F, Maurois P, Bac P, German-Fattal M. Allogeneic activation is attenuated in a model of mouse lung perfused with magnesium-deficient blood. Transpl Immunol. 2006;16(3-4):200–7.

65. Zhao M, Fernandez LG, Doctor A, Sharma AK, Zarbock A, Tribble CG, et al. Alveolar macrophage activation is a key initiation signal for acute lung ischemia-reperfusion injury. Am J Physiol Lung Cell Mol Physiol. 2006;291(5):L1018–26.

66. Institutional Animal Care and Use Committee: Biomethodology of the rat. University of Iowa;

67. Kanekal S, Plopper C, Morin D, Buckpitt A. Metabolism and cytotoxicity of naphthalene oxide in the isolated perfused mouse lung. J Pharmacol Exp Ther [Internet]. 1991 Jan; 256(1):391–401.

68. Sakagami M, Byron PR, Venitz J, Rypacek F. Solute disposition in the rat lung in vivo and in vitro: determining regional absorption kinetics in the presence of mucociliary escalator. J Pharm Sci [Internet]. 2002 Feb;91(2):594–604.

69. Cryan S-A, Sivadas N, Garcia-Contreras L. In vivo animal models for drug delivery across the lung mucosal barrier. Adv Drug Deliv Rev. 2007;59(11):1133–51.

70. Ravnic DJ, Konerding MA, Pratt JP, Wolloscheck T, Huss HT, Mentzer SJ. The murine bronchopulmonary microcirculation in hapten-induced inflammation. J Thorac Cardiovasc Surg. 2007;133(1):97–103.

71. Al-jayyoussi G, Price DF, Francombe D, Taylor G, Smith MW, Morris C, et al. Selectivity in the Impact of P-Glycoprotein Upon Pulmonary Absorption of Airway-Dosed Substrates : A Study in Ex Vivo Lung Models Using Chemical Inhibition and Genetic Knockout. 2013;1–13.

72. Francombe D, Taylor G, Taylor S SG, Edwards C GM. Functional role of P-gp efflux in limiting pulmonary drug absorption within an intact lung: Application of an isolated perfused rat lung model. Proc Resp Drug Deliv. 2008;2:461–4.

73. Roerig DL, Audi SH, Ahlf SB. Kinetic characterization of P-glycoprotein-mediated efflux of rhodamine 6G in the intact rabbit lung. Drug Metab Dispos [Internet]. 2004/08/21 ed. 2004;32(9):953–8.

74. Ejendal KF, Hrycyna CA. Differential sensitivities of the human ATP-binding cassette transporters ABCG2 and P-glycoprotein to cyclosporin A. Mol Pharmacol [Internet]. 2004/12/16 ed. 2005;67(3):902–11.

75. Annaert PP, Turncliff RZ, Booth CL, Thakker DR, Brouwer KL. P-glycoprotein-mediated in vitro biliary excretion in sandwich-cultured rat hepatocytes. Drug Metab Dispos [Internet]. 2001/09/19 ed. 2001;29(10):1277–83.

76. Mistry P, Stewart AJ, Dangerfield W, Okiji S, Liddle C, Bootle D, et al. In vitro and in vivo reversal of P-glycoprotein-mediated multidrug resistance by a novel potent modulator, XR9576. Cancer Res [Internet]. 2001/02/24 ed. 2001;61(2):749–58.

77. Huisman MT, Smit JW, Wiltshire HR, Beijnen JH, Schinkel AH. Assessing safety and efficacy of directed P-glycoprotein inhibition to improve the pharmacokinetic properties of saquinavir coadministered with ritonavir. J Pharmacol Exp Ther [Internet]. 2003/01/23 ed. 2003;304(2):596–602.

78. Letrent SP, Pollack GM, Brouwer KR, Brouwer KL. Effects of a potent and specific P-glycoprotein inhibitor on the blood-brain barrier distribution and antinociceptive effect of morphine in the rat. Drug Metab Dispos [Internet]. 1999/06/29 ed. 1999;27(7):827–34.

79. Kemper EM, van Zandbergen AE, Cleypool C, Mos HA, Boogerd W, Beijnen JH, et al. Increased penetration of paclitaxel into the brain by inhibition of P-Glycoprotein. Clin Cancer Res [Internet]. 2003/07/12 ed. 2003;9(7):2849–55.

80. Pichler A, Prior JL, Piwnica-Worms D. Imaging reversal of multidrug resistance in living mice with bioluminescence: MDR1 P-glycoprotein transports coelenterazine. Proc Natl Acad Sci U S A [Internet]. 2004/02/03 ed. 2004;101(6):1702–7.

81. Rautio J, Humphreys JE, Webster LO, Balakrishnan A, Keogh JP, Kunta JR, et al. In vitro p-glycoprotein inhibition assays for assessment of clinical drug interaction potential of new drug candidates: a recommendation for probe substrates. Drug Metab Dispos [Internet]. 2006/02/04 ed. 2006;34(5):786–92.

82. Rao V V, Dahlheimer JL, Bardgett ME, Snyder AZ, Finch RA, Sartorelli AC, et al. Choroid plexus epithelial expression of MDR1 P glycoprotein and multidrug resistance-associated protein contribute to the blood-cerebrospinal-fluid drug-permeability barrier. Proc Natl Acad Sci U S A [Internet]. 1999/03/31 ed. 1999;96(7):3900–5.

83. Tannergren C, Petri N, Knutson L, Hedeland M, Bondesson U, Lennernas H. Multiple transport mechanisms involved in the intestinal absorption and first-pass extraction of fexofenadine. Clin Pharmacol Ther [Internet]. 2003/10/31 ed. 2003;74(5):423–36.

84. Williams GC, Liu A, Knipp G, Sinko PJ. Direct evidence that saquinavir is transported by multidrug resistance-associated protein (MRP1) and canalicular multispecific organic anion transporter (MRP2). Antimicrob Agents Chemother [Internet]. 2002/10/18 ed. 2002;46(11):3456–62.

85. Polli JW, Jarrett JL, Studenberg SD, Humphreys JE, Dennis SW, Brouwer KR, et al. Role of P-glycoprotein on the CNS disposition of amprenavir (141W94), an HIV protease inhibitor. Pharm Res [Internet]. 1999/09/01 ed. 1999;16(8):1206–12.

86. Francombe D, Hons BS. Examining the Functional Role of Transporters in Modulating Drug Absorption across Lung Epithelium . 2011;(June).

87. Patton JS, Fishburn CS, Weers JG. The lungs as a portal of entry for systemic drug delivery. Proc Am Thorac Soc [Internet]. 2004 Jan [cited 2012 Jul 23];1(4):338–44.

88. Fisher A. The Isolated Perfused Lung, in Handbook of experimental pharmacology. Witschi H., editor. Springer Berlin / Heidelberg; 1985. 149-179.

89. Czartolomna J, Voelkel NF, Chang SW. Permeability characteristics of isolated perfused rat lungs. J Appl Physiol. 1991;70(4):1854–60.

90. Sakagami M, Byron PR, Rypacek F. Biochemical evidence for transcytotic absorption of polyaspartamide from the rat lung: Effects of temperature and metabolic inhibitors. J Pharm Sci. 2002;91(9):1958–68.

91. Ingbar A. Measurement of Lung Water, in Pulmonary Edema (Lung Biology in Health and Disease). Informa Healthcare; 1998. 638.

92. Reinoso RF, Telfer BA, Rowland M. Tissue water content in rats measured by desiccation. J Pharmacol Toxicol Methods. 1997;38(2):87–92.

93. Schinkel AH, Mayer U, Wagenaar E, Mol CA, van Deemter L, Smit JJ, et al. Normal viability and altered pharmacokinetics in mice lacking mdr1-type (drug-transporting) P-glycoproteins. Proc Natl Acad Sci U S A [Internet]. 1997/04/15 ed. 1997;94(8):4028–33. 94. Lankas GR, Cartwright ME, Umbenhauer D. P-glycoprotein deficiency in a subpopulation of CF-1 mice enhances avermectin-induced neurotoxicity. Toxicol Appl Pharmacol [Internet]. 1997/04/01 ed. 1997;143(2):357–65.

95. Umbenhauer DR, Lankas GR, Pippert TR, Wise LD, Cartwright ME, Hall SJ, et al. Identification of a P-glycoprotein-deficient subpopulation in the CF-1 mouse strain using a restriction fragment length polymorphism. Toxicol Appl Pharmacol [Internet]. 1997/09/23 ed. 1997;146(1):88–94.

96. Schinkel AH, Smit JJ, van Tellingen O, Beijnen JH, Wagenaar E, van Deemter L, et al. Disruption of the mouse mdr1a P-glycoprotein gene leads to a deficiency in the blood-brain barrier and to increased sensitivity to drugs. Cell [Internet]. 1994/05/20 ed. 1994;77(4):491–502.

97. Kwei GY, Alvaro RF, Chen Q, Jenkins HJ, Hop CE, Keohane CA, et al. Disposition of ivermectin and cyclosporin A in CF-1 mice deficient in mdr1a P-glycoprotein. Drug Metab Dispos [Internet]. 1999/04/30 ed. 1999;27(5):581–7.

98. Van Asperen J, Schinkel AH, Beijnen JH, Nooijen WJ, Borst P, van Tellingen O. Altered pharmacokinetics of vinblastine in Mdr1a P-glycoprotein-deficient Mice. J Natl Cancer Inst [Internet]. 1996/07/17 ed. 1996;88(14):994–9.

99. Lagas JS, Sparidans RW, van Waterschoot RA, Wagenaar E, Beijnen JH, Schinkel AH. P-glycoprotein limits oral availability, brain penetration, and toxicity of an anionic drug, the antibiotic salinomycin. Antimicrob Agents Chemother [Internet]. 2008/01/16 ed. 2008;52(3):1034–9.

100. Huisman MT, Smit JW, Wiltshire HR, Hoetelmans RM, Beijnen JH, Schinkel AH. P-glycoprotein limits oral availability, brain, and fetal penetration of saquinavir even with high doses of ritonavir. Mol Pharmacol [Internet]. 2001/03/22 ed. 2001;59(4):806–13.

101. Mayer U, Wagenaar E, Beijnen JH, Smit JW, Meijer DK, van Asperen J, et al. Substantial excretion of digoxin via the intestinal mucosa and prevention of long-term digoxin accumulation in the brain by the mdr 1a P-glycoprotein. Br J Pharmacol [Internet]. 1996/11/01 ed. 1996;119(5):1038–44.

102. De Lange EC, de Bock G, Schinkel AH, de Boer AG, Breimer DD. BBB transport and P-glycoprotein functionality using MDR1A (-/-) and wild-type mice. Total brain versus microdialysis concentration profiles of rhodamine-123. Pharm Res [Internet]. 1998/12/02 ed. 1998;15(11):1657–65.

103. Jonker JW, Wagenaar E, van Deemter L, Gottschlich R, Bender HM, Dasenbrock J, et al. Role of blood-brain barrier P-glycoprotein in limiting brain accumulation and sedative side-effects of asimadoline, a peripherally acting analgaesic drug. Br J Pharmacol [Internet]. 1999/06/16 ed. 1999;127(1):43–50.

104. Van Asperen J, van Tellingen O, Tijssen F, Schinkel AH, Beijnen JH. Increased accumulation of doxorubicin and doxorubicinol in cardiac tissue of mice lacking mdr1a P-glycoprotein. Br J Cancer [Internet]. 1999/07/17 ed. 1999;79(1):108–13.

105. Sparreboom A, van Asperen J, Mayer U, Schinkel AH, Smit JW, Meijer DK, et al. Limited oral bioavailability and active epithelial excretion of paclitaxel (Taxol) caused by P-glycoprotein in the intestine. Proc Natl Acad Sci U S A [Internet]. 1997/03/04 ed. 1997;94(5):2031–5.

106. Smit JJ, Schinkel AH, Oude Elferink RP, Groen AK, Wagenaar E, van Deemter L, et al. Homozygous disruption of the murine mdr2 P-glycoprotein gene leads to a complete absence of phospholipid from bile and to liver disease. Cell [Internet]. 1993/11/05 ed. 1993;75(3):451–62.

107. OligoCalc [Internet]. Northwestern University Feinberg. 2013.

108. Fromm MF, Kim RB, Stein CM, Wilkinson GR, Roden DM. Inhibition of P-glycoprotein-mediated drug transport: A unifying mechanism to explain the interaction between digoxin and quinidine [seecomments]. Circulation [Internet]. 1999/02/02 ed. 1999;99(4):552–7.

109. Brady JM, Cherrington NJ, Hartley DP, Buist SC, Li N, Klaassen CD. Tissue distribution and chemical induction of multiple drug resistance genes in rats. Drug Metab Dispos [Internet]. 2002/06/18 ed. 2002;30(7):838–44.

110. Campbell L, Abulrob AN, Kandalaft LE, Plummer S, Hollins AJ, Gibbs A, et al. Constitutive expression of p-glycoprotein in normal lung alveolar epithelium and functionality in primary alveolar epithelial cultures. J Pharmacol Exp Ther [Internet]. 2002/12/20 ed. 2003;304(1):441–52.

111. Cordon-Cardo C, O'Brien JP, Boccia J, Casals D, Bertino JR, Melamed MR. Expression of the multidrug resistance gene product (P-glycoprotein) in human normal and tumor tissues. J Histochem Cytochem [Internet]. 1990/09/01 ed. 1990;38(9):1277–87.

112. Valk P Van Der, Kalken CK Van, Ketelaars H, Broxterman HJ, Scheffer G, Kuiper CM, et al. Distribution of multi-drug resistance-associated P-glycoprotein in normal and neoplastic human tissues Analysis with 3 monoclonal antibodies recognizing different epitopes of the P-glycoprotein molecule. 1990;56–64.

113. Lechapt-Zalcman E, Hurbain I, Lacave R, Commo F, Urban T, Antoine M, et al. MDR1-Pgp 170 expression in human bronchus. Eur Respir J [Internet]. 1997/08/01 ed. 1997;10(8):1837–43.

114. Scheffer GL, Pijnenborg AC, Smit EF, Muller M, Postma DS, Timens W, et al. Multidrug resistance related molecules in human and murine lung. J Clin Pathol [Internet]. 2002/05/03 ed. 2002;55(5):332–9.

115. Endter S, Becker U, Daum N, Huwer H, Lehr CM, Gumbleton M, et al. P-glycoprotein (MDR1) functional activity in human alveolar epithelial cell monolayers. Cell Tissue Res [Internet]. 2006/12/14 ed. 2007;328(1):77–84.

116. Brillault J, De Castro W V, Harnois T, Kitzis A, Olivier JC, Couet W. P-glycoprotein-mediated transport of moxifloxacin in a Calu-3 lung epithelial cell model. Antimicrob Agents Chemother [Internet]. 2009/02/04 ed. 2009;53(4):1457–62.

117. Ehrhardt C, Kneuer C, Laue M, Schaefer UF, Kim KJ, Lehr CM. 16HBE14o- human bronchial epithelial cell layers express P-glycoprotein, lung resistance-related protein, and caveolin-1. Pharm Res [Internet]. 2003/05/13 ed. 2003;20(4):545–51.

118. Kuhlmann O, Hofmann HS, Muller SP, Weiss M. Pharmacokinetics of idarubicin in the isolated perfused rat lung: effect of cinchonine and rutin. Anticancer Drugs [Internet]. 2003/07/11 ed. 2003;14(6):411–6.

119. Sakagami M. In vivo, in vitro and ex vivo models to assess pulmonary absorption and disposition of inhaled therapeutics for systemic delivery. Adv Drug Deliv Rev [Internet]. 2006 Oct 31 [cited 2013 Apr 6];58(9-10):1030–60.

120. Icard P, Saumon G. Alveolar sodium and liquid transport in mice. Am J Physiol [Internet]. 1999 Dec;277(6 Pt 1):L1232–8.

121. Loetchutinat C, Saengkhae C, Marbeuf-Gueye C, Garnier-Suillerot A. New insights into the P-glycoprotein-mediated effluxes of rhodamines. Eur J Biochem [Internet]. 2003/01/25 ed. 2003;270(3):476–85.

122. Shapiro AB, Ling V. Positively cooperative sites for drug transport by P-glycoprotein with distinct drug specificities. Eur J Biochem [Internet]. 1998/02/07 ed. 1997;250(1):130–7.

123. Research, F.a.D.A.C.f.D.E.a. Guidance for Industry: Bioanalytical Method Validation. Drug Inf Branch Rockville, MD. :25.

124. Juliano RL, Ling V. A surface glycoprotein modulating drug permeability in Chinese hamster ovary cell mutants. Biochim Biophys Acta [Internet]. 1976/11/11 ed. 1976;455(1):152–62.

125. Schinkel AH, Wagenaar E, van Deemter L, Mol CA, Borst P. Absence of the mdr1a P-Glycoprotein in mice affects tissue distribution and pharmacokinetics of dexamethasone, digoxin, and cyclosporin A. J Clin Invest [Internet]. 1995/10/01 ed. 1995;96(4):1698–705.

126. Thiebaut F, Tsuruo T, Hamada H, Gottesman MM, Pastan I, Willingham MC. Immunohistochemical localization in normal tissues of different epitopes in the multidrug transport protein P170: evidence for localization in brain capillaries and crossreactivity of one antibody with a muscle protein. J Histochem Cytochem [Internet]. 1989/02/01 ed. 1989;37(2):159–64.

127. Hamilton KO, Topp E, Makagiansar I, Siahaan T, Yazdanian M, Audus KL. Multidrug resistance-associated protein-1 functional activity in Calu-3 cells. J Pharmacol Exp Ther [Internet]. 2001/08/16 ed. 2001;298(3):1199–205.

128. Schuetz EG, Umbenhauer DR, Yasuda K, Brimer C, Nguyen L, Relling M V, et al. Altered expression of hepatic cytochromes P-450 in mice deficient in one or more mdr1 genes. Mol Pharmacol [Internet]. 2000/01/05 ed. 2000;57(1):188–97.

129. Committee JF. British National Formulary. BMJ Gr Pharm Press. 2008;

130. Varma M V, Sateesh K, Panchagnula R. Functional role of P-glycoprotein in limiting intestinal absorption of drugs: contribution of passive permeability to P-glycoprotein mediated efflux transport. Mol Pharm [Internet]. 2005/04/05 ed. 2005;2(1):12–21.

131. Valenzuela B, Nácher A, Casabó VG, Martín-Villodre A. The influence of active secretion processes on intestinal absorption of salbutamol in the rat. Eur J Pharm Biopharm [Internet]. 2001 Jul [cited 2012 Dec 4];52(1):31–7.

132. Valenzuela B, Nacher A, Ruiz-Carretero P, Martin-Villodre A, Lopez-Carballo G, Barettino D. Profile of P-glycoprotein distribution in the rat and its possible influence on the salbutamol intestinal absorption process. J Pharm Sci [Internet]. 2004/05/05 ed. 2004;93(6):1641–8.

133. Chang C, Bahadduri PM, Polli JE, Swaan PW, Ekins S. Rapid identification of P-glycoprotein substrates and inhibitors. Drug Metab Dispos [Internet]. 2006/09/26 ed. 2006;34(12):1976–84.

134. Hochhaus G, Möllmann H. Pharmacokinetic/pharmacodynamic characteristics of the beta-2-agonists terbutaline, salbutamol and fenoterol. Int J Clin Pharmacol Ther Toxicol. 1992;30(9):342–62.

135. Valenzuela B, Lopez-Pintor E, Perez-Ruixo JJ, Nacher A, Martin-Villodre A, Casabo VG. Modelling intestinal absorption of salbutamol sulphate in rats. Int J Pharm [Internet]. 2006/04/01 ed. 2006;314(1):21–30.

136. Anderson PJ, Zhou X, Breen P, Gann L, Logsdon TW, Compadre CM, et al. Pharmacokinetics of (R,S)-albuterol after aerosol inhalation in healthy adult volunteers. J Pharm Sci. 1998;87(7):841–4.

137. Borgström L. The pharmacokinetics of inhaled hydrofluoroalkane formulations. J Allergy Clin Immunol. 1999;104(6):S246–9.

138. Nolting A, Sista S, Abramowitz W. Single-dose study to compare the pharmacokinetics of HFA flunisolide and CFC flunisolide. J Pharm Sci. 2002;91(2):424–32.

139. Crim C, Pierre LN, Daley-Yates PT. A review of the pharmacology and pharmacokinetics of inhaled fluticasone propionate and mometasone furoate. Clinical Therapeutics. 2001. p. 1339–54.

140. Winkler J, Hochhaus G, Derendorf H. How the lung handles drugs: pharmacokinetics and pharmacodynamics of inhaled corticosteroids. Proc Am Thorac Soc [Internet]. 2004 Jan [cited 2012 Apr 27];1(4):356–63.

141. Miller-Larsson A, Mattsson H, Hjertberg E, Dahlbäck M, Tunek A, Brattsand R. Reversible fatty acid conjugation of budesonide: Novel mechanism for prolonged retention of topically applied steroid in airway tissue. Drug Metab Dispos. 1998;26(7):623–30.

142. Allen DB, Bielory L, Derendorf H, Dluhy R, Colice GL, Szefler SJ. Inhaled corticosteroids: past lessons and future issues. J Allergy Clin Immunol. 2003;112(3 Suppl):S1–40.

143. Wieslander E, Delander EL, Järkelid L, Hjertberg E, Tunek A, Brattsand R. Pharmacologic importance of the reversible fatty acid conjugation of budesonide studied in a rat cell line in vitro. Am J Respir Cell Mol Biol. 1998;19(3):477–84.

144. Andes D, Craig W a. Pharmacodynamics of a new streptogramin, XRP 2868, in murine thigh and lung infection models. Antimicrob Agents Chemother. 2006;50(1):243–9.

145. Dudhani R V., Turnidge JD, Coulthard K, Milne RW, Rayner CR, Li J, et al. Elucidation of the pharmacokinetic/pharmacodynamic determinant of colistin activity against Pseudomonas aeruginosa in murine thigh and lung infection models. Antimicrob Agents Chemother. 2010;54(3):1117–24.

146. Wiederhold NP, Tam VH, Chi J, Prince RA, Kontoyiannis DP, Lewis RE. Pharmacodynamic activity of amphotericin B deoxycholate is associated with peak plasma concentrations in a neutropenic murine model of invasive pulmonary aspergillosis. Antimicrob Agents Chemother. 2006;50(2):469–73.

147. Schmidt EW. Pharmacokinetics of beta2-sympathomimetics at the example of fenoterol and conclusion for the administration. Wiadomosci lekarskie (Warsaw, Poland : 1960). 1998.

148. Eytan GD, Regev R, Oren G, Hurwitz CD, Assaraf YG. Efficiency of P-glycoprotein-mediated exclusion of rhodamine dyes from multidrug-resistant cells is determined by their passive transmembrane movement rate. Eur J Biochem [Internet]. 1997/08/15 ed. 1997;248(1):104–12.

149. Yamamoto A, Iseki T, Ochi-sugiyama M, Okada N, Fujita T, Muranishi S. Absorption of water-soluble compounds with different molecular weights and [Asu 1 . 7] -eel calcitonin from various mucosal administration sites. 2001;76:363–74.

150. Varma M V, Panchagnula R. Prediction of in vivo intestinal absorption enhancement on P-glycoprotein inhibition, from rat in situ permeability. J Pharm Sci [Internet]. 2005/06/30 ed. 2005;94(8):1694–704.

151. Thiebaut F, Tsuruo T, Hamada H, Gottesman MM, Pastan I, Willingham M. Cellular localization of the multidrug-resistance gene product P-glycoprotein in normal human tissues. Proc Natl Acad Sci U S A. 1987;84:7735–8.

152. Hunter J, Jepson MA, Tsuruo T, Simmons NL, Hirst BH. Functional expression of P-glycoprotein in apical membranes of human intestinal Caco-2 cells. Kinetics of vinblastine secretion and interaction with modulators. J Biol Chem [Internet]. 1993/07/15 ed. 1993;268(20):14991–7. Available from: http://www.ncbi.nlm.nih.gov/entrez/query.fcgi?cmd=Retrieve&db=PubMed&dopt=Citation&list_uids=8100817

153. Fricker G, Drewe J, Huwyler J, Gutmann H, Beglinger C. Relevance of p-glycoprotein for the enteral absorption of cyclosporin A: in vitro-in vivo correlation. Br J Pharmacol [Internet]. 1996/08/01 ed. 1996;118(7):1841–7.

154. Englund G, Rorsman F, Rönnblom A, Karlbom U, Lazorova L, Gråsjö J, et al. Regional levels of drug transporters along the human intestinal tract: Co-expression of ABC and SLC transporters and comparison with Caco-2 cells. Eur J Pharm Sci. 2006;29(3-4 SPEC. ISS.):269–77.

155. Berggren S, Gall C, Wollnitz N, Ekelund M, Karlbom U, Hoogstraate J, et al. Gene and protein expression of P-glycoprotein, MRP1, MRP2, and CYP3A4 in the small and large human intestine. Mol Pharm [Internet]. 2007/02/01 ed. 2007;4(2):252–7.

156. Zimmermann C, Gutmann H, Hruz P, Gutzwiller JP, Beglinger C, Drewe J. Mapping of multidrug resistance gene 1 and multidrug resistance-associated protein isoform 1 to 5 mRNA expression along the human intestinal tract. Drug Metab Dispos [Internet]. 2004/11/04 ed. 2005;33(2):219–24.

157. Taipalensuu J, Tornblom H, Lindberg G, Einarsson C, Sjoqvist F, Melhus H, et al. Correlation of gene expression of ten drug efflux proteins of the ATP-binding cassette transporter family in normal human jejunum and in human intestinal epithelial Caco-2 cell monolayers. J Pharmacol Exp Ther [Internet]. 2001/09/19 ed. 2001;299(1):164–70.

158. Mouly S, Paine MF. P-glycoprotein increases from proximal to distal regions of human small intestine. Pharm Res [Internet]. 2003/11/19 ed. 2003;20(10):1595–9.

159. MacLean C, Moenning U, Reichel A, Fricker G. Closing the gaps: A full scan of the intestinal expression of P-glycoprotein, breast cancer resistance protein, and multidrug resistance-associated protein 2 in male and female rats. Drug Metab Dispos. 2008;36(7):1249–54.

160. Tamura S, Tokunaga Y, Ibuki R, Amidon GL, Sezaki H, Yamashita S. The site-specific transport and metabolism of tacrolimus in rat small intestine. J Pharmacol Exp Ther [Internet]. 2003/04/05 ed. 2003;306(1):310–6.

161. Valenzuela B, Nacher A, Casabo VG, Martin-Villodre A. The influence of active secretion processes on intestinal absorption of salbutamol in the rat. Eur J Pharm Biopharm [Internet]. 2001/07/05 ed. 2001;52(1):31–7.

162. Yumoto R, Murakami T, Sanemasa M, Nasu R, Nagai J, Takano M. Pharmacokinetic interaction of cytochrome P450 3A-related compounds with rhodamine 123, a P-glycoprotein substrate, in rats pretreated with dexamethasone. Drug Metab Dispos [Internet]. 2001/02/13 ed. 2001;29(2):145–51.

163. Chiou WL, Chung SM, Wu TC, Ma C. A comprehensive account on the role of efflux transporters in the gastrointestinal absorption of 13 commonly used substrate drugs in humans. Int J Clin Pharmacol Ther [Internet]. 2001/06/09 ed. 2001;39(3):93–101.

164. Gallois L, Fiallo M, Laigle A, Priebe W, Garnier-Suillerot A. The overall partitioning of anthracyclines into phosphatidyl-containing model membranes depends neither on the drug charge nor the presence of anionic phospholipids. Eur J Biochem. 1996;241(3):879–87.

165. Regev R, Eytan GD. Flip-flop of doxorubicin across erythrocyte and lipid membranes. Biochem Pharmacol [Internet]. 1998/02/17 ed. 1997;54(10):1151–8.

166. Eytan GD, Regev R, Oren G, Assaraf YG. The role of passive transbilayer drug movement in multidrug resistance and its modulation. J Biol Chem [Internet]. 1996/05/31 ed. 1996;271(22):12897–902.

167. Aller SG, Yu J, Ward A, Weng Y, Chittaboina S, Zhuo R, et al. Structure of P-glycoprotein reveals a molecular basis for poly-specific drug binding. Science [Internet]. 2009 Mar 27 [cited 2013 Jan 29];323(5922):1718–22.

168. Schinkel AH. P-Glycoprotein, a gatekeeper in the blood-brain barrier. Adv Drug Deliv Rev [Internet]. 2000/06/06 ed. 1999;36(2-3):179–94.

169. Clarke LL. A guide to Ussing chamber studies of mouse intestine. Am J Physiol Gastrointest Liver Physiol [Internet]. 2009 Jun [cited 2013 Aug 12];296(6):G1151–66.

170. Fortuna A, Alves G, Falcão A, Soares-da-Silva P. Evaluation of the permeability and P-glycoprotein efflux of carbamazepine and several derivatives across mouse small intestine by the Ussing chamber technique. Epilepsia [Internet]. 2012 Mar [cited 2013 Sep 16];53(3):529–38.

171. Stephens RH, Neill CAO, Bennett J, Humphrey M, Henry B, Rowland M, et al. Resolution of P-glycoprotein and non-P-glycoprotein e ects on drug permeability using intestinal tissues from mdr1a (7 / 7) mice. 2002;2038–46.

172. Collett A, Stephens RH, Harwood MD, Humphrey M, Dallman L, Bennett J, et al. Investigation of regional mechanisms responsible for poor oral absorption in humans of a modified release preparation of the alpha-adrenoreceptor antagonist, 4-amino-6,7-dimethoxy-2-(5-

methanesulfonamido-1,2,3,4 tetrahydroisoquinol-2-yl)-5-(2-pyridyl)quin. Drug Metab Dispos [Internet]. 2007/10/13 ed. 2008;36(1):87–94.

173. Effros RM, Mason GR. Measurements of pulmonary epithelial permeability in vivo. Am Rev Respir Dis. 1983;127(5 Pt 2):S59–65.

174. Gumbleton M, Hollins AJ, Omidi Y, Campbell L, Taylor G. Targeting caveolae for vesicular drug transport. Journal of Controlled Release. 2003. p. 139–51.

175. Taylor G, Colthorpe P, Farr S. Pulmonary absorption of proteins, influence of deposition site and competitive elimination processes. Proc Resp Drug Deliv. 1994;IV:25–37.

176. Cabral-Marques, H.M Hadgraft J, Kellaway I., Taylor G. Studies of cyclodextrin inclusion complexes IV The pulmonary absorption of salbutamol from a complex with 2-hydroxy-propyl b-cyclodextrin in rabbits. Int J Pharm. 1991;(77):303–7.

177. Lanman RC, Gillilan RM, Schanker LS. Absorption of cardiac glycosides from the rat respiratory tract. J Pharmacol Exp Ther [Internet]. 1973/10/01 ed. 1973;187(1):105–11.

178. Krämer SD, Lombardi D, Primorac A, Thomae A V, Wunderli-Allenspach H. Lipid-bilayer permeation of drug-like compounds. Chem Biodivers [Internet]. 2009 Nov;6(11):1900–16.

179. Veber DF, Johnson SR, Cheng H-Y, Smith BR, Ward KW, Kopple KD. Molecular properties that influence the oral bioavailability of drug candidates. J Med Chem [Internet]. 2002 Jun

180. Acree WE, Grubbs LM, Abraham MH. Prediction of Partition Coefficients and Permeability of Drug Molecules in Biological Systems with Abraham Model Solute Descriptors Derived from Measured Solubilities and Water-to-Organic Solvent Partition Coefficients. 2008;

181. Abraham MH. The Permeation of Neutral Molecules , Ions , and Ionic Species Through Membranes : Brain Permeation as an Example. 2011;100(5):1690–701.

182. Ribeiro MMB, Melo MN, Serrano ID, Santos NC, Castanho MARB. Drug-lipid interaction evaluation: Why a 19th century solution? Trends Pharmacol Sci. 2010;31(10):449–54.

183. J S. Octanol-water partition coefficients. New York, NY: John Wiley and Sons; 1997.

184. Leo A. Calculating logPoct from structures. Chem Rev. 1993;93:1281–306.

185. Braumann T. Determination of hydrophobic parameters by reversed-phase liquid chromatography: theory, experimental techniques, and application in studies on quantitative structure-activity relationships. J Chromatogr. 1986;373(2):191–225.

186. Hauser H, Pascher I, Pearson RH, Sundell S. Preferred conformation and molecular packing of phosphatidylethanolamine and phosphatidylcholine. Biochim Biophys Acta. 1981;650(1):21–51.

187. Pidgeon C, Ong S, Liu H, Qiu X, Pidgeon M, Dantzig AH, et al. IAM chromatography: an in vitro screen for predicting drug membrane permeability. J Med Chem. 1995;38(4):590–4.

188. Ong S, Liu H, Pidgeon C. Immobilized-artificial-membrane chromatography: Measurements of membrane partition coefficient and predicting drug membrane permeability. Journal of Chromatography A. 1996. p. 113–28.

189. Ottiger C, H. W-A. Immobilized artificial membrane (IAM)-HPLC for partition studies of neutral and ionized acids and bases in comparison with the liposomal partition system. Pharm Res. 1999;16:643–50.

190. Kaliszan R, Nasal R, Bucinski A. Chromatographic hydrophobicity parameter deterimed on an immobilized aritificial membrane column: relationships to standard measures of hydrophobicity and bioactivity. Eur J Med Chem. 1994;29:163–70.

191. Barbato F, La Rotonda M, Quaglia F. Chromatographic indices determined on an immobilised artificial membrane (IAM) column as descriptors of lipophilic and polar interactions of 4-phenyldihydropyridine calcium-channel blockers with biomembranes. Eur J Med Chem. 1996;31:311–8.

192. Salminen T, Pulli a, Taskinen J. Relationship between immobilised artificial membrane chromatographic retention and the brain penetration of structurally diverse drugs. J Pharm Biomed Anal [Internet]. 1997 Jan;15(4):469–77.

193. Kotecha J, Shah S, Rathod I, Subbaiah G. Prediction of oral absorption in humans by experimental immobilized artificial membrane chromatography indices and physicochemical descriptors. Int J Pharm [Internet]. 2008 Aug [cited 2013 Jun 25];360(1-2):96–106.

194. Platts JA, Butina D, Abraham MH, Hersey A. Estimation of Molecular Linear Free Energy Relation Descriptors Using a Group Contribution Approach. 1999;835–45.

195. Giaginis C, Tsantili-kakoulidou A. Alternative Measures of Lipophilicity : From Octanol – Water Partitioning to IAM Retention. 2008;97(8):2984–3004.

196. Mintz C. Predicting Chemical and Biochemical Properties Using the Abraham General Solvation Model. 2009;

197. Thomas L. Lemke DAW, Wilkins LW&, editors. Foye's Principles of Medicinal Chemistry. 7th ed. Wolters Kluwer; 2012.

198. Dressman JB, Amidon GL, Fleisher D. Absorption potential: estimating the fraction absorbed for orally administered compounds. J Pharm Sci. 1985;74(5):588–9.

199. Lentz KA, Polli JW, Wring SA, Humphreys JE, Polli JE. Influence of passive permeability on apparent P-glycoprotein kinetics. Pharm Res [Internet]. 2001/04/17 ed. 2000;17(12):1456–60.